Earth-Science Reviews 253 (2024) 104774

Contents lists available at ScienceDirect

Earth-Science Reviews

journal homepage: www.elsevier.com/locate/earscirev

Unveiling the history and nature of paleostorms in the Holocene

Kenta Minamidate [a,b,*], Kazuhisa Goto [b]

[a] Graduate School of Science, Tohoku University, Aoba 468-1, Aramaki, Aoba-ku, Sendai 980-0845, Japan
[b] Department of Earth and Planetary Science, The University of Tokyo, 7-3-1 Hongo, Tokyo 113-0033, Japan

ARTICLE INFO

Keywords:
Tropical cyclones
Storm deposit
Paleotempestology
Natural hazards
Holocene

ABSTRACT

Tropical and extratropical cyclones have a profound impact on coastal morphology, ecosystems, and human lives. Given the ongoing global warming and the rising coastal populations, it is an urgent task to evaluate their impact on coastal regions ranging from low to high latitudes. Although the observation records show both significant and insignificant changes in tropical cyclone activity over recent decades, detecting long-term trends and attributing them to anthropogenic warming remains challenging due to the relatively short observation records and substantial natural variability. Paleotempestology is an emerging research field to reveal past storm activity prior to observation records based on geological, geomorphological, and biological records. This review summarizes the current progress and challenges of paleotempestology and provides insight into the response of storm activity to climate variability in the Holocene. Integrating interdisciplinary perspectives from geology, paleoclimatology, and numerical climate modeling, this review underscores the non-stationarity of storm activity, which is intricately related to climate variability through diverse mechanisms in each basin. Exploring the links and discrepancies between paleotempestological, paleoclimate, and modeling studies improves our understanding of the relationship between climate environment and storm activity.

1. Introduction

Storm-induced wind, precipitation and, waves drastically change coastal morphology through hydrodynamic and sedimentological processes. Ecosystems are severely impacted by temporally or irreversible environmental changes associated with seawater and sediment supply. The compounded hazards posed by approaching or landfalling storms, particularly tropical and extratropical cyclones, make it imperative to evaluate their impact on coastal regions ranging from low to high latitudes, given the rising coastal populations and vulnerability.

Tropical cyclones (TCs) are among the most severe geophysical phenomena that pose a threat to human lives and property. TCs are defined as warm-core, non-frontal, low-pressure systems of synoptic scale that originate over tropical or subtropical waters (Hobgood, 2005). The main source of energy for TCs is the latent heat of water vapor. The release of thermal energy through the condensation of water leads to an increase in wind speed and a decrease in air pressure, drawing in warm, moist air. As such, TCs are considered mesoscale convective complexes with self-sustaining heat engines. TCs are classified by their maximum sustained wind speeds as follows: (1) tropical depression, with winds up to 17 m/s, (2) tropical storm, with winds of 18–32 m/s (3) hurricane, typhoon, tropical cyclone, and very severe cyclonic storm depending on the basin with the winds of 33 m/s or greater. Climatologically, of about 85 tropical storms that occur annually on the Earth, 44 develop into tropical cyclone/hurricane/typhoon (WMO, 2021a). TCs accounted for one-third of the deaths and economic losses from weather, climate, and water disasters in the past 50 years (WMO, 2021b).

Atmospheric and oceanic environmental conditions are responsible for the genesis and development of TCs. The following conditions are necessary for the TC formation (Gray, 1968): (1) sufficient ocean thermal energy (sea surface temperature, hereinafter referred to as SST, >26 °C), (2) enhanced mid-troposphere (700 hPa) relatively humidity, (3) conditional instability, (4) enhanced lower troposphere relative vorticity, (5) weak vertical shear of the horizontal winds, and (6) displacement by at least 5° latitude away from equator. In other words, although ocean heat is important as an energy source for a TC, a disturbance in the atmosphere is also needed. TC activity, including formation location, frequency, intensity, size, life span, and tracks, is affected by various time-scale internal climate variability from intra-seasonal (e.g., Madden-Julian Oscillation) and interannual (e.g., El Niño-Southern Oscillation, hereinafter referred to as ENSO), to inter-decadal (e.g., Atlantic Multidecadal Variability and Pacific Decadal

* Corresponding author at: Atmosphere and Ocean Research Institute, The University of Tokyo, Kashiwa 277-8564, Japan.
E-mail address: minamidate@aori.u-tokyo.ac.jp (K. Minamidate).

https://doi.org/10.1016/j.earscirev.2024.104774
Received 14 February 2023; Received in revised form 7 April 2024; Accepted 8 April 2024
Available online 13 April 2024

Variability). Still, the relationship between centennial- to millennial-scale climate variability and TC activity is poorly understood due to the lack of long-term record of TCs.

Concerning the possibility of an increase in TC-related hazards due to anthropogenic global warming, TC-climatology is a major research topic paramount importance to society. Observational records have indicated a decrease in the annual counts of global TCs (Klotzbach et al., 2022), an increase in the proportion of major TCs (Saffir-Simpson categories 3–5) (Kossin et al., 2020) as well as poleward migration of latitude of maximum TC intensity in the western North Pacific (Kossin et al., 2014) within the satellite era—a short time span of the past 40 years. However, assessing the role of anthropogenic warming from the observational data alone in the presence of large natural variability is challenging and has led to inconsistent conclusions on the detection and attribution of TC trends (Emanuel, 2021; Knutson et al., 2019; Moon et al., 2019; Vecchi et al., 2021). Observational records have the following fundamental difficulties:

- Low-frequency but large-scale TC events (e.g., once in a century) are less likely to occur in the observational record (~40 years).
- It is difficult to detect long-term variabilities in TC activity from relatively short observational records.
- Our understanding of TC characteristics is likely to be biased by the fact that satellite observations have only begun in the latter half of the 20th century, when global warming is at an accelerated pace.
- There is spatio-temporal heterogeneity due to differences in observation methods and accuracy depending on the time and region.

As a result, observation records alone are insufficient to understand the true characteristics of TCs. Historical records are useful for obtaining information prior to the instrumental era, but they are relatively short and lack universality.

Extratropical cyclones (e.g., winter storms) are low-pressure systems characterized by the presence of cold and warm fronts. They are particularly prevalent in the mid-latitudes, approximately between 30 and 60° latitudes, including regions such as the North Atlantic, North Pacific, Southern Ocean, and Mediterranean Sea. Compared to TCs, extratropical cyclones, especially those making landfall in Europe, are more frequent (Dullaart et al., 2021). Intense winter storms can cause impacts including flooding, infrastructure damage, and geomorphological alterations, attributable to their winds and precipitation patterns (Bentley et al., 2019; Castelle et al., 2018; Eisenstein et al., 2022). According to Banerjee et al. (2023), the annual average insured loss attributed to winter storms during the period 2013–2022 amounted to 2.68 billion USD. While our review primarily focuses on TCs, we also address extratropical cyclones as a secondary consideration, particularly concerning regions like Europe where the influence of extratropical cyclones is substantial.

Paleotempestology is the study of past storm activity prior to observational records based on geological and geomorphological records. While sedimentological research on tempestites has long been conducted, the conceptualization of paleotempestology as a discipline integrating paleoclimatological aspects was advanced by Dr. Kerry Emanuel in 1996 (Liu, 2004). The key objectives of paleotempestology are to:

- Reconstruct the local history including frequency and magnitude of storm events
- Understand climatology of tropical and extratropical cyclones on centennial- to millennial-scale
- Detect changes in storm activity before and after anthropogenic climate change (around the 19th century)
- Impose physical constraints on numerical climate models.

Given the high level of social and scientific interest in storms, the knowledge of paleotempestology should now be made available to a wide variety of people, including geoscientists, socioeconomic planners, local governments, and policymakers. In order to incorporate the paleotempestological findings into hazard and climate risk assessments, such as the assessment report of the Intergovernmental Panel on Climate Change (IPCC), it is crucial to identify which geological records can be used as paleostorm proxies and what is currently understood. The recent progress in paleotempestology has been remarkable, and the techniques and knowledge related to each approach used in this field have been developed independently. Therefore, understanding the knowledge of a certain paleotempestological approach requires a high degree of professionalism, which makes it difficult for researchers in other fields to assess the findings, reliability, and challenges.

This paper aims to synthesize current knowledge and challenges of paleostorm research, which is still in its infancy, based on different disciplines such as geology, paleoclimatology, and numerical modeling. The article is organized as follows (Fig. 1): In chapter 2, we comprehensively describe various characteristics of geological proxy-based paleotempestological records, basic principles, current progress, and issues in paleostorm reconstruction. Chapter 3 reviews paleoclimatological and climatological findings that influence Holocene-scale storm activity. Chapter 4 discusses long-term variability in basin-scale storm activity and its mechanism. Chapter 5 reviews the paleoclimatological studies using numerical models. Finally, chapter 6 compares paleotempestological findings and modeling studies to interpret paleostorm activity and evaluate models, and provides a future perspective of the paleostorm study.

2. Paleostorm archives

In this chapter, we describe the geological and geomorphological records used to reconstruct the paleostorm information (Fig. 2). Deposits that are formed by hydrodynamic process, such as storm waves, storm surges, floods, and wind related to storm events are collectively referred to as storm deposits. Although there are number of proposed proxies, here we introduce four types of major storm deposits in the following sections: (1) overwash deposits, (2) deposits in coastal karst basin, (3) coastal boulder deposits, and (4) beach ridges. In the final section, we introduce (5) chemically and biologically formed laminae such as tree rings, speleothems, and corals, which record storm-related high precipitation.

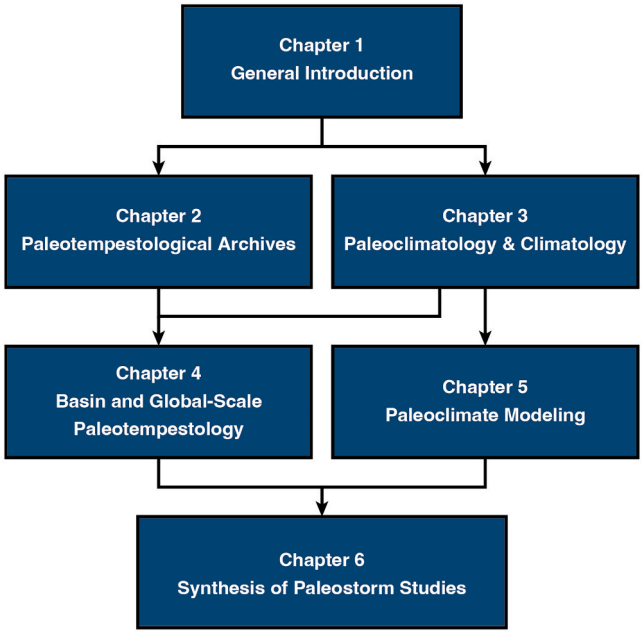

Fig. 1. Structure of the article.

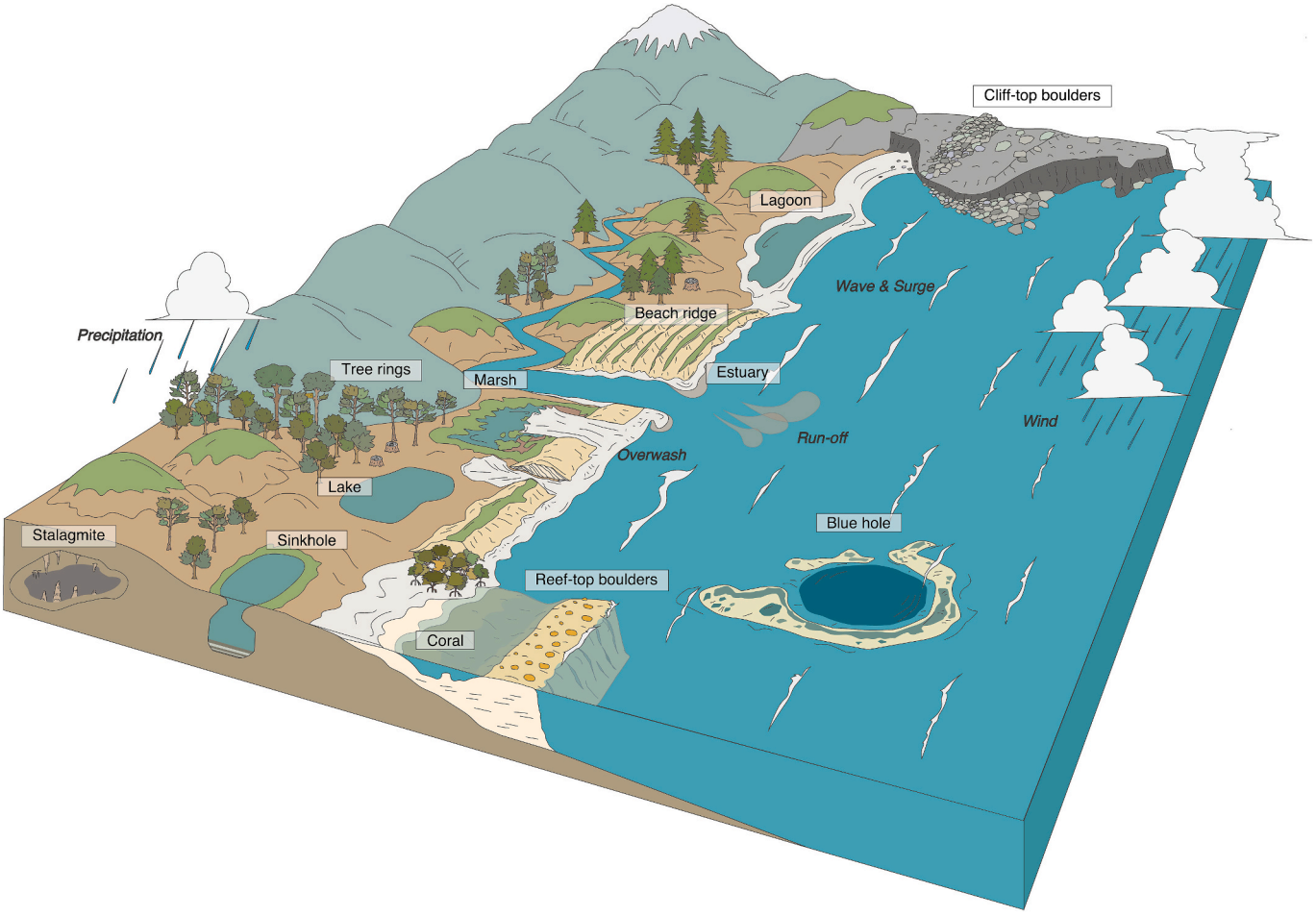

Fig. 2. Conceptual diagram of coastal environment with storm-associated phenomena.

2.1. Overwash deposit

2.1.1. Characteristics of overwash deposit

Overwash is overflowing water over onshore during storms and may cause shoreface erosion and sediment transport. Overwash deposits are sedimentary units deposited as a result of overwash event (Fig. 3a). Briefly, the impacts of storm waves and surges on the coastal zone are determined by extreme water level (combined effects of storm surge, astronomical tide, wave setups and run-up) and beach morphology (Masselink and van Heteren, 2014; Sallenger, 2000). In the Storm Impact Scale model (SIS model) proposed by Sallenger (2000), overwash is classified into the following two types: i) Overwash regime and ii) inundation regime.

i) The overwash regime occurs when the average water level during a storm (R_{low}) is below the crest or dune height (D_{high}), but the swash runup height (R_{high}) is above D_{high} ($R_{high} > D_{high} > R_{low}$). Wave overtopping can cause foreshore sediments to be deposited over the crest/dune. When many waves pass over the crest/dune, sediments eroded from the surface of offshore/foreshore/dune/crest are transported to the backshore and deposited. When the crest/dune is uneven, the overwash funnels through a gap (known also as a throat) and lower part of the foredune and then spreads laterally to the backshore. The flow velocity of the overwash decreases due to the action of friction and penetration. Consequently, suspended sediment deposits, forming a leaf-like or spray-like pattern called a washover fan behind the barrier (May et al., 2017; Williams, 2015).
ii) The inundation regime occurs when R_{low} exceeds D_{high}. This regime is defined as a crest/dune completely and continuously submerged by constantly flowing water. When the crest/dune height is constant, sheets of water and sediment flow over the crest. Sediments are deposited by the action of friction and penetration, forming sheet-like sediments (Phantuwongraj et al., 2013). Inconsistent crest/dune height or concentration of flow can cause localized overwash and form washover fans similar to the overwash regime. Overwash flow often forms channels and causes temporary breaches. Breaches involve large topographical changes, sediment supply to the back barrier, hydrological changes through the reconstruction of river systems and channels, and the destruction of ecosystems. Temporary breaches close once the water level returns, whereas full breaches may remain open for extended periods.

These basic concepts have been supported by physical process, numerical modeling, and field survey (Chaumillon et al., 2017; Donnelly et al., 2006). See Chaumillon et al. (2017) for a review of recent advances in interdisciplinary approaches. Studies on modern overwash events, utilizing observational and historical records, have revealed diverse sedimentological features of overwash deposits. Sedimentary patterns of these deposits are complicated due to hydrodynamic factors, geographic factors related to storm and site location, and local geomorphological factors. Overwash deposits consist of one or multiple layers that are rich in beachface materials (Nanayama et al., 2000; Soria et al., 2017). Laminations and sharp basal contacts are commonly found in overwash deposits (Brill et al., 2016; Hawkes and Horton, 2012). The sedimentary facies of overwash deposits can be characterized as graded, degraded, or both (Phantuwongraj et al., 2013; Sedgwick and Davis, 2003). Graded structures are interpreted to be formed by the turbulence and suspension associated with the overwash flow (Brill et al., 2016).

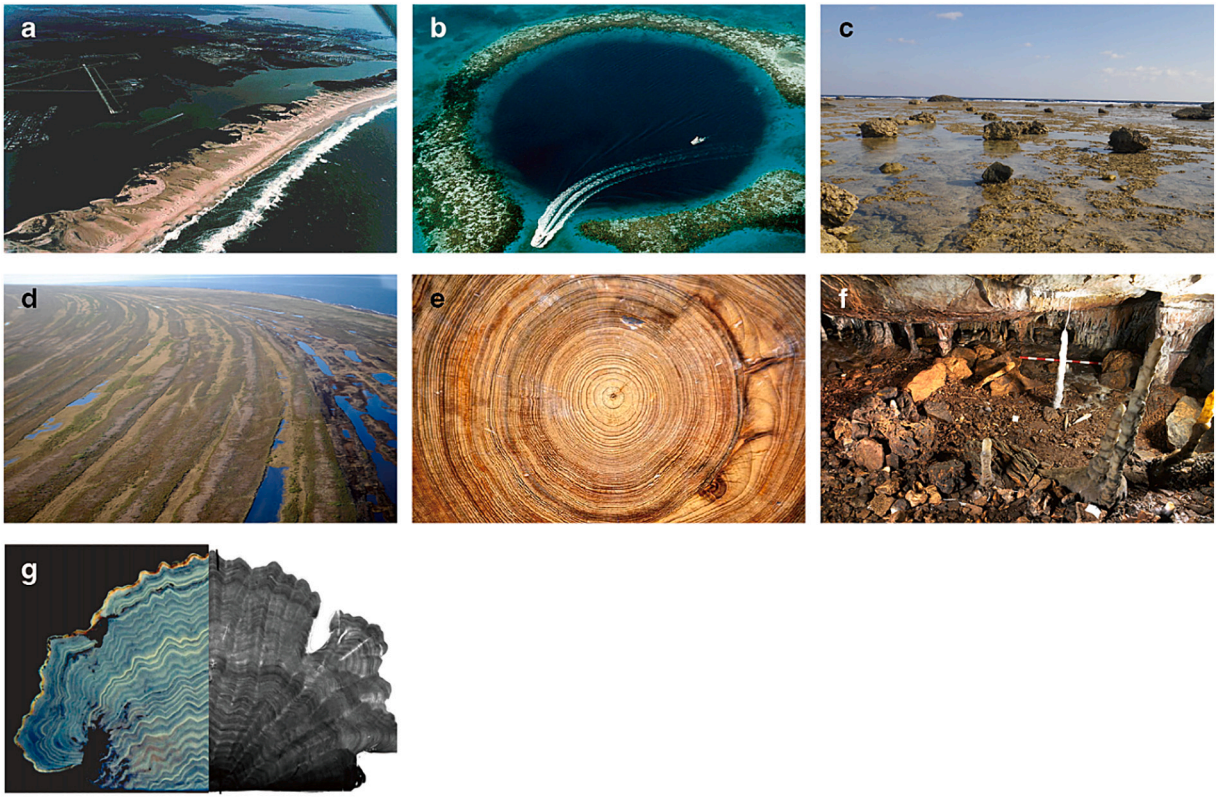

Fig. 3. Example photographs of proxies used for paleotempestology. (a) Overwash deposit at the barrier. (b) Blue hole. (c) Coastal boulder deposit. (d) Beach ridge. (e) Tree rings. (f) stalagmite in the cave. (g) Coral (Right: positive print of X-ray. Left: Illuminated by UV light). Photo credit information: (a) Figure from Donnelly et al. (2006). Reproduced and modified with permission from the Coastal Education and Research Foundation, Inc. (b) U.S. Geological Survey (USGS), Public domain, via Wikimedia Commons. (c) This study. (d) Education Specialist, CC BY 2.0, via Wikimedia Commons. (e) James *St.* John, CC BY 2.0, via Wikimedia Commons. (f) Figure from Baldini et al. (2015). Licensed by Elsevier. (g) Figure from Lough (2010). Licensed by John Wiley and Sons. (For interpretation of the references to colour in this figure legend, the reader is referred to the web version of this article.)

The mechanism behind the formation of the reversed structure remains unclear, but it has been suggested that it results from increase in flow velocity (Spiske and Jaffe, 2009), dispersion pressure (Bagnold, 1954), dynamic sieving effect (Knight et al., 1993), and settling of heavy minerals after sedimentation (Leatherman and Williams, 1983).

These sedimentary structures are generally accompanied by inland sorting. Typically, the average grain size of overwash deposit gradually decreases in response to decreasing flow velocity (Woodruff et al., 2008a). Macroscopically, overwash sheets over backbarrier plains often show an inland thinning trend (Williams, 2012). However, those systematic features are not always observed (Castagno et al., 2021; Soria et al., 2017).

2.1.2. *Principles behind the use of overwash deposits as storm proxy*

Through the overwash process, sediments are transported inland and overwash deposits are formed on the backbarrier. Subsequently, normal low-energy sediments (e.g., soil and peat) are deposited on the top of the overwash deposit, and thus the overwash deposit layers are buried within the strata. Therefore, information on storm events can be reconstructed by identifying paleostorm deposits in the strata. Storm deposits are identified based on grain size distribution, elemental composition, mineral composition, microfossils (foraminifera, diatoms, and dinoflagellates), organic content, and sedimentary structures. Dating methods are used to construct chronostratigraphy and determine the approximate age of storm events.

Reconstruction of paleostorm information such as storm frequency and/or intensity has been conducted using overwash deposits in the coastal regions of western North Atlantic (Boldt et al., 2010; Donnelly et al., 2015; Hippensteel, 2011; Hippensteel and Garcia, 2014; Kiage et al., 2011; Scileppi and Donnelly, 2007), Gulf of Mexico (Aharon and Lambert, 2009; Bregy et al., 2018; Das et al., 2013; Ercolani et al., 2015; Lambert et al., 2008; Lane et al., 2011; Liu and Fearn, 1993, 2000; Rodysill et al., 2020), Caribbean Sea (Donnelly and Woodruff, 2007; McCloskey and Keller, 2009; McCloskey and Liu, 2012, 2013; Peros et al., 2015), North Europe (Orme et al., 2015; Sorrel et al., 2009, 2012), Mediterranean Sea (Degeai et al., 2015; Dezileau et al., 2011, 2016; Kohila et al., 2021; Raji et al., 2015; Sabatier et al., 2012), western North Pacific (Kongsen et al., 2021a, 2021b; Williams et al., 2016; Woodruff et al., 2009, 2015), Central Pacific (Toomey et al., 2013), eastern North Pacific (Bianchette et al., 2022; Hemphill-Haley et al., 2019), and South Indian Ocean (May et al., 2015a).

The intensity of a storm event determines the magnitude of storm surge and waves it produces (Lin et al., 2010). Roughly speaking, the extent and thickness of the resulting overwash deposit can be expected to be correlated with the intensity of the storm, assuming that storm track is direct to the study site and other parameters remaining constant. A pioneering study by Liu and Fearn (1993) found that category 3 Hurricane Frederic (1979) did not supply overwash sediment across the barrier, whereas category 4 or higher TCs did so at Lake Shelby, US. Liu and Fearn (1993) inferred that only category 4–5 hurricanes were capable of forming the sandy overwash layers on the floor of Lake Shelby, given that the geomorphologic setting has not altered significantly over the past 5000 years. Using a similar modern analogue approach, Liu and Fearn (2000) reconstructed the history of hurricanes above category 4 that struck Western Lake in the US over the past 3200 years. Boldt et al. (2010) reported a 2000-year record of overwash events in the backbarrier saltmarsh of southeastern New England. They found a good agreement between the timing of storms that caused storm

surge comparable to barrier height and the ages of overwash deposits, based on the historical tide gauge records and storm surge modeling.

Hippensteel and Martin (1999) and Collins et al. (1999) utilized microfossil records to identify overwash deposits, which were not detectable from lithology alone. Scott et al. (2003) reconstructed the storm activity on the South Carolina coast dating back to 5700 years BP based on the overwash layers characterized by the peak abundance of calcareous offshore foraminifera.

Dezileau et al. (2011) identified records of storm overwash in sediments from a lagoon on the French Mediterranean coast, spanning a period of 15,000 years, through the use of grain size distribution and geochemical methods. Subsequently, Sabatier et al. (2012) conducted additional grain and geochemical analyses, as well as faunal, mineral, and dating, on the same site. This resulted in the identification of seven distinct episodes of heightened storm activity over the last 7000 years (Sabatier et al., 2012).

There are interesting coincidences between the historical and geological records of storms in East Asia. Legend states that the Mongol Empire, one of the world's largest armadas of its time, twice attempted to invade Japan in the 13th century, but both times, the Japanese defenses were saved when the Mongol fleet was destroyed by storms referred to as *Kamikaze* (meaning "divine winds" in Japanese; Uda, 2003). Woodruff et al. (2015, 2009) described overwash sediment records characterized by grain size peaks and heavy mineral enrichment from sediment cores of two coastal lakes in southwestern Japan near the location of the Mongol invasions. These sedimentary reconstruction of the overwash events indicate that there were periods of greater flood activity relative to modern times in this region, supporting the historical lore.

2.1.3. Challenges

Overwash deposits are commonly used for paleostorm reconstruction, however, several issues must be considered. One issue is the selection of coring locations. Overwash deposit can extend heterogeneously across the backbarrier (Fig. 3a). In general, it is thickest on the seaward side of the washover fan and thinnest on the inland edge of the fan. Liu (2004) pointed out that the presence and thickness of the overwash layer in cores taken from coastal lakes depends on the position of the coring relative to the overwash fan. Therefore, it is important to sample and correlate multiple cores to reconstruct the complete storm history of the region.

Second, the geomorphological setting must be considered as changes in barrier height can affect the sensitivity of the lake/marsh/pond in the backbarrier to storms. Also, if the current freshwater lake was once a saltwater lake or brackish lake, sedimentological features and paleontological records formed by overwash may differ from the present. Thus, it is recommended to reconstruct the paleoenvironment and ensure that the geomorphological setting is preserved.

Third, the estimation of storm magnitude using overwash deposits is limited. Several studies have attempted to estimate storm intensity or overwash magnitude based on grain size distributions (Toomey et al., 2013; Woodruff et al., 2008b). It is likely that, assuming other parameters such as storm tracks and sediment source conditions are the same, larger storms would transport larger grained sediments to the backbarrier. However, extreme water level rises associated with storms depends not only on the storm intensity, but also on meteorological and geomorphological factors, and the relative positions of the storm and the site. Caution should be exercised when directly estimating event intensity from sediment records. Numerical computation of storm surge and sediment transport is useful to constrain the storm condition satisfying the distribution of overwash deposits (Brandon et al., 2014).

The identifiable temporal intervals of storm events differ from site to site. If the interval between two or more storms is short, overwash layers formed by both events may be difficult to distinguish unless enough fine-grained sediments have been deposited inter-event. Especially in coastal lowlands and marshes, the sedimentation rate is slow relative to storm event frequency and the upper part of deposit may be eroded by the overwash process. Coastal lakes are suitable for identification of overwash layers because of their high sedimentation rate and relatively low erosion.

Finally, the uncertainty in dating techniques makes it difficult to estimate the absolute age of storm events. The high frequency of storm events compared to tsunami events caused by earthquakes and landslides makes it more difficult to determine their ages. Therefore, it is common to estimate the frequency of events over a period of centuries to millennia.

2.2. Coastal karst basin

2.2.1. Characteristics of coastal karst basins

Coastal karsts are basin-like landforms formed by dissolution and alteration on a Quaternary scale and buried below sea level in carbonate landforms (Mylroie et al., 1995). They come in forms such as sinkholes, blue holes, and submarine caves (Fig. 2). Among coastal karst basins, blue holes located in shallow waters are, in particular, favored for paleostorm reconstruction (Fig. 3b).

Blue holes are open, basin-like underground cavity filled with tidal-influenced freshwater, seawater, or mixed water formed on a carbonate platform (Mylroie et al., 1995; Fig. 3b). These holes open directly into the present marine environment and contain ocean water, usually accompanied by tidal currents. In contrast, inland sinkholes, separated from oceanic conditions by the present topography, open to the ground surface or to ponds and lakes and contain waters of varying chemical composition from freshwaters to seawaters. The formation of blue holes reflects the consequences of many sea level changes, as Quaternary sea level oscillations cause the freshwater lens and its mixing zone passes up and down many times through hole-bearing rocks (Mylroie et al., 1995). Limestone platforms dissolve internally to form caves, and cave ceilings eventually collapse (Mylroie et al., 1995). After formation, blue holes that open to the outside become natural sediment traps, recording paleoenvironmental proxies.

Blue holes are generally protected by walls made of limestone, and are low-energy environments that are less affected by ocean currents, waves, and bioerosion. Thus, during normal quiescence, fine particles settle and deposit on the karst floor (Gischler et al., 2008). Fine-grained sediments consist mainly of carbonate clastic produced in lagoons and reefs. Fine-grained sediments often have laminar structures that are thought to be formed by seasonal fluctuations in organic matter production and may be regarded as varve (Denommee et al., 2015). Deep enough holes are free from bioturbation due to the anoxic environment at the bottom. Inland sinkholes tend to be composed of mud-silt, dominated by organic sediments such as trees and leaves (van Hengstum et al., 2016).

Field surveys include coring, seismic surveys, bathymetric surveys, temperature and salinity profile measurements. Cores are analyzed for grain size, X-ray CT scan, trace element composition, organic matter content, and isotope composition. Isotopic records from normal sediment provide paleoclimate proxies (Gischler et al., 2008), paleoenvironmental reconstructions (van Hengstum et al., 2020), and hydroclimatic reconstructions related to summer precipitation (Sullivan et al., 2021).

2.2.2. Principles behind the use of coastal karst as storm proxy

Over the past two decades, an increasing number of studies have used sediments within coastal karst basins to reconstruct storm history (Bramante et al., 2020; Brandon et al., 2013; Brown et al., 2014; Denommee et al., 2015; Gischler et al., 2008; Lane et al., 2011; Rodysill et al., 2020; Schmitt et al., 2020; van Hengstum et al., 2016; Wallace et al., 2019, 2021a, 2021b, 2021c; Winkler et al., 2020, 2022). When a storm passes around a carbonate platform, a significant bottom shear stress is generated by the storm waves, leading to the supply of sediment to the blue hole, either through the transport of reef or lagoon sediment,

or through the collapse of the hole's rim. Storm waves form relatively coarse-grained sedimentary layers, which can be distinguished from the fine-grained sediments that accumulate during quiescent conditions. Similarly, when a storm passes around an inland sinkhole, large sediments from the reef and coast may be supplied to the hole by overtopping waves or falling into the hole from the surrounding area.

Sediments within coastal karst basins can also be used for chronostratigraphy, similar to inland overwash deposits. Paleostorm frequency is reconstructed by identifying event layers and creating chronostratigraphy. The holes are topographically protected and the water depth is deep, resulting in little physical and biological erosion. Due to these factors, the sediments are highly preservable. Additionally, it is possible to detect relatively weaker events than those captured by inland overwash deposits because of the likelihood of sediment supply by storms.

Gischler et al. (2008) collected sediment cores at the bottom of the blue hole at Lighthouse Reef, Belize. The core consists of undisturbed annually-laminated mud and silt layers and interrupted coarse-grained storm event bed. Schmitt et al. (2020) also surveyed the lighthouse Reef and reconstructed the annually-resolved record of TCs for 1885 years.

In Bahamas, lots of surveys for paleostorm reconstruction have been conducted at blue holes of Abaco (van Hengstum et al., 2014; Winkler et al., 2020), South Andros (Wallace et al., 2019; Winkler et al., 2020), Cay Sal Bank (Winkler et al., 2022), Long Island (Wallace et al., 2021c), and Middle Caicos (Wallace et al., 2021a). Wallace et al. (2019) interpreted that in the blue hole deposits near the inland, foliage originating from mangrove forests is supplied into the blue hole during storms. A compilation of Bahamas records suggested that TC activity in Bahamas synchronously fluctuated on a centennial time scale (Winkler et al., 2022).

Bramante et al. (2020) reconstructed a 3000-year record of cyclone activity from blue hole sediments in Jaluit Atoll, Marshall Islands. Their results indicate the variability of cyclogenesis in the low latitudes of the North Pacific (Bramante et al., 2020).

2.2.3. Challenges

Grain size analysis serves as the primary method for identifying storm beds in coastal karst basins. Determining the threshold of grain size for identification of storm event deposit poses a challenge. In many cases, both non-event and event deposits comprise carbonate clastic, complicating identification. While differences in texture, colour, and the presence or absence of lamina may exist, grain size is typically the most commonly used method for certification. It is important to note that normal low-energy sediment may be affected by reef productivity, sea level, and climatic conditions, so it is crucial to select a site with high degree of accuracy in certification.

Constraining the magnitude of past storm events that make each event beds presents challenges. Blue holes, facing the open ocean, readily admit storm waves entering. Generally, blue holes and sinkholes exhibit a lower threshold for the magnitude of storm events forming event beds compared to inland backbarrier settings (Denommee et al., 2015; Schmitt et al., 2020). Consequently, determining the magnitude of the events forming each event layer is more challenging.

2.3. Coastal boulder deposit

2.3.1. Characteristics of coastal boulder deposit

Coastal boulder deposits are coarse-grained clastics distributed individually or in groups on coastal areas such as rocky coast, reef flat, cliff top, sandy beach, and coastal terraces (Fig. 2, 3c). The dimensions of boulders are measured from field survey and aerial photographs. In general, boulders with a long axis length of 1 m or more are often studied, although pebbles and cobbles with a diameter of several tens of centimeters are also studied (Lau and Autret, 2020). This section mainly refers to boulders of 1 m or more. Because coastal boulder deposits are formed by high-energy waves such as storm waves and tsunamis, these deposits and their sedimentary features provide adequate evidence of past extreme wave events (Cox et al., 2018; Goto et al., 2010a).

Coastal boulder deposits are typically produced when upper coastal and submarine bedrocks or biochemical sedimentary rocks (e.g., coral) are detached during high-energy wave events. Boulder fields formed on reef flats and unobstructed flat platforms tend to be dispersive (Goto et al., 2010b). Boulders on reef flats are found in tropical and subtropical regions such as the western North Pacific, South Pacific, and the Caribbean (Goto et al., 2009; Morton et al., 2006; Terry and Lau, 2018). The energy of storm waves attenuates as they break on the reef, resulting in boulders concentrated only with in the limited distance (~300 m), and the boulders' distribution exhibits an inland fining trend (Goto et al., 2009; Lau et al., 2016). The long axes of boulders tend to be oriented perpendicular to the flow direction (May et al., 2015b). Waves amplified by refraction, reflection, and local topography cause high run-up and carry boulders onto clifftops (Autret et al., 2016; Fichaut and Suanez, 2011). Boulder ridges formed by overlapping boulders are commonly found on rocky coasts (Etienne and Paris, 2010; Paris et al., 2011). Boulder ridges are frequent on the storm-prone, open-sea coasts of Western Europe (Autret et al., 2018; Cox et al., 2012), but they are also observed on less energetic coasts around the Mediterranean Sea (Causon Deguara and Gauci, 2017). The direction of imbrication typically indicates the flow direction (Cox et al., 2019; Erdmann et al., 2018). The distribution of boulders is determined by wave climate, geomorphological setting, and the availability as a sediment source, including lithology and fragility of basement.

Coastal boulder deposits are valuable geological evidences of coastal hazard events for the following reasons: (1) their preservation even in a high-energy environment over time, (2) their mass which requires large wave forces to move them, and (3) the relative simplicity of describing their transportation compared to that of sandy or muddy sediments.

2.3.2. Principle behind the use of coastal boulder deposit as storm proxy

Coastal boulder deposits serve as a record of the magnitude and timing of past storm events. Physical equations for boulder transportation are utilized to estimate the magnitude of wave conditions, such as flow speed, wave height, wave period and wave force. Nott (1997, 2003) proposed a hydrodynamic model for estimating the wave height required for the initial movement of boulders, demonstrating the feasibility of inferring hydrodynamic conditions from measurable data of boulders. However, subsequent studies have identified limitations in these models, such as assumptions of the unique value of Froude number and equivalent treatment of onshore flow height and offshore wave height in the equation (Cox et al., 2020; Watanabe et al., 2020). On the other hand, Nandasena et al. (2011, 2013) proposed a model for estimating the minimum flow velocity required for boulder transport via sliding, rolling, and lifting under more reasonable assumptions. Through comparisons of these inverse models and wave simulation results, not only the onshore wave conditions but also the incident offshore wave conditions can be estimated. Rovere et al. (2017) estimated incident wave conditions for transportation of clifftop boulders in Elauthera, Bahamas by comparing the estimated current velocity from the inverse model with wave run-up calculation results. Watanabe et al. (2019) developed a model accounting for vertical hydrodynamic forces and demonstrated that the clifftop boulders in Hachijojima Island, Japan were formed by storm waves rather than tsunamis.

Another approach is to compute the forward model for wave and boulder movement simultaneously. This approach calculates how much the boulders move under arbitrary conditions, making it possible to constrain the incident wave conditions that explain the actual distribution of boulders (Minamidate et al., 2020, 2022). In general, forward boulder transport models (Imamura et al., 2008; Nandasena and Tanaka, 2013; Noji et al., 1993) solve motion equations based on Morison's equation (O'Brien and Morison, 1952). The movement of boulders is determined by the action of fluid force, bottom friction force, gravity

force, and lift force. Minamidate et al. (2020) performed numerical simulations of storm surges, waves, and boulder transport under the constraint of explaining the distribution of the boulders in Kudaka Island, Japan, and determined the maximum intensity of typhoons and associated storm waves that hit the island over the past 3500 years.

Boulder components and biological remains are dated to determine when the boulder was dislodged from water onto land or when the wave events were active (Cox et al., 2012; Hansom and Hall, 2009; Kench et al., 2018; Lau et al., 2016; Tao et al., 2021; Terry et al., 2016b; Terry and Etienne, 2014; Yu et al., 2004; Zhao et al., 2009; Zhou et al., 2021). Coral boulders have a special advantage that they can be directly dated by radiocarbon dating or uranium series dating. By measuring the ages of coral boulders in Thailand, Terry et al. (2018) identified four separated periods of high storm activity, 600–700 CE, 900–1000 CE, 1150–1250 CE, and 1400–1650 CE, and clarified that areas around Bangkok Bay have potential typhoon risks.

2.3.3. Challenges

The research field of coastal boulder deposits is still developing and met with several challenges. Firstly, it should be noted that the inverse model using dimensions of boulders indicates the minimum flow velocity required to transport boulders but not necessarily the actual flow velocity. The dimensions and sizes of boulders depend not only on the magnitude of the wave event, but also on the local topographic setting, including the existence and orientation of faults, joints and cracks, and reef microtopography. Basically, the inverse model yields a larger estimated flow velocity for larger boulders. If topographical factors limit the size of the supplied boulders, the resulting velocity will also be limited. Conversely, if a given event were to supply the largest class of transportable boulders, the lower bound on the estimated minimum flow velocity would be maximized. Therefore, large or difficult-to-move boulders are suitable for the inverse model. In contrast, using the spatial distribution as a constraint in addition to the boulder dimension compensates for these shortcomings, and allows us to estimate the wave magnitude that forms the boulder distribution (Minamidate et al., 2020).

Secondly, there is a concern that the spatial distribution of the boulders may change due to subsequent events after the distribution has been formed once. For example, in the Ryukyu Islands, Japan, a region where TCs frequently pass through, storm-derived boulders are distributed throughout the archipelago. However, on Ishigaki Island, the large tsunami of 1771 swept away the boulders on the reef crest, thus it can be interpreted that the boulders observed on the reef crest today were supplied by the storm waves over the next 250 years (Goto et al., 2010b). It is necessary to consider the possibility that the boulders have moved multiple times to estimate the wave and storm conditions that carried them to their present locations.

Finally, there is the problem that age estimation is limited by multiple factors. The accuracy of dating is limited by post-depositional preservation due to weathering and abrasion, growth rate of coral, difficulty in sampling the youngest parts, and the presence or absence of marine organisms. In general, organic materials such as plant fragments and pollen, which are generally used for sandy sediments, cannot be used for boulders. For these reasons, it may be hard to estimate the age with high precision and accuracy compared to sandy sediments based on stratigraphy. In addition, when the number of boulders that are dated is limited, there is a possibility that past events cannot be detected. A statistically sufficient amount of age data would be necessary to detect the age of the event and the period when the event was active.

2.4. Beach ridge

2.4.1. Characteristics of beach ridge

Beach ridges are prograding sedimentary systems consisting of alternating ridges and flat planes parallel to the coastline (Fig. 3d). They are primarily composed of sand, gravel, or a mixture of them. The formation mechanism of beach ridges is controlled by allogenic and/or autogenic processes. Allogenic process includes changes in meteorological and oceanographic conditions such as storm activity (Tamura et al., 2018), tectonic activity (Monecke et al., 2015), and eustatic- and isostatic-induced sea level change (Brooke et al., 2019). Autogenic process includes local change in sediment budget (Hein et al., 2016), topography, and vegetation (Moore et al., 2016). The attribution of each formative factor depends on local and/or regional regimes (Short, 2006; Tamura, 2012).

The formation of beach ridges is a result of coastal plain progradation, although the specific mechanisms of formation are still being debated. The formation of prograding beach ridge involves two phases: the initial advance of the beach berm, followed by the growth of the ridge both vertically and horizontally through sediment supply from normal and storm waves (Tamura, 2012). New ridges form on the seaward side of past ridges. Each ridge can be distinguished by its sedimentary profile. Additionally, aeolian processes may also contribute to the formation of the ridge top through processes such as ridge crest concentration, erosion, and ridge growth around vegetation (Tamura, 2012; Tamura et al., 2018). Techniques such as Ground Penetrating Rader (GPR), drilling, and Optically Stimulated Luminescence (OSL) dating are commonly used to study the underground structures, age, and sedimentary processes of beach ridges.

2.4.2. Principles behind the use of beach ridge as storm proxy

Beach ridges on wave-dominated or wave-influenced coasts may potentially retain information on past storms, as storm waves play one of the significant roles in the formation and erosion of beach ridges (Bendixen et al., 2013; Clemmensen et al., 2009; Fairbridge and Hillaire-Marcel, 1977; Forsyth et al., 2010, 2012; Goslin and Clemmensen, 2017; Lindhorst and Schutter, 2014; Nott et al., 2009; Nott, 2011; Nott et al., 2013; Nott and Hayne, 2001; Scheffers et al., 2012; Tamura et al., 2018, 2019).

Some researchers have reported beach ridges along the northeastern and western coasts of Australia, interpreting them as being formed by waves associated with TCs (Forsyth et al., 2010, 2012; Nott, 2011; Nott et al., 2009; Nott and Forsyth, 2012; Nott and Hayne, 2001). Each ridge forms 10 to 30 rows on the coastal plain. A marine inundation event higher than the ridge height is required to add sediment along the ridge elevation. Therefore, Nott and his coauthors propose that the final sedimentary layer on top of each ridge records the maximum flooding event that deposited the ridge. Nott et al. (2009) showed that 29 ridges with heights of 3.5–5.5 m in Queensland, Australia were formed by storms of category 4 or higher using storm surge simulation. This method is based on the hypothesis that the magnitude of storm events can be estimated from the height of each ridge, and the event interval can be estimated from the age difference of the ridges.

Clemmensen et al. reconstructed the relative ridge height at the time of its formation by subtracting sea level changes from the current ridge profile (Clemmensen et al., 2012, 2016; Goslin and Clemmensen, 2017). The beach ridges along the coast of Anholt, Denmark have been formed in the last 7000 years, with one ridge forming in about 15 years (Clemmensen et al., 2012). They mapped the downlap points corresponding to the sea level at the time of ridge formation and estimated the relative height of the ridge. They concluded that the storm intensity was high during the period between 4000 and 3500 years ago when the beach ridge developed significantly (Goslin and Clemmensen, 2017).

2.4.3. Challenges

Despite the significant interest in beach ridges as indicators of paleostorm activity, a robust method for estimating paleostorm activity from them has yet to be established. Tamura et al. (2018) reevaluated the usefulness of ridges as paleostorm indicators, focusing on coarse-grained beach ridges in Queensland, which had been previously used to reconstruct paleostorm activity. The previously surveyed older inland ridges do not exhibit separate sedimentary layers, but instead show

massive structures (Forsyth et al., 2010; Tamura et al., 2018). Tamura et al. (2018) suggested that the temporarily formed sedimentary structure may have been erased by bioturbation, thereby limiting our ability to identify the number of cyclones that have formed a ridge. Additionally, variation in the thickness of the storm deposit makes it more difficult to estimate realistically the thickness of sediment layer delivered by a single event (Nott et al., 2013).

To model ridge construction over longer periods, it is important to determine the amount of time required for a single ridge to form. In general, storm waves cause substantial topographical changes through erosion (Masselink and van Heteren, 2014). Most of the investigated coarse-grained ridges contain truncation surfaces in trench profiles and GPR phases (Bristow and Pucillo, 2006; Tamura et al., 2018). There are also gaps of several hundred years between the ridges (Tamura et al., 2018). It is unclear whether this reflects a period of non-ridge formation or is caused by significant erosion. In the latter case, it is inappropriate to assume the apparent mean interval of ridge formation.

The validity of using coarse-grained ridge elevation as an index of storm surge run-up and storm magnitude has not yet been robustly tested. Without an accurate reference sea-level curve, it is impossible to quantify the run-up level above mean sea level. The presence of astronomical tides with ranges of several meters and spatial variations in the maximum surge rise level produced by a single cyclone introduce uncertainty into estimates of past cyclone magnitude based on ridge elevations (Tamura et al., 2018). Therefore, Tamura et al. (2018) concluded that coarse-grained ridges do not provide a reliable record of past storm inundation. On a gravel beach, aeolian ridge remobilization is unlikely to have occurred, but erosion effects and difficulty in recognizing separate storm layers remain significant issues.

It is important to determine whether a ridge was formed by a single storm event or multiple storm events. Bendixen et al. (2013) found that the formation of the beach ridges along the Baltic coast was only observed in about 20% of all storms passing the study area, indicating that not all extreme events form ridges. If a ridge is formed by a single event, the chronological difference between ridges probably correspond to the storm interval. However, if a ridge is formed by multiple events, the age difference of inter-ridges does not indicate the storm interval and the height of the ridge may characterize the event that formed the top unit. When the speed of coastal progradation is high, forming the topmost unit may represent the largest event in a period of time. Therefore, the information gleaned from the ridge differs depending on whether it was formed by one event or multiple events.

It should be noted that storms act not only as formation factors, but also as erosion factors (Scheffers et al., 2012). Wave-built ridges are also known to be later modified by aeolian forces and covered with aeolian sand (Bendixen et al., 2013; Tamura, 2012). Additionally, modification by vegetation and accumulation of sand due to increased ground density cannot be ignored (Tamura et al., 2018). Clemmensen et al. (2016) have suggested that well-preserved gravel beach ridges may provide a better record. The beach ridges in Vesterlying beach, Denmark, which are considered to be relatively well preserved. However, they are not formed only by gravel, but are mixed sand and gravel ridges, with vegetation growing on the surface, which make paleostorm reconstruction difficult.

Lastly, it is unclear whether the height of a beach ridge can be quantitatively regarded as the magnitude of a specific storm event. This is because pre-event ridge height, beach width and slope can affect post-event height (Stockdon et al., 2006). Even for events of the same magnitude, the higher the original ridge, the higher the run-up height. Furthermore, since the run-up distance varies depending on the slope and width of the beach, it is expected that the narrower the beach, the higher the run-up height. Therefore, the final ridge height that can be observed today is the result of a combination of storm magnitude and other factors.

2.5. Chemically and biologically formed laminae as tree rings, speleothem, and corals

2.5.1. Characteristics of chemically and biologically formed laminae

In this section, the use of tree rings, speleothem, and corals as layered records of paleostorms is described. Tree rings (Bregy et al., 2018, 2022; Collins-Key and Altman, 2021; Cook et al., 2013; Knapp et al., 2021; Knapp and Hadley, 2012), stalagmites (Baldini et al., 2015; Denniston et al., 2015; Frappier et al., 2007; Zhang et al., 2008), and corals (Chen et al., 2018; Cobb et al., 2003; Greer and Swart, 2006; Kilbourne et al., 2011; Nyberg et al., 2007) are well-established paleoclimatic and paleoenvironmental proxies with high temporal resolution (annual to intra-annual), and have also been used as paleostorm proxies.

The tree profiles in many temperate forests display alternating bright (earlywood) and darker (latewood) bands that are continuous around the tree (Bradley, 2014; Fig. 3e). A single set of earlywood and latewood corresponds to one year of tree growth, and is called a tree ring. The average width of tree rings is a function of several variables, including tree species and age, storage in trees, soil nutrients, and climatic factors such as solar radiation, precipitation, temperature, wind speed, and humidity (Vaganov et al., 2011). Climatic information can be obtained from annual changes in tree-ring width, tree-ring density, and isotope ratios. In the tropics, most trees do not form annual rings because seasonal temperature changes are small. However, in many tropical forests, there are strong seasonal variations in rainfall and evaporation, which affect annual variability in tree growth and oxygen isotope composition. Therefore, it has been confirmed that annual growth can be identified and measured even in the absence of tree rings (Poussait et al., 2006).

Stalagmites are one of the speleothems that rise from the floor of limestone caves due to dripping water (Fig. 3f). The formation process of stalagmites, along with other speleothems, is the reprecipitation of limestone that constitutes caves (Fairchild et al., 2006; Fairchild and Baker, 2012). The water in the stalagmite cave originates from precipitation in the limestone area. In caves, calcite is precipitated by CO_2 outgassing and evaporation (Fairchild and Baker, 2012). Isotopic equilibrium is maintained when sedimentation occurs by gentle degassing, and isotopic values of groundwater are recorded (White, 2007). If rapid outgassing and/or evaporation occurs, the precipitation reaction is too rapid to maintain isotopic equilibrium (White, 2007). The growth rate of stalagmites is controlled by the chemical conditions of water and the drip rate. The partial pressure of carbon dioxide in the cave atmosphere varies significantly seasonally, reflecting the chemical conditions of dripping water and the precipitation rate. Changes in the seasonal growth rate of stalagmites results in the formation of bands (Tan et al., 2003). Annual bands can also be formed that reflect the organic acid content of soil origin (Tan et al., 2003). Stalagmites can record climatic information such as temperature and precipitation by capturing oxygen isotope signals in seasonally deposited calcite layers (Fairchild and Baker, 2012). In addition to isotopes, trace elements, optical characteristics (luminescence), and layer thicknesses are also used (Fairchild and Baker, 2012).

Corals, which form calcium carbonate skeletons, also used for paleoclimate reconstruction (Bradley, 2014; Fig. 3g). Reef-building massive corals (*Porites* and *Mondastaea*) are commonly used in paleoclimate studies (Gagan et al., 2000). *Porites* grow concentrically and spherically, and annual rings are formed by seasonal changes in the skeletal density of precipitates. The annual growth rate is about 1–2 cm, and colonies reaching several meters may record environmental information for the past several hundred years. Analysis with high temporal resolution is possible because they precipitate a dense skeleton. Samples for analysis are cut from coral slabs or cores at regular intervals along the growth axis or specific skeleton. For example, sub-sampling a 1-cm-wide annual ring with a resolution of 1 mm can provide a monthly environmental record. The oxygen isotope ratio ($\delta^{18}O_c$) in coral skeletons is determined by the surrounding seawater temperature and the oxygen isotope ratio ($\delta^{18}O_w$) of sea water at the time of skeleton precipitation (Grottoli and

Eakin, 2007). $\delta^{18}O_w$ is controlled by mixing, evaporation and precipitation of seawater, so it roughly corresponds to salinity. Since isotopically lighter water tends to evaporate, increasing evaporation increase $\delta^{18}O_w$. On the other hand, since the oxygen isotope ratio of precipitation is lighter than that of seawater, the decrease in salinity due to precipitation works to reduce $\delta^{18}O_w$. Therefore, $\delta^{18}O_c$ reflect seawater temperature and salinity (precipitation and evaporation) (Grottoli and Eakin, 2007). In addition, the growth rate, trace metal elements (Sr, Mg, Ba) incorporated by substituting Ca in calcium carbonate, and optical characteristics (luminescence) are also used as indicator of seawater temperature, salinity, and flooding events (Bradley, 2014).

2.5.2. Principle behind the use of chemically and biologically formed laminae as storm proxy

Rain fall during TCs is known to have significantly lower oxygen and hydrogen isotope ratios than other weak rains due to strong isotope fractionation (Lawrence and Gedzelman, 1996; Munksgaard et al., 2015; Sánchez-Murillo et al., 2019). By detecting such changes in isotope signals from tree rings, stalagmites, and corals, it may be possible to identify past precipitation events associated with storms.

For isotope analysis of tree rings, the monocomponent alpha-cellulose is extracted to avoid chemical heterogeneity problems (Bradley, 2014). Oxygen isotope ratios of cellulose contained in the tree rings reflect summer rainfall (directly, summer relative humidity, and rainfall isotope ratio). Miller et al. (2006) provided a 220-year oxygen isotope record for alpha-cellulose in longleaf pine in the southeastern United States, whose variability coincided with the passage of historical TCs in the 19th and 20th centuries. Their results suggested that the oxygen isotope record of tree rings can serve as proxies for TC frequencies over centuries.

Some studies have indicated that the growth of trees is affected by temporary changes in rainfall associated with TCs, and their accompanying groundwater fluctuations, seawater inundation, and peak wind speeds. Harley et al. (2011) constructed a dendrochronology between 1871 CE and 2009 CE using a total of 23 slash pine in South Florida, and found that changes in growth rate correlated with events such as hurricanes and wildfires. Trouet et al. (2016) combined a chronology of tree growth suppression with a Caribbean shipwreck record. They hypothesized that storm related seawater inundation inhibited tree growth, and estimated that the frequency of TC passage decreased by 75% during the Maunder Minimum in around the 17th century. In order to detect changes in TCs from tree rings, comparison with other meteorological factors that may affect tree growth is important. In the Oregon coast, Knapp and Hadley (2012) showed that variations in tree growth over 350 years were weakly related to temperature, precipitation, and drought, but strongly correlated to peak wind speed of storms. Knapp et al. (2021) also reconstructed the variability of TC precipitation from 1750 to 2015 using longleaf pine in North Carolina. Collins-Key and Altman (2021) examined whether tree ring width of longleaf pine from Georgia, US shows past TC activity, and concluded that the signals of TC activity could not be significantly detected from the original chronology data of tree ring width because they were strongly influenced by other climatic factors. They, however, suggested that the TC signal could be detected by removing other external factors from the raw data.

Oxygen isotope ratios in stalagmites can serve as proxy for recording short-term climatic events (meteorological events) if the water residence time is sufficiently short. Consequently, it is possible to reconstruct past precipitation events by sampling at a high enough resolution compared to the growth rate of the stalagmite. For instance, Frappier et al. (2007) presented a 23-year oxygen isotope record of stalagmites from caves in Belize, showing negative $\delta^{18}O$ peaks corresponding to TC rainfall events. Baldini et al. (2016) also used the Belize stalagmite and successfully reconstructed 450 years of western Caribbean TC activity from oxygen and carbon isotope record. Haig et al. (2014) proposed a TC activity index based on stalagmite oxygen isotope ratios for Australia, suggesting that the current storm activity on the mid-west and northeast coasts of Australia is unprecedently lower over the past 550 and 1500 years, respectively. Medina-Elizalde et al. (2016a, 2016b) constructed an about 1400-year oxygen isotope record from the Yucatan Peninsula stalagmite in Mexico, and proposed a hypothesis that the frequency of TCs influenced the collapse of the Classical Maya civilization.

Corals may also record isotope ratio changes associated with heavy precipitation events and runoff events from continents. Runoff events have been reported to be recorded as fluorescent bands in corals (Grove et al., 2010; Isdale et al., 1998). These bands are produced by incorporating land-derived fulvic acid into coral structures. Nyberg et al. (2007) used coral luminescence as an index of hurricane frequency over a 270-year period, showing a steady decline in hurricane frequency in the northern Caribbean from 1750 to 1995 CE. Lough (2007, 2011) also used coral luminescence in northeastern Australia to reconstruct the history of runoff events. Considering the runoff to the coastal area of the Great Barrier Reef is mainly derived from summer rainfall due to TCs, they calibrated the luminescent signals to TC-related rainfall from 1685 CE. Hetzinger et al. (2008) reconstructed about 80 years of SST and precipitation variability from coral $\delta^{18}O$ records in the southeastern Caribbean Sea, and showed that corals reflected the variability of Atlantic decadal oscillations and TC activity.

2.5.3. Challenges

The three types of lamina records discussed in this section are considered indirect indicators of storms, and there are several issues to consider when using them as proxies for paleostorm events. Firstly, it is important to verify that the obtained records, such as isotope records, growth pattern, and runoff indices, are actually indicative of heavy precipitation events. As with any paleoclimate reconstruction, it is necessary to ensure that the climate index of interest can be distinguished from other sources of noise (Bradley, 2014). Lewis et al. (2011) have noted the presence of undetected and false positives in tree rings. Additionally, Yang et al. (2021) have stated that while precipitation events certainly provide rainwater with low $\delta^{18}O$, the isotopic changes in cave water are minimal and difficult to detect. Therefore, it is essential to understand which proxies, species, and sites are available and their respective sensitivities (Frappier, 2008; Lases-Hernández et al., 2020).

Secondly, even if proxies are indicators of precipitation, it is not always easy to determine whether they are specifically detecting TC or other precipitation events such as summer or winter monsoons. Kilbourne et al. (2011) verified the sensitivity of $\delta^{18}O$ in coral skeletons in Puerto Rico as a proxy for past TCs and found that TC-related precipitation cannot be distinguished from other precipitation events. It may be possible to consider that the variability in a proxy is mainly caused by TC if the record is from where summer-time precipitation is predominantly induced by TCs (Lough, 2007).

Thirdly, these proxies assume that the same climatic factors influence lamina formation in the same way over the past and present. The fact that a proxy is consistent with the observed record is a necessary but not sufficient for it to be used as a proxy for past storms. To make paleostorm reconstruction more robust, it is important to compare and verify records from multiple sources, not just from a single record (Black et al., 2019).

2.6. Common challenges of the origin of event deposits: Storm or Tsunami?

Distinguishing whether wave-induced event deposits originate from a storm or a tsunami is one of the largest challenges in storm deposit identification. Both storm deposits and tsunami deposits contain marine detritus transported by waves and currents, and often exhibit similar sedimentary characteristics and patterns. Despite considerable research aimed at characterizing both storm and tsunami deposits (Morton et al., 2007; Nanayama et al., 2000; Switzer and Jones, 2008), there is no universally applicable method to distinguish between them.

Sedimentary patterns can serve as valuable indicators for identifying storm deposits, considering geomorphological, climatological, and tectonic settings, hydrodynamic processes, and local sedimentary environments. Landward washover fans are typical features of storm deposits, whereas they are rarely formed by tsunami (Morton et al., 2007). Rip-up crusts are less frequently observed in storm deposits compared to tsunami deposits, attributed to the weaker bottom shear stress during onshore flow of storm surge (Kortekaas and Dawson, 2007).

Tsunami and storm waves have different characteristics, leading to disparate patterns in boulder distributions. In general, tsunamis are characterized by one or two waves with long wavelengths (long wave period). Storm waves manifest as groups of hundreds of waves, each possessing shorter wavelength (short wave period). Boulders originating from the tsunami tend to exhibit long distribution distances, often spanning on the order of 10^3 m (Goto et al., 2007, 2010b). These tsunami boulders are typically sparse and lack pronounced sorting (Paris et al., 2009). In contrast, boulders resulting from storm waves display shorter distribution distances, typically on the order of 10^2 m, and exhibit a landward fining trend due to the wave attenuation as they interact with the reef (Goto et al., 2009; Lau et al., 2016).

Characteristics of sediment composition may be useful in identifying the sediment sources. Storm deposits typically exhibit better sorting compared to tsunami deposits, as storm waves generally scour only limited coastal sources; however, tsunami deposits originate from diverse material sources from the outer shelf to inland. Due to the long wavelength of tsunamis, they have the potential to transport molluscs from greater depths and distances. Nanayama et al. (2000) and Kortekaas and Dawson (2007) reported that tsunami deposits, such as those from the 1993 Hokkaido-nansei-oki and the 1775 Lisbon events, contained more abundant shells than storm deposits from the same sites. Recently, sedimentary DNA analysis has also been attempted to differentiate between tsunami and storm deposits (Yap et al., 2021).

Numerical simulations of storm surges, tsunamis, and associated sediment transport are invaluable for understanding sedimentary mechanisms and distinguishing between storm and tsunami deposits. When simulating storm surge, various parameters such as storm intensity, path, and size are considered (Minamidate et al., 2020; Watanabe et al., 2018). For tsunami simulations, historical or hypothetical tsunami sources can be assumed based on the local tectonic setting of study area (Minamidate et al., 2022; Sugawara, 2021).

To assess tsunami potential, it is recommended to compare dates of known tsunami events from convincing historical, archaeological, and geological records around the study area (Goff et al., 2012). The higher the risk of tsunami exposure, the more challenging it becomes to identify storm deposits. In regions where the recurrence interval of tsunamis can be interpreted as significantly longer compared to storms, attributing tsunamis to the formation of event deposits becomes less likely compared to storms. Nevertheless, considering the possibility of a tsunami as an uncertainty is advisable.

3. Paleoclimatology and climatology

We review researches on climate variability and climatic events during the Holocene that have influenced long-term storm activity in the sections 3.1 and 3.2, respectively. The Holocene, the most recent geological epoch, began 11,650 years BP and is divided into the early, middle, and late Holocene, with lower limits of 11,650 years BP, 8186 years BP, and 4200 years BP, respectively Table 1. Sections 3.3 and 3.4 present findings on climate patterns and internal factors involved in storm dynamics, respectively. Section 3.5 gives a brief review of observed trends in storm activity under the current global warming.

3.1. Millennial and centennial scale climatic trends

Proxy-based paleoclimate reconstruction indicates that the global annual mean temperature rose for several thousand years from the beginning of the Holocene, and then declined after a peak around 6 ka until around the 19th century (Kaufman et al., 2020a; Marcott et al., 2013; Fig. 4a). Several global and regional temperature reconstructions have been proposed, but there is little consensus on the most suitable one (Kaufman et al., 2020a; Marcott et al., 2013). Kaufman et al. (2020a) compared between five reconstruction methods and analyzed a multimethod ensemble (Fig. 4a). On average, the warmest millennium was centered at 6.5 ka, which was 0.6 °C warmer than in the 19th century (Kaufman et al., 2020a). The warmest 200-year interval was also centered around 6.5 ka, which was 0.7 °C warmer than in the 19th century (Kaufman et al., 2020a). On the other hand, recent climate model simulation did not show a cooling trend from 8 ka, instead, they showed a slight uptrend to pre-industrial times (Osman et al., 2021). Clarifying discrepancy between proxy-based reconstructions and climate models have been considered as important future work (Erb et al., 2022; Kaufman and Broadman, 2023; Osman et al., 2021).

Table 1
Holocene division and major paleoclimatic features.

Division	Lower Limit	General features of temperature	General feature of other features
Early Holocene	11,650 years BP	Warming trend	Melting ice sheets
Middle Holocene	8276 years BP	Sustained warm	Increased vegetation
Late Holocene	4200 years BP	Cool	Increase in greenhouse gasses
Industrial Era	1800 CE	Rapidly warming	Increase in anthropogenic greenhouse gasses

The onset of the early Holocene (~11 ka) marks the end of Greenland Stadial 1, also known as the Younger Dryas stage, and is followed by the warming of climate. Climate change during this transition led to a temperature increase of approximately 15 °C in central Greenland over a period of 1500 years, with 5–10 °C of that increase occurring within decades (Fig. 4b). Additionally, global SST also increased around 12 ka, though the exact extent of variation is uncertain due to the seasonal bias of the oceanic proxy records (Bereiter et al., 2018; Bova et al., 2021; Kaufman et al., 2020a, 2020b).

The middle Holocene is characterized by a relatively warm period. The sustained warm period of ~9.5 ka is called as the Holocene Thermal Maximum (HTM). The HTM was concentrated in the northwestern part of North America between 11 and 9 ka, whereas in the northeastern part it occurred 4 k years later due to residual ice sheet and the asymmetry of the atmosphere-ocean circulation (Kaufman et al., 2004). Renssen et al. (2012) have shown that the warmest HTM conditions were found at high latitudes in both hemispheres, with temperature reaching up to 5 °C above pre-industrial levels, while the smallest signals were found in the tropics (<0.5 °C). This latitudinal contrast in the HTM is mainly related to orbital forcing (Renssen et al., 2012). Globally, a cooling trend began with a peak at ~6.5 ka (Kaufman et al., 2020a; Fig. 4a) and is thought to be caused by orbital factors (Wanner et al., 2015; Fig. 4c). The IPCC AR6 concluded with moderate confidence that the mean temperature peak during the Holocene was 0.2–1.0 °C higher than in the late 1800s. Marine sediment-based surface temperature reconstructions also show a warm climate during the middle Holocene and a cooling trend after around 6 ka, similar to terrestrial sediment records (Kaufman et al., 2020a, 2020b).

The late Holocene is a relatively stable and cold period in the Holocene. Multiple compilations have shown a consistent global cooling trends in the late Holocene (Kaufman et al., 2020b; Marcott et al., 2013; Fig. 4a). Mean millennial-scale temperature declined by 0.08 °C/k year from 6 ka until the 19th century (Kaufman et al., 2020a). Paleoclimatic and paleoceanic changes in the Common Era over the past 2000 years have been analyzed with particularly high resolution and exhaustiveness (McGregor et al., 2015; PAGES2k Consortium, 2013, 2017; Fig. 5).

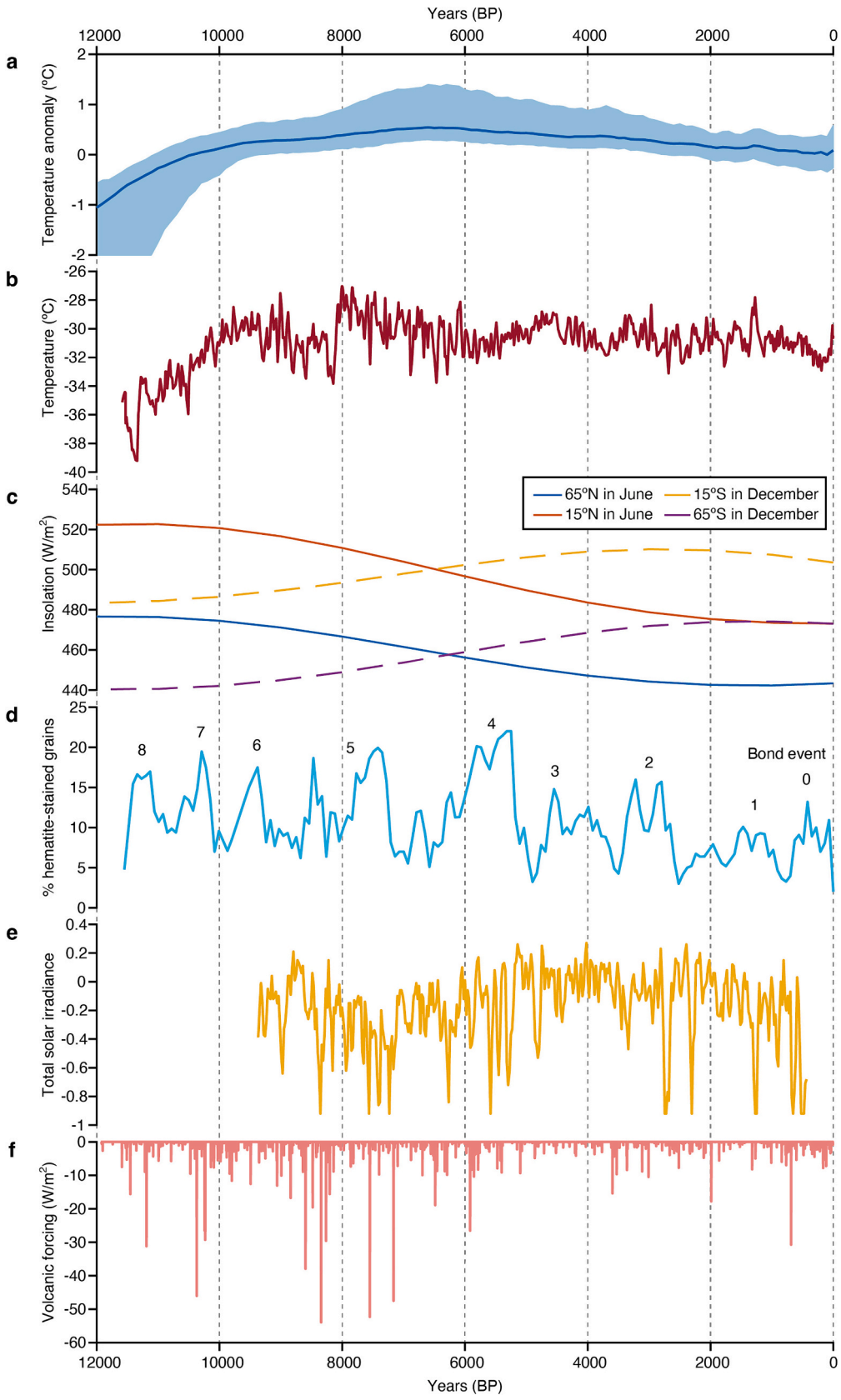

Fig. 4. Climate variability and external forcing in the Holocene. (a) Global mean temperature anomaly (Kaufman et al., 2020a). (b) Greenland temperature reconstruction (Kobashi et al., 2017). (c) Average calculated insolation on 65°N, 15°N, 15°S, and 65°S in summer. (d) Content of hematite-stained grains in the core for MC52-VM29–191 as record of drift-ice record (Bond et al., 2001). (e) 40-year averaged Total Solar Irradiance (Steinhilber et al., 2009). (f) Volcanic forcing (Kobashi et al., 2017).

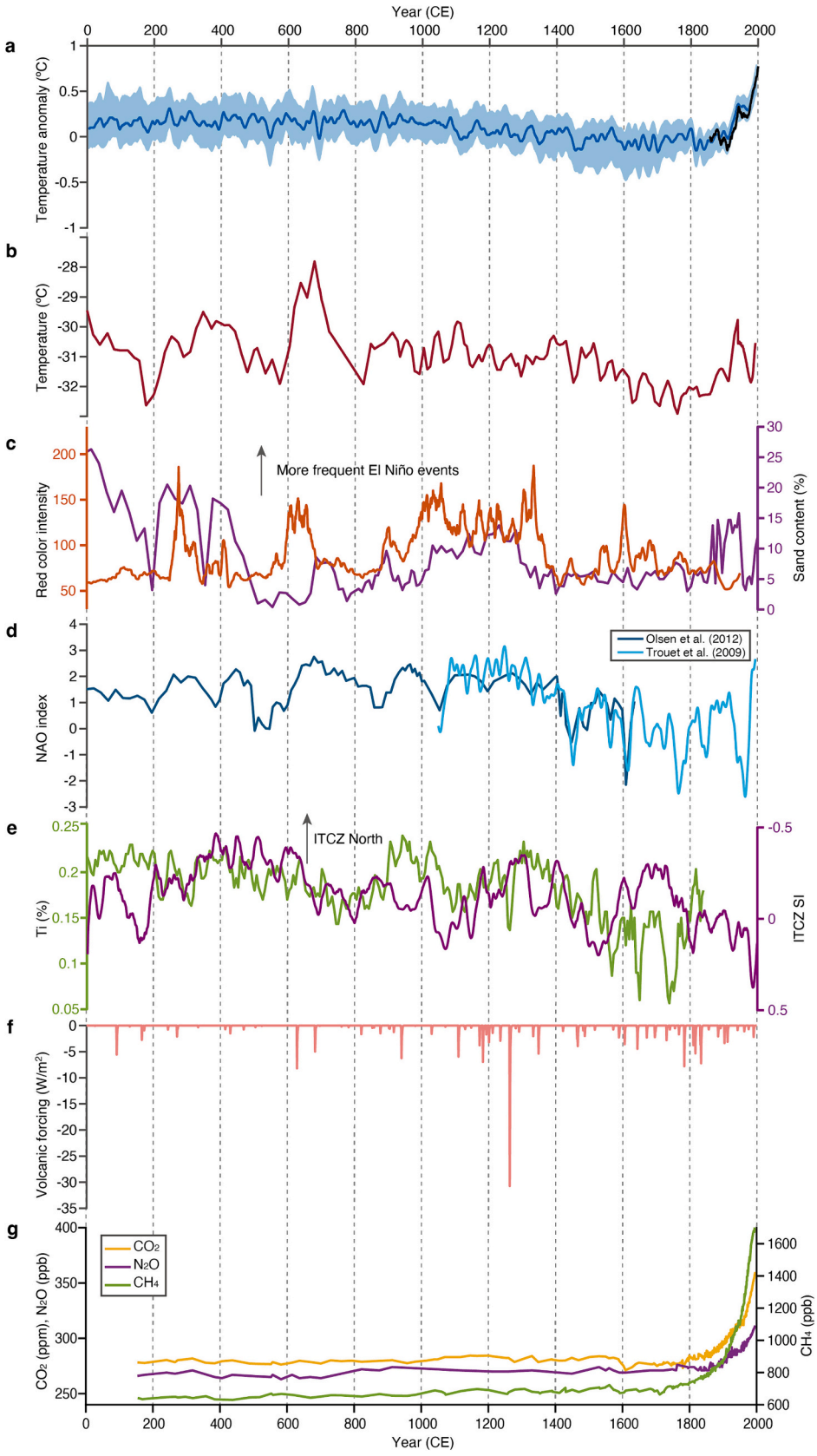

(caption on next page)

Fig. 5. Climate variability and external forcing in the Common Era. (a) Reconstructed global mean temperature anomaly (blue line) with 95% confidence level (blue shade) and observed global mean temperature anomaly (black line) (Intergovernmental Panel on Climate Change (IPCC), 2021). (b) Greenland temperature reconstruction (Kobashi et al., 2017). (c) El Niño proxy reconstruction. Red colour intensity (red) from Laguna Pallacacocha, Ecuador (Moy et al., 2002) and sand content (magenta) of El Junco, Galápagos (Conroy et al., 2008). (d) NAO reconstruction (Olsen et al., 2012; Trouet et al., 2009). (e) Record of the ITCZ position. Titanium content (light green) of Cariaco Basin sediment (Haug et al., 2001) and reconstructed ITCZ shift index (purple) based on speleothem record from Klang Cave, Thailand (Tan et al., 2019). (f) Volcanic forcing (Kobashi et al., 2017). (g) CO_2, N_2O, and CH_4 reconstruction from Antarctica ice core (Bereiter et al., 2015; Spahni et al., 2005). (For interpretation of the references to colour in this figure legend, the reader is referred to the web version of this article.)

The PAGES2k Consortium has reconstructed temperature variations in seven continents over the past 2000 years, with the most consistent feature being a long-term cooling trend until the 19th century (PAGES2k Consortium, 2013). McGregor et al. (2015) conducted a global synthesis of the SST in the common era based on 57 individual reconstructions and found a globally robust SST cooling to the 19th century.

After the industrial revolution (1850 CE–present), anthropogenically induced global warming occurred against the background cooling trend in the late Holocene (Mann et al., 2009b; Fig. 5a). IPCC AR6 concluded that human impacts have caused warming of the climate at an unprecedented rate over the past 2000 years, and that global temperatures have reached levels unprecedented in the last 100 k years (Fig. 5a). The global mean temperature during the first 20 years of the 21st century was ~0.99 °C higher than that during 1850–1900 CE (Intergovernmental Panel on Climate Change (IPCC), 2021). Moreover, for 80% of ensemble members according to Kaufman et al. (2020a), temperatures in the most recent decade were higher than in any 200-year interval in the last 12 k years. Note that changes in older time intervals may have been smoothed out compared to temperature changes in relatively short intervals in the 20th century (Kaufman et al., 2020a). IPCC AR6 has deemed the warming of oceans shallower than 700 m since 1970s CE to be virtually certain, while the warming of oceans between 700 m and 2000 m is considered very likely, and the warming of the oceans deeper than 2000 m is deemed likely (Intergovernmental Panel on Climate Change (IPCC), 2021). SST compilation by McGregor et al. (2015) shows a significant warming trend from 1801 to 2000 CE. IPCC AR6 also indicated that the mean SST increased by 0.88 °C from the late nineteenth century (1850–1900 CE) to the last two decades (2011−2020). The increase in CO_2 and CH_4 since 1750 CE far exceed natural variability over at least the last 800 k years, and the increase in N_2O is similar to the variation during this period (Intergovernmental Panel on Climate Change (IPCC), 2021; Fig. 5g).

3.2. Climatic events

In this section, we describe warm and cold climatic events that occurred in the Holocene in chronological order (Table 2). The most prominent recurring events during the Holocene are Bond events. Bond et al. (2001) identified periodic cold climatic events that existed throughout the Holocene, based on the ice-rafted debris from marine sediments in the North Atlantic, later called Bond events (Fig. 4d). Bond events are thought to have been triggered by southward and eastward advection of surface waters from the Nordic & Labrador Seas, resulting in centennial-scale cooling reversals in the North Atlantic and Europe (Bond et al., 2001). The nine bond events are numbered from 0 to 8 and have peaks at around 0.4, 1.4, 2.8, 4.3, 5.9, 8.1, 9.4, 10.3, and 11.1 ka (Wanner and Butikofer, 2008; Fig. 4d). These events occurred at intervals of about 1–1.6 k year, but there is still no plausible explanation for the mechanism of this cycle. Several processes are thought to be involved in the formation of the cycle, including orbit-driven insolation, changes in solar irradiance, large volcanic eruptions, the Atlantic Meridional Oceanic Circulation (AMOC), and variations in the internal climate system (Wanner et al., 2015). The 8.2 ka and 4.2 ka abrupt global climate changes, which are also used to define the Holocene subdivision, are introduced in Subsections 3.2.1 and 3.2.2, respectively. The Little Ice Age (LIA) which corresponds to Bond event 0 that occurred in the late Holocene is introduced in Subsection 3.2.4.

Table 2
Climatic Events.

	Start time	Period	Feature	Main region
Bond Event 8	~11.1 ka	~300 years	Cold	North Atlantic
Bond Event 7	~10.3 ka	~300 years	Cold	(North Atlantic)
Bond Event 6	~9.4 ka	~300 years	Cold	(North Atlantic)
8.2 ka event (Bond Event 5)	~8.2 ka	~160 years	Cold	North Hemisphere, South America
Bond Event 4	~5.9 ka	~400 years	Cold	North Atlantic
4.2 ka event (Bond Event 3)	~4.2 ka	~300 years	Cold	Global
Bond Event 2	~2.8 ka	~300 years	Cold	(North Atlantic)
Roman Warm Period	~2.2 ka	~600 years	Warm	Europe, North Atlantic
Late Antique Little Ice Age (Bond Event 1)	~1.4 ka	~300 years	Cold	North Atlantic, Europe
Medieval Climate Anomaly	~1.0 ka	~300 years	Warm	Global
Little Ice Age (Bond Event 0)	~0.5 ka	~300 years	Cold	Global, Especially North hemisphere
Current Warm Period	1850 CE	~170 years	Warm	Global

3.2.1. 8.2 ka event

At the beginning of the middle Holocene (8.2 ka), Greenland experienced a rapid cooling, which lasted for about 160 years over the northern hemisphere (Matero et al., 2017; Thomas et al., 2007). This 8.2 ka cold event is considered to be the most significant climatic event in the Holocene, with estimated average annual temperature decreases in Greenland by 6 ± 2 °C (Thomas et al., 2007; Fig. 4b). Evidences of this climate change have also been found in various regions such as Europe, North America, South America, Africa, Central Asia, and East Asia (Alley and Ágústsdóttir, 2005; Wang et al., 2005). The 8.2 ka event is believed to have been caused by the weakening of the AMOC by the massive outflow of freshwater from the glacial lake Agasiiz-Ojibway into the North Atlantic Ocean, resulting from the melting of the Laurentide Ice Sheet (Alley and Ágústsdóttir, 2005).

3.2.2. 4.2 ka event

At the beginning of the late Holocene (4.2 ka), a rapid drying and cooling event is thought to have occurred across a wide area of the Earth. Based on the $\delta^{18}O$ record obtained from the Mawmluh stalactites, a sharp decrease in precipitation occurred with the weakening of the Indian monsoon (Berkelhammer et al., 2013). At 4.2 ka, monsoon weakening and accompanying drying occurred in India, Oman, the Middle East, and East Africa (Dixit et al., 2014; Nakamura et al., 2016). There is a decrease in surface water temperature in the western tropical Pacific during this period (Stott et al., 2004).

The mechanism behind the 4.2 ka event remains unclear. Like the 8.2 ka event, previous studies have suggested that climate shifts in the North Atlantic may have been the primary cause of this event (Mayewski et al., 2004), but little evidence has been found for the 4.2 ka event in northern high-latitude regions (Walker et al., 2012). Other proposed

causes include the southward movement of the ITCZ (Mayewski et al., 2004), a decrease in surface water temperature in the North Atlantic Ocean (Bond et al., 2001), and intensification of El Niño-type conditions (Walker et al., 2012).

3.2.3. Medieval Climate Anomaly

The Medieval Climate Anomaly (MCA) is a period of warming that occurred primarily in the North Atlantic Ocean, spanning the 9th to 13th centuries (Mann et al., 2009b). However, its duration and scale are spatio-temporally heterogeneous, and no globally consistent warm period has been found (Mann et al., 2009b; Neukom et al., 2019; PAGES2k Consortium, 2013). Continental-scale temperature reconstructions of the Common Era have found that the period between 830 and 1100 CE featured warm periods in all four Northern Hemisphere regions, such as Arctic, Europe, North America, and Asia (PAGES2k Consortium, 2013). Whereas, in South America and Australasia, a sustained warm period was observed later, from around 1160 to 1370 CE (PAGES2k Consortium, 2013).

3.2.4. Little Ice Age

The Little Ice Age (LIA) was a period with a cooler condition that occurred around the 13th to 19th centuries, mainly in Europe, but it was also observed outside of Europe (Mann et al., 2009b; Fig. 5a, b). According to a continental compilation by PAGES2k, the transition to cooler climates occurred earlier in the Arctic, Europe, and Asia, and later in North America and the Southern Hemisphere. This transition was sustained in all regions except Antarctica by 1580 CE (PAGES2k Consortium, 2013). These regional differences may be attributed to internal climate variability, including major modes of atmospheric variability (PAGES2k Consortium, 2013). Considered associated with Bond event 0, the LIA was probably the coldest period since the 8.2 ka event (Wanner et al., 2015).

3.3. Climatic pattern

3.3.1. El Niño and Southern Oscillation

ENSO is a recurring climatic pattern associated with changes in atmospheric circulation and ocean temperature in the central to eastern tropical Pacific Ocean. El Niño and La Niña are two phases of ENSO. El Niño is characterized by weaker easterly winds, higher SST in the central to eastern tropical Pacific, and an eastward shift of the active convection area. By contrast, La Niña is characterized by stronger easterly winds, higher SST in the western tropical Pacific, lower SST in the eastern Pacific, and a westward retraction of the area of convection toward Indonesia and the western Pacific. ENSO affects the climate of Asia, North America, South America, Africa, Australia, Indonesia and other regions either directly or through teleconnections.

ENSO is the climatic pattern has the most influence on regional TC activity. From observation records and modeling, it is well known that the location of TC generation shifts to the southeast (northwest) during El Niño (La Niña) in the western North Pacific. Along with this southeastward shift, TCs tend to have longer lifespans (Wang and Chan, 2002) and the number of strong TCs tends to increase during El Niño (Camargo and Sobel, 2005). The shift of the occurrence position is considered to be caused by the eastward expansion of the monsoon trough and westerly winds (Wang and Chan, 2002), the decrease in wind shear near the International Date Line (Wang and Chan, 2002), and the suppression of TC genesis in the western North Pacific due to the decrease in relative humidity near the continent (Camargo et al., 2007). The impact of ENSO on TC activity in the western North Pacific is also seen in the shape of the track, and during El Niño, TC tends to turn northeast and move further north (Wang and Chan, 2002).

A clear relationship between TC activity in the eastern North Pacific and ENSO has been found, with a westward shift of the occurrence position during El Niño (Camargo et al., 2007). In the central Pacific, TC occurrence increases due to low vertical shear and large sublayer vorticity during El Niño although the average annual TC occurrence is generally low (Camargo et al., 2007).

North Atlantic TC activity is strongly associated with ENSO. During El Niño, hurricane activity in the Atlantic decreases, but increases during La Niña. This negative correlation is evident across a wide range of indices, including hurricane numbers, TC numbers, and Accumulated Cyclone Energy (ACE). The effect of ENSO on the number of TC occurrences is due to the dynamic effect of decreasing vertical shear during El Niño (Camargo et al., 2007). There are twice as many hurricanes during La Niña as during El Niño. Furthermore, the number of landings in the United States increases during La Niña (Larson et al., 2005).

In the North Indian Ocean, ENSO affects TC activity mainly during the post-monsoon season (October–December). An increase in frequency, intensity, and the rate of rapid intensification of TC is observed especially in the Bay of Bengal during La Niña compared to during El Niño (Bhardwaj et al., 2019; Felton et al., 2013).

In the western South Pacific, the location of TC generation shifts eastward during El Niño, and TC may occur in French Polynesia, where it is usually less affected by TCs (Camargo et al., 2007; Kuleshov et al., 2008). Overall, the total number of TCs increase in the South Pacific during El Niño (Basher and Zheng, 1995). On the other hand, during La Niña, the number of TC landing in northeastern Australia increases (Kuleshov et al., 2008).

Many geological proxies suggest that ENSO has millennial-scale variability, although there are some discrepancies. Paleoclimate records in the tropical Pacific show a decrease in ENSO variability from the early Holocene to the middle Holocene and an increase over the few thousand years (Carré et al., 2014; Conroy et al., 2008). A 12,000-year reconstruction of alluvial sediments from Laguna Pallcacocha, Ecuador, showed an increasing ENSO frequency up to 1.2 ka, followed by a decreasing trend (Moy et al., 2002; Fig. 5c). Sediment records of Holocene ENSO frequency reconstructed from Lake Eljunco, Galapagos suggest an increase in frequency at 9 ka and 4.2 ka (Conroy et al., 2008; Fig. 5c). Carré et al. (2014) reconstructed ENSO variability over the past 10 k years in the eastern equatorial Pacific from Peruvian mollusk fossils showing that the variability was close to the present level in the early Holocene and decreased significantly at 4–5 ka. Some paleoclimate proxies show La Niña-like consistency of cooling in the eastern equatorial Pacific (Mann et al., 2009b), dryness in the southwestern US (Cook et al., 2014), and wetness in the western North Pacific (Steinman et al., 2014) in the early past millennium (1000–1400 CE).

3.3.2. Arctic Oscillation and North Atlantic Oscillation

Arctic Oscillation (AO) is a climatic pattern characterized by counterclockwise circulating winds in the Arctic around latitude 55°N, in which the Arctic and mid-latitudes of Northern Hemisphere vary in antiphase (Thompson and Wallace, 1998). The North Atlantic Oscillation (NAO) is a climatic pattern in which the intensity of both the Icelandic low and the Azores high in winter season (Hurrell et al., 2001). AO and NAO are closely linked with a high correlation coefficient of 0.95 (Wanner et al., 2001).

NAO affects storm activity mainly in the North Atlantic. NAO shifts the pressure pattern and the position of the jet stream, thus affecting the North Atlantic storm track (Elsner, 2003). Boudreault et al. (2017) statistically investigated the effects of climatic factors on TC activity in the North Atlantic and found a strong negative correlation between NAO and the annual number of TCs and hurricanes in the entire North Atlantic, and the number of TC landfalls in the United States. Frank and Young (2007) found a positive correlation between TC in the Indian and Atlantic Oceans that TC activity in the Indian Ocean decreases during the positive phase of NAO.

NAO plays an important role in winter storm activity in Europe. Positive NAO phases lead to more frequent and intense storms affecting Europe during the winter season (Pinto et al., 2009). There is a positive correlation of NAO indices with winter storms in northern Europe and smaller or negative correlations in southern Europe (Hanna et al., 2008).

The Alkenone-based Holocene-scale SST records show cooling in the eastern North Atlantic and warming in the eastern Mediterranean, northern Red Sea, and subtropical Atlantic from the early to late Holocene, suggesting an AO/NAO-like weakening of the atmospheric circulation in the northern hemisphere (Rimbu et al., 2003). Summer cooling in the Northern Hemisphere from the mid-Holocene to the pre-industrial period, combined with changes in global temperature gradients, could probably explain a negative NAO index (Wanner et al., 2008). In the last millennium, the LIA and MCA correspond to negative and positive AO/NAO patterns, respectively (Mann et al., 2009b; Fig. 5d). This response may be caused by the interaction of solar radiation with lower stratospheric and upper tropospheric atmospheric dynamics, resulting in negative patterns during periods of low irradiance such as the LIA and conversely positive patterns during the period of high irradiance such as the MCA (Mann, 2021).

3.3.3. *Atlantic Meridional Oscillation*

Atlantic Meridional Oscillation (AMO), also known as Atlantic Medieval Variability (AMV), is a natural climate variability that is observed in the multidecadal variability of SST in the tropical North Atlantic and in the variability of the Atlantic thermohaline circulation (Delworth and Mann, 2000). AMO has been investigated as a factor that explains the multidecadal TC variability in the North Atlantic (Goldenberg et al., 2001). Klotzbach and Gray (2008) found that the index which described from the North Atlantic SST and sea level pressure anomalies is consistent with the observed multidecadal variation in Atlantic TC numbers and frequency of landfalls in the United States. Boudreault et al. (2017) also confirmed that there is a positive correlation between the number of TCs and hurricanes in the North Atlantic and the AMO index.

3.4. *Internal factor of climate system*

Atmospheric and oceanic circulation systems vary in position and intensity on the Holocene timescale. Here we briefly describe the characteristics and known variations of the main constituents of the climate system.

3.4.1. *Atlantic Meridional Overturning Circulation*

The Atlantic Meridional Overturning Circulation (AMOC) is a thermohaline circulation characterized by the northward current of warm, saline surface water and the southward current of cold, deep water in Atlantic Ocean. AMOC is thought to have a significant influence on climate and storm activity in the North Atlantic, Europe, and globally, although the relationship between AMOC strength and storm activity is not completely clear. Yan et al. (2017b) conclude that the decline of the frequency of major Atlantic TCs from 2005 to 2015 is likely related to increased vertical wind shear due to a weakening of AMOC. The strengthening (weakening) of AMOC results in the weakening (strengthening) of the winter storm track and Aleutian Low, which affect European climate (Zhang et al., 2019).

Ayache et al. (2018) statistically analyzed the integration of 22 proxy records over the Holocene covering the North Atlantic and reconstructed the variation of AMOC. The results suggested that AMOC reached a maximum at 6–7 ka and then weakened until ~2 ka (Ayache et al., 2018). Rahmstorf et al. (2015) estimated AMOC variability over the past millennium by integrating paleoclimate proxies. They found an anomalous decline in AMOC intensity over the last 100 years in the last 1000 years (Rahmstorf et al., 2015). Compilation of proxy records by Caesar et al. (2021) also supports the unprecedented slowdown in AMOC over the past century.

3.4.2. *Intertropical Convergence Zone*

The Intertropical Convergence Zone (ITCZ) is the area where the northeast and southeast trade winds converge around the Earth near the equator. The ITCZ is accountable for the ascending portion of the Hadley circulation, where energetic convective activity takes place. A significant number of TCs in the tropical oceans are generated within the ITCZ (Studholme et al., 2022). Idealized simulations have found a strong relationship between the characteristics of ITCZ and the frequency of TCs (Burnett et al., 2021; Merlis and Held, 2019). A statistical analysis by Liao et al. (2023) showed that in the North Atlantic and western North Pacific, the frequency of TC genesis is significantly correlated with the position of the ITCZ, with more TC genesis occurring in years when the ITCZ is further poleward.

Haug et al. (2001) showed a drying trend after 5400 years BP and a decrease in precipitation during the period 3800–2800 years BP and the LIA (Fig. 5e). They conclude that this change in precipitation is best explained by changes in the mean latitude of the ITCZ in the Atlantic (Haug et al., 2001). Fleitmann et al. (2007) provided records of precipitation variability along latitudinal transects from four-site stalagmite records in Oman and Yemen. Their results indicate a rapid migration of the summer ITCZ during the early Holocene and a gradual migration southward during the middle to late Holocene (Fleitmann et al., 2007).

3.5. *Observed trends in storm activity under the current global warming*

As mentioned in the previous section, the magnitude of natural variability across various temporal scales makes it difficult to detect anthropogenic influences on storm activity. Identifying past trends in TC metrics remains a challenge due to the heterogeneous nature of historical instrumental data, which are known as best-track data (Schreck et al., 2014). Inhomogeneities in data quality and limited temporal length are insufficient to provide robust trend detection statements, especially in the presence of multi-decadal natural variability (Intergovernmental Panel on Climate Change (IPCC), 2021).

While observational records do not exhibit a clear trend in global TC frequency, they do reveal a significant decreasing trend in the western North Pacific (Knutson et al., 2019). The sixth assessment report of IPCC indicates low confidence in the existence of long-term (decades to centuries) trends in the frequency of all categories of TCs (Intergovernmental Panel on Climate Change (IPCC), 2021). On the other hand, the proportion of category 3–5 TCs among global TCs likely increased over the past 40 years (Klotzbach et al., 2022; Kossin et al., 2020; Walsh et al., 2016).

The poleward migration in the peak position of TCs has been confirmed in both the Northern and Southern Hemispheres (Kossin et al., 2014), which is particularly pronounced in the western North Pacific (Daloz and Camargo, 2018; Lee et al., 2020). This poleward shift of TCs in the western North Pacific offsets changes in overall TC intensity (Kossin et al., 2020; Lee et al., 2012). The poleward shift of TCs is interpreted to be associated with changes in the Hadley circulation (Sharmila and Walsh, 2018; Studholme and Gulev, 2018). Over the past 40 years, the annual mean extent of the Hadley circulation has shifted poleward by approximately 0.1–0.5° per decade (Grise and Davis, 2020; Studholme and Gulev, 2018). While the trend in the Hadley circulation strength since 1979 varies among reanalyses, there is a tendency for the Hadley circulation to strengthen (D'Agostino and Lionello, 2017; Studholme and Gulev, 2018).

The sixth assessment report of IPCC concluded that there is overall low confidence in recent changes in the total number of extratropical cyclones across both hemispheres, with medium confidence in a poleward shift of extratropical cyclone tracks since the 1980s (Intergovernmental Panel on Climate Change (IPCC), 2021).

4. Basin-scale Paleotempestology

This chapter discusses the topic of regional paleostorm variability, and delves into paleotempestological studies that have reconstructed local information such as frequency and intensity. The chapter specifically discusses trends in the western North Atlantic, Europe, the western North Pacific, and the western and central South Pacific, but does not

cover the Indian Ocean and Eastern Pacific due to a scarcity of available case studies (Fig. 6).

4.1. Western North Atlantic

The western North Atlantic coast has been the most extensively studied region for paleostorm reconstruction. Donnelly and Woodruff (2007) reconstructed variability in storm frequency over the past 5000 years from Puerto Rico overwash sediments, showing frequent periods of 5400–3600 years BP and 2500–1000 years BP, as well as quiet periods of 3600–2500 years BP and 1000–250 years BP. These quiet periods may correspond to the active periods of El Niño events (Moy et al., 2002). Additionally, Donnelly and Woodruff (2007) found a link between TC activity in Puerto Rico and tropical African precipitation patterns, which are associated to the strength of the West African monsoon (Nguetsop et al., 2004). The West African monsoon forms African Easterly Waves,

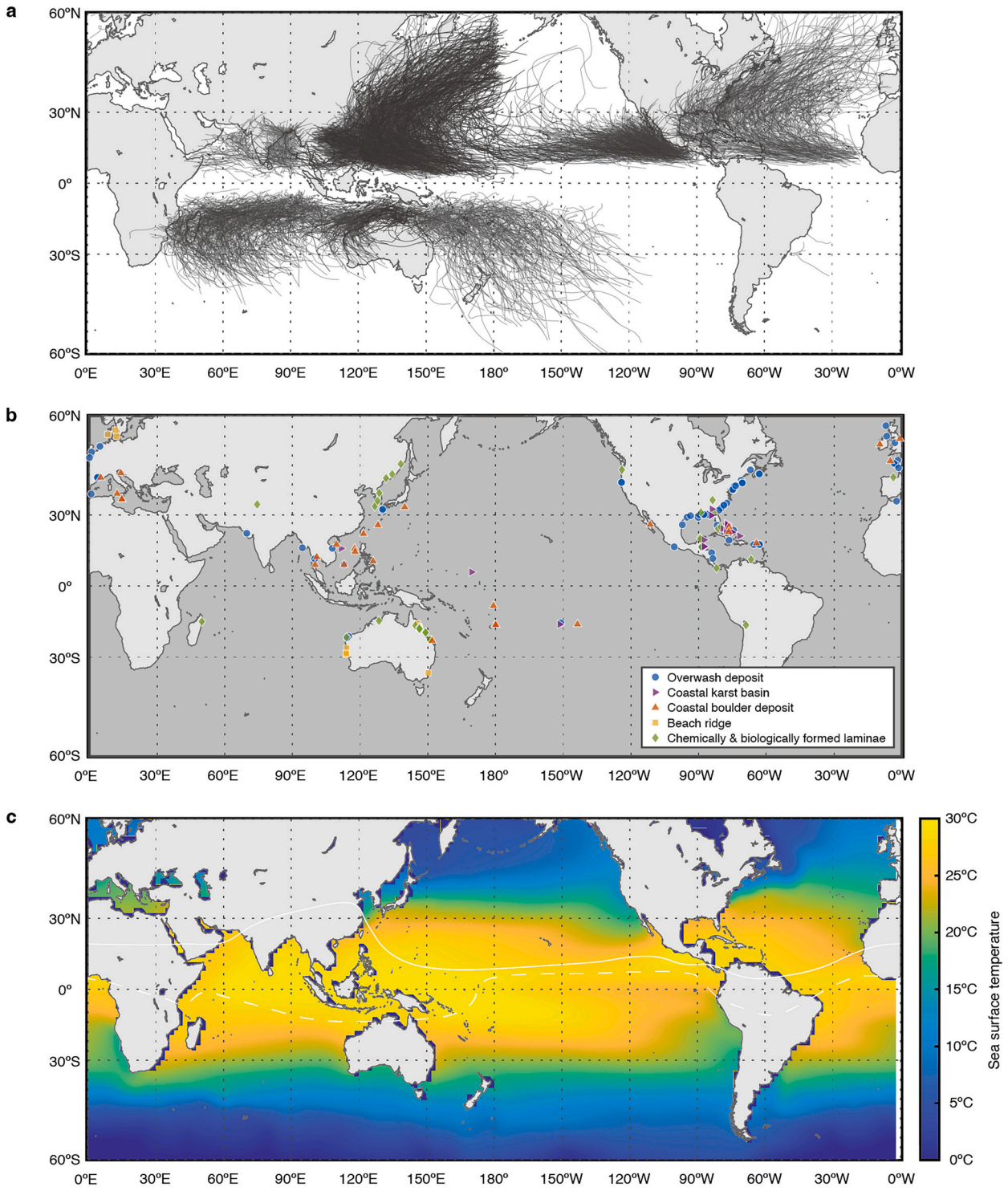

Fig. 6. Paleostorm records and observation record of tropical cyclones and ocean temperature. (a) Tracks of all tropical cyclones in 1980–2022 (data from IBTrACS). (b) Distribution of paleostorm records in this review. (c) Annual mean sea surface temperature in 1991–2020 (data from NOAA). Solid and dashed white lines represent the modern mean positions of the Intertropical Convergence Zone in July, and January, respectively.

synoptic-scale disturbances that propagate westward from tropical Africa to the North Atlantic Ocean (Burpee, 1972). These African Easterly Waves contribute to the genesis of approximately 72% of TCs in the North Atlantic (Russell et al., 2017). It is plausible that the West African monsoon plays an important role in seeding cyclogenesis in the North Atlantic over millennial timescales (Donnelly and Woodruff, 2007).

Mann et al. (2009a) compiled the overwash sediment record from eight sites along the coasts of the western North Atlantic for the past 1500 years. They indicated that the annual number of cyclones peaked at 900–1100 CE before decreasing from 1200 CE and suggested the medieval peak of TC activity results from the reinforcing effects of La Niña-like climate conditions and relative tropical Atlantic warmth based on a statistical climate model (Mann et al., 2009a). Mann et al. (2009a) concluded that Atlantic TC activity was unusual in the decades leading up to 2009 CE, but not unprecedented over the past 1500 years.

Wallace et al. (2021a, 2021c)) conducted a comprehensive analysis of paleostorm records from Florida, Bahamas, and New England dating back to 500 CE (Fig. 7). They found that during 600–800 CE, there were fewer storms detected in New England, while frequent storms were detected in Bahamas and Florida (Fig. 7). The MCA (950–1250 CE) partially overlaps with active storm periods in all three regions (E. Wallace et al., 2021a). The authors suggested that warmer SST in the North Atlantic Main Development Region and La Niña-like conditions in the eastern Pacific from 900 to 1000 CE may have facilitated the

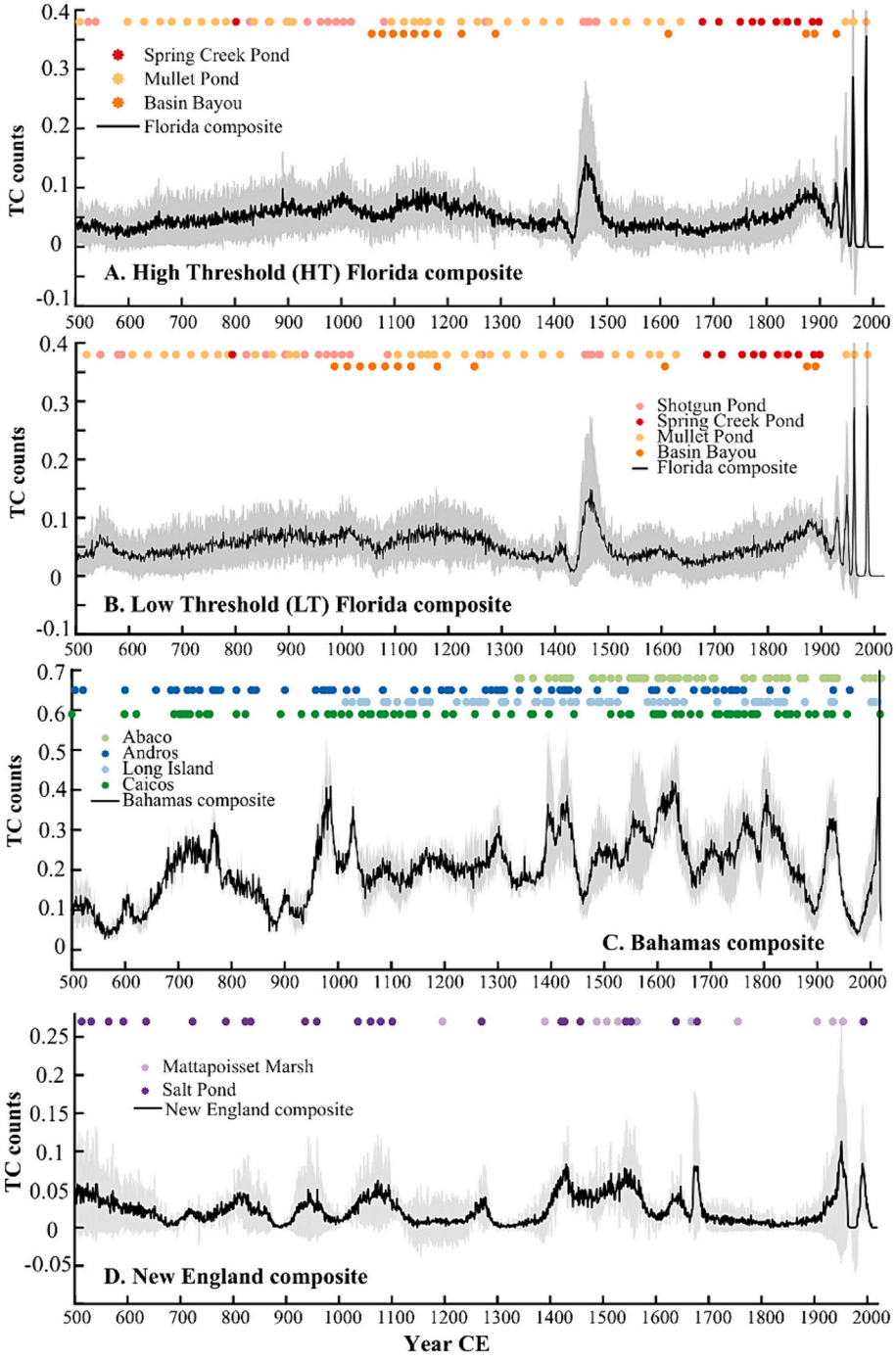

Fig. 7. Regional compilations of tropical cyclone counts from 500 to 2019 CE for the (A) Florida with high threshold, (B) Florida with low threshold, (C) the Bahamas, and (D)New England. For more details, please refer to (Wallace et al., 2021a). This figure is from Wallace et al., 2021a. © Elsevier. Used with permission.

occurrence of hurricanes in the North Atlantic (Wallace et al., 2021a; Fig. 5c). During the period 1200–1400 CE, following peak of the MCA, storms became less frequent in both the Bahamas and New England (Wallace et al., 2021c; Fig. 7). In the same period, storms were frequent in Florida up until 1300 CE. Conversely, during the LIA, frequent storms were detected in Bahamas and New England, while Florida was relatively quiet (E. Wallace et al., 2021a). Over the last 200 years, storm activity has decreased significantly in the Bahamas compared to other periods in the last 1000 years, but increased in Florida from 1780 CE and in New England from 1900 CE (Wallace et al., 2021c; Fig. 7). Winkler et al. (2022) also compiled blue hole deposits in five Bahamian sites dating back to 1400 CE, and divided the storm active period of Bahamas noted by Wallace et al. (2021c) into two periods: 1530–1625 CE and 1725–1830 CE. A recent compilation by Winkler et al. (2023) suggested that despite a globally cooler climate, the Bahamian TC activity during the LIA was enhanced by an increase of African Easterly Waves originating from a stronger West African Monsoon.

In summary, the western North Atlantic region has been the subject of numerous paleostorm reconstructions, which have shown regional-scale variations in storm patterns. A recent compilation of these records has indicated that storm frequencies are not uniform across different regions, such as the north (New England), middle (Florida), and south (Bahamas and Puerto Rico) of the western Atlantic coast. This regional variation may be due to different climatic drivers such as ENSO and West African monsoon. A notable commonality among these records is that an increase in storm frequency was observed between 900 and 1100 CE across the broader western North Atlantic. This increase in storm activity is thought to have been influenced by both La Niña-like climate conditions and the MCA.

4.2. Europe

In Europe, both TCs and winter storms produce strong winds and waves. It is noted that paleostorm records reflect the impacts of both TCs and winter storms. The difficulty of distinguishing between TCs and winter storms based on sedimentary features alone hampers our understanding of the long-term variability of storm activity. However, in terms of frequency, winter storms pass through Europe more frequently than TCs (Dullaart et al., 2021). Most of TC-origin storms generally transform into extratropical cyclones by the time they influence on Europe (Baker et al., 2021). In Europe, extratropical cyclones may contribute more to the formation of the paleostorm record than TCs.

Sorrel et al. (2012) compiled a collection of nine overwash records from coastal environment in England, Scotland, Ireland, the Netherlands, Denmark, and Sweden (Fig. 6). Their compilation shows five periods of active storms in northern Europe over the past 6500 years, i.e., 5800–5500 years BP, 4500–3950 years BP, 3300–2400 years BP, 1900–1050 years BP, and 600–250 years BP (Fig. 6). The last period coincides with the LIA. Sorrel et al. (2012) suggested that this ~1500-year cycle of storm activity corresponds to Bond events, primarily characterized by cold European climatic conditions (Bond et al., 2001; Fig. 4d). On the other hand, this variability does not match the periodicity of the solar irradiance record (Steinhilber et al., 2009; Fig. 4e), suggesting that solar radiation is not the primary external force driving millennial-scale storm activity in northern Europe. For the compilation, Sorrel et al. (2012, 2009) divided the estuary sediments into storm-dominated and tidal-dominated sequences based on sedimentological features. It is noted that the recognition of the storm sequences within an estuary does not correspond to a specific storm event and thus includes an element of uncertainty.

Sabatier et al. (2012) found frequent storms during the periods of

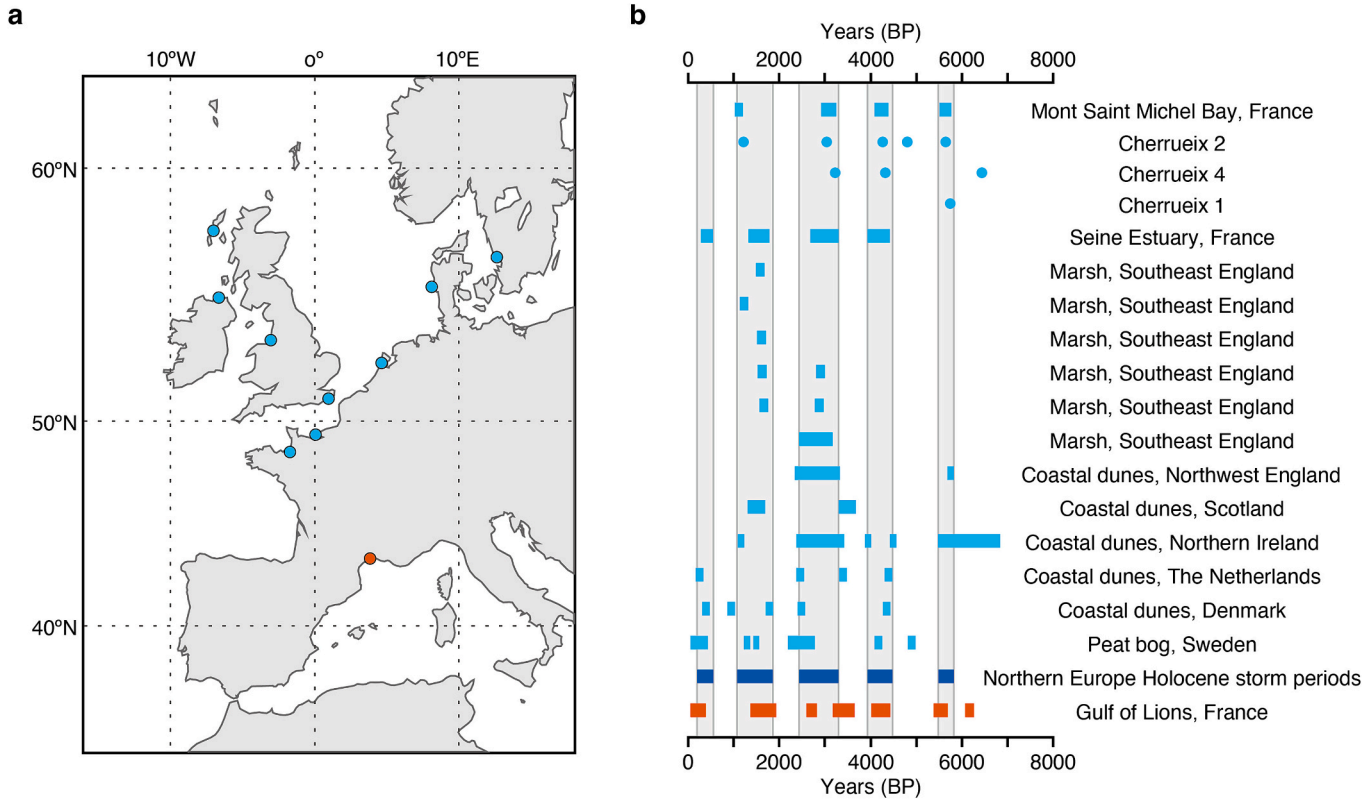

Fig. 8. Compilation of the European paleostorm records. (a) Location of the studies. (b) active storm period suggested from each record. Light blue plots in (a) and periods in (b) are based on the studies collected by Sorrel et al. (2012). Blue periods in (b) are the Holocene storm periods of the Northern Europe by Sorrel et al. (2012). Red plots in (a) and periods in (b) are based on the record along the Gulf of Lions by Sabatier et al. (2012). (For interpretation of the references to colour in this figure legend, the reader is referred to the web version of this article.)

6300–6100 years BP, 5650–5400 years BP, 4400–4050 years BP, 3650–3200 years BP, 2800–2600 years BP, 1950–1400 years BP, and 400–50 years BP (LIA) from a 7000-year storm record on the northwest coast of the Mediterranean Sea (Fig. 8). This result aligns with the period of active storms confirmed by Sorrel et al. (2012) in northern Europe. Sorrel et al. (2012) posit that the periods of frequent storm activity in the northern Europe may be explained by the condition such as positive NAO phases. However, Sabatier et al. (2012) argued that the NAO alone does not predominantly drive millennial-scale variability, as its positive phase typically fails to explain concurrent activation of storms in both northern Europe and the Mediterranean.

Generally, the positive NAO phase involves more frequent and intense winter storms affecting the North Atlantic and Europe (Pinto et al., 2009). Conversely, during positive NAO phases, the formation of TCs in the North Atlantic and their landfall in North America tends to decrease (Boudreault et al., 2017). It is plausible that conditions resembling positive NAO during the LIA might have activated winter storms in Europe while suppressing TCs in the North Atlantic, as described in the section 4.1.

Coastal barrier dynamics are influenced by complex physical processes such as dune breaches, recovery, and sediment supply, which exhibit spatio-temporal effects. However, coastal boulder deposits on rocky coasts remain unaffected by these processes, making them valuable indicators of long-term storm activity. Many coastal boulder deposits have been reported in European coastal regions (Autret et al., 2018; Cox et al., 2012; Hansom and Hall, 2009). Boulder ridges in the Aran Islands and Ireland have been observed to change significantly in distribution during periods unaffected by tsunamis, but were affected by storms. This is evidenced by photographs, comparisons with old maps from 1839 CE, and dating (Cox et al., 2012). Local eyewitness accounts also confirm that the 1991 CE storm displaced 78 tons of clifftop boulders located at an elevation of 11 m and a distance of 145 m from the cliff edge (Cox et al., 2012). These boulder ridges are believed to have been formed by the cumulative impact of waves during the Holocene, providing evidence of past high-energy wave events. Hansom and Hall (2009) conducted radiocarbon and OSL dating on sediments within and beneath the boulder ridges in the Shetland Islands, Scotland, identifying the periods of exceptionally high storm activity in 400–550 CE, 700–1050 CE, 1300–1900 CE, and since 1950 CE.

Sedimentary records suggest a possible cycle of storm intensification in northern Europe and the northwestern Mediterranean with a periodicity of approximately 1500 years. Yet, the specific climatic pattern responsible for enhancing regional storm activity remains unclear. The NAO, a climate pattern often associated with storm activity in Europe, is a candidate factor governing this variability of storm activity (Sorrel et al., 2012). However, the NAO alone may not fully explain the observed storm patterns in both regions, as the impact of positive NAO phases on storm activity is limited to the northern sector, while the southern sector remains largely unaffected. Importantly, the recent reconstructions suggest that the NAO was neutral or negative during the LIA (Ortega et al., 2015; Trouet et al., 2012). Therefore, it is necessary to consider other mechanisms which activate storminess during the LIA.

The winter season of 2013/2014 CE, marked by exceptional winter storms and waves, recorded the highest mean winter wave energy in at least the last 67 years along the broad Atlantic coast of Europe (55°N–38°N) (Masselink et al., 2016; Matthews et al., 2014). This winter was not captured by NAO or other climate indices. Recently, the Western Europe Pressure Anomaly (WEPA) has been proposed as a climate index that most effectively explains the winter wave height variation based on 66 years of weather and wave hindcasts (Castelle et al., 2017). The positive phase of WEPA reflects the strengthening and southward shift of the pressure gradient between Ireland (Icelandic low) and the Canary Islands (Azores high), resulting in extreme waves over Western Europe south of 52°N (Castelle et al., 2017, 2018). Castelle et al. (2017) demonstrated that WEPA was the climate index that best explained the extreme winter of 2013/2014 CE, which caused widespread coastal erosion and inundation.

The extreme winter of 2013/2014 CE, marked by storms and associated waves affecting Western and Southern Europe (e.g., France, Spain, and Portugal) to Northern Europe (e.g., Ireland, UK, and Norway), could potentially account for the elevated storm activity recorded in sedimentary records across Europe. Autret et al. (2018) investigated morphological changes in coastal boulder deposits in western Brittany, France during 2013–2017 CE and found that most of the morphological changes were caused by extreme water level events at the decennial level. Furthermore, a 70-year hindcast of maximum winter water levels revealed that extreme events that caused changes in boulder distribution were more correlated with the WEPA index ($r = 0.46$) than the NAO index ($r = 0.1$) (Autret et al., 2018). Although the WEPA reconstructions on centennial to millennial scales have not yet been performed, climatic conditions similar to positive WEPA phases may explain millennial-scale regional storm activation in the northeastern Atlantic including both the northern Europe and the Mediterranean.

The combined effects of several atmospheric and oceanic patterns may be driving storm activity in Europe. To clarify the relationship between the atmosphere-ocean variability associated with Bond events and storm activity, it is necessary to deepen our understanding the link between paleoclimatology, paleoceanography, and past storm records.

In summary, sedimentary records from both northern Europe and the northwest Mediterranean suggest that storm activity in Europe exhibits a cyclical variation of approximately 1500 years, consistent with Bond events. Generally, the climate pattern most commonly associated with storm activity in Europe is the NAO; however, it may be difficult to explain the high storm activity in both northern Europe and Mediterranean solely through the positive NAO-like condition. Climate patterns similar to the positive WEPA phase, with the strengthening and southward shift of the Icelandic and Azores highs, may better explain the widespread storm and wave activity over Europe. However, the generation mechanism of Bond events, as well as the associated atmospheric and oceanic changes, remain not fully understood. To clarify the variability of long-term storm activity in Europe and its underlying controlling factors, further collection of past storm records, particularly in southwestern Europe and the Mediterranean, is necessary.

4.3. Western North Pacific

Woodruff et al. (2009) reconstructed the past 6400 years of TC history from two lake sediments in southwestern Japan. They found that TCs are active at 4800–4300 years BP, 3600–2500 years BP, and 1000–300 years BP, and these periods were consistent with the period that frequent El Niño events occurred (Moy et al., 2002; Fig. 5c). In the subsequent study, Woodruff et al. (2015) reconstructed overwash records for the past 2000 years from lake sediments from southwestern Japan. While the sites of Woodruff et al. (2009) were north-facing, the site in Woodruff et al. (2015) was south-facing and exposed to more common typhoon paths in the western North Pacific. Woodruff et al. (2015) found that there was a period of high TC activity in the 11th–13th centuries, followed by a gradual decline in activity. These two records of southwestern Japan show the inverse-correlation with historical TC landfall records in southern China (Liu et al., 2001), implying that the sediment records representing changes in TC track rather than overall TC activity.

Variations in the grain size of marine sediment cores from the Zhejiang-Fujian mud belt located offshore east of China have been regarded as proxies for past storm activity (Yang et al., 2022; Zhou et al., 2019). By comparing the TC observation records from 1984 CE to 2018 CE with the sand (>64 μm) content in the core, Yang et al. (2022) found a high positive correlation ($R = 0.72$) between the annual TC maximum wind speed and the sand content. According to a series of studies, high TC activity in the Zhejiang-Fujian mud belt was assumed to have occurred during 0–480 CE, 790–1230 CE, and 1940–2018 CE (Yang et al., 2022; Zhou et al., 2019).

On the Gulf of Thailand coast, Williams et al. (2016) conducted an analysis of overwash deposits spanning the past 8000 years, suggesting that inundation events occurred with a frequency two to five times higher during the 7800–3900 years BP period compared to the subsequent period of 3900 years BP to present. The study posits that the increased frequency of overwash events in the middle Holocene may be attributed to several factors, including changes in site sensitivity resulting from sea-level rise (Williams et al., 2016). Conversely, the late Holocene saw a relative rarity of overwash events in the Gulf of Thailand during the periods of 3600–2500 years BP and 1000–300 years BP, as opposed to the trends observed in southwest Japan record (Williams et al., 2016; Woodruff et al., 2009). This opposite trend between southwest Japan and Gulf of Thailand supports that patterns in the overwash records represent changes in TC tracks (Williams et al., 2016).

Numerous coastal boulder deposits have been reported on the coral reefs in the western North Pacific, which are evidence of high-energy wave events. Boulders are highly conserved even in tropical and subtropical regions with few overwash records. In the Ryukyu Islands, Japan, a significant number of reef boulders and coral blocks originating from storm waves are distributed on coral reefs (Goto et al., 2009, 2011; Fig. 3c). Minamidate et al. (2020) conducted numerical computations of typhoons, storm waves, surge, and boulder movement under the constraint of the distribution of boulders on Kudaka Island, Japan, and estimated the maximum intensity of typhoons over the past 3500 years. The estimated maximum intensity of typhoons and storm waves exceeded those observed in the Ryukyu Islands over the past 70 years (Minamidate et al., 2020). On the other hand, this intensity is meteorologically reasonable and comparable to Super Typhoon Nancy (1961) and Super Typhoon Haiyan (2013).

In the South China Sea, Tao et al. (2021) conducted the U—Th dating on coral blocks carried by storms on the reef flat of Xisha Island and Huangyan Island. The results of their 16-point U—Th dating revealed that the boulder age frequency was low during the warm period (the MCA) and high during the cold period (the LIA) in the South China Sea (Tao et al., 2021). Additionally, relatively small (<1.5 t) carbonate boulders have also been reported on the islands of the Gulf of Thailand (Terry et al., 2016a, 2016b, 2018). These boulders are thought to have been transported by wave events with onshore velocity of at least 5 m/s. The ages of these boulders are concentrated in the periods 600–700 CE, 900–1000 CE, 1150–1250 CE, and 1400–1650 CE, with the last period being the longest and comprising over half of the boulders (Terry et al., 2018). Since 1650 CE to the present, a long quiet period of storm activity has been inferred in the Gulf of Thailand (Terry et al., 2018).

Yu et al. (2009) reconstructed the frequency of extreme wave events for the past 4000 years using coarse fraction from the lagoonal deposit at Yongshu Reef in the South China Sea. The coarse fraction record indicates more frequent storm events during the LIA than that during the MCA although the proxy record relates to not only storm events but also the sedimentation rate on the reef and the reef morphology (Yu et al., 2009).

Bramante et al. (2020) provided a 3000-year record of the occurrence of TCs, identified as a coarse-grained event layers in a blue hole of the Marshall Islands. The estimated TC frequency was 1 event per century on average for the entire period, but reached a maximum of 3.75 events per century during the period of 1300–1700 CE. This peak coincides with the LIA and the southward migration of the ITCZ (Bramante et al., 2020; Fig. 5e).

The paleostorm records in this review show that storm activity is elevated in the northern part of western North Pacific (southwest Japan and the East China Sea) during the warm period such as the MCA, while it is active in the southern part (South China Sea and the tropical central Pacific) during the cold period such as the LIA. A recent compilation by Han et al. (2023), independent of the compilation in this paper, also showed an increase in TC activity in mid-latitudes during the MCA and an increase in TC activity in low latitudes during the LIA. Han et al. (2023) hypothesized that there is a transition boundary of asynchronous storm activity between 24.74°–25.87°N.

Why is TC activity increased in the north (south) during warm (cold) periods? This is possibly explained by a latitudinal shift in the location of favorable climatic conditions for TC formation and development, with ocean temperature changes. Bramante et al. (2020) noted correlations between tropical central North Pacific TC activity and the ITCZ proxy variability, and suggested that low-latitude TC activity may have increased due to the southward migration of the ITCZ during the LIA. Over the past few decades, when anthropogenic warming progressed, a poleward shift in the location of TC genesis was observed in the western North Pacific (Studholme and Gulev, 2018; Studholme et al., 2022). As a notable example, the number of TC landing in Thailand has decreased significantly since the 1960s (Lee et al., 2020). The position where TC reaches its peak has also moved poleward (Kossin et al., 2014, 2016). Modeling and theoretical studies suggest that the observed changes are caused by shifts in the location of climatic conditions favorable to TC formation and development (e.g., vertical wind shear and potential intensity) (Kossin et al., 2014, 2016; Sharmila and Walsh, 2018). Therefore, in the western North Pacific, during the transition from the MCA to the LIA, it is possible that zones with a favorable large-scale environment for TC activity moved southward due to the southward migration of the ITCZ, resulting in high TC activity observed at relatively low latitudes.

ENSO is widely acknowledged as the most dominant internal oscillation in the western North Pacific. During El Niño, the location of TC genesis shifts southeast, individual TC's lifetime increases, and the number of strong TCs increases (see details in the section 3.3.1). Additionally, TCs tend to move north and turn east in El Niño years, whereas they are more likely to move west and make landfall in southern China in La Niña years. Frequent ENSO events or El Niño like condition in the MCA may have caused an increase in the number of TCs heading toward southwest Japan (Woodruff et al., 2009, 2015). However, the ENSO variation alone cannot fully explain the overall TC activity in the western North Pacific, especially the multi-centennial scale variability in low latitudes. The enhanced magnitude of ENSO activity or El Niño-like condition during the RWP cannot explain the increase and decrease of TC frequency near Yongshu Reef (Yu et al., 2009) and southwest Japan (Woodruff et al., 2009, 2015), respectively. Besides, the weakened ENSO activity or La Niña-like condition during the LIA, which may lead fewer TCs in the South China Sea, conflicts with high TC activity in Yongshu Reef in this period (Yu et al., 2009). Thus, the long-term variation of ENSO seems to be less dominant on paleo-TC activity in the western North Pacific than SST in this ocean and the global and associated changes in atmospheric circulation. ENSO plays a subdominant role in TC activity through its influence on SST and atmospheric circulation over a wide area in the western North Pacific.

In summary, no consistent millennial-scale variability was found across all regions in the western North Pacific. Rather, anti-phase variability in centennial-scale TC activity was observed in the southern and northern parts of western North Pacific (Fig. 9): TC activity was high in the northern part (southern part) during the periods when the Northern Hemisphere was relatively warm (cold). It is hypothesized that this north-south shift in the TC activity is caused by a latitudinal shift of the environment favorable to TC generation and development accompanying changes in ocean temperature (Fig. 6c, 9). Therefore, SST variability can be the most important factor driving storm activity in the western North Pacific. Overwash events increased in southwestern Japan under the El Niño-dominant condition of the MCA, suggesting that the ENSO variability over the Holocene is also important for storm activity in the western North Pacific. Further collection of records in each region (e.g., East Asia and South East Asia) is needed to detect more robust trends in regional variation.

4.4. Western South Pacific

In the South Pacific, storm records are not as abundant as in other

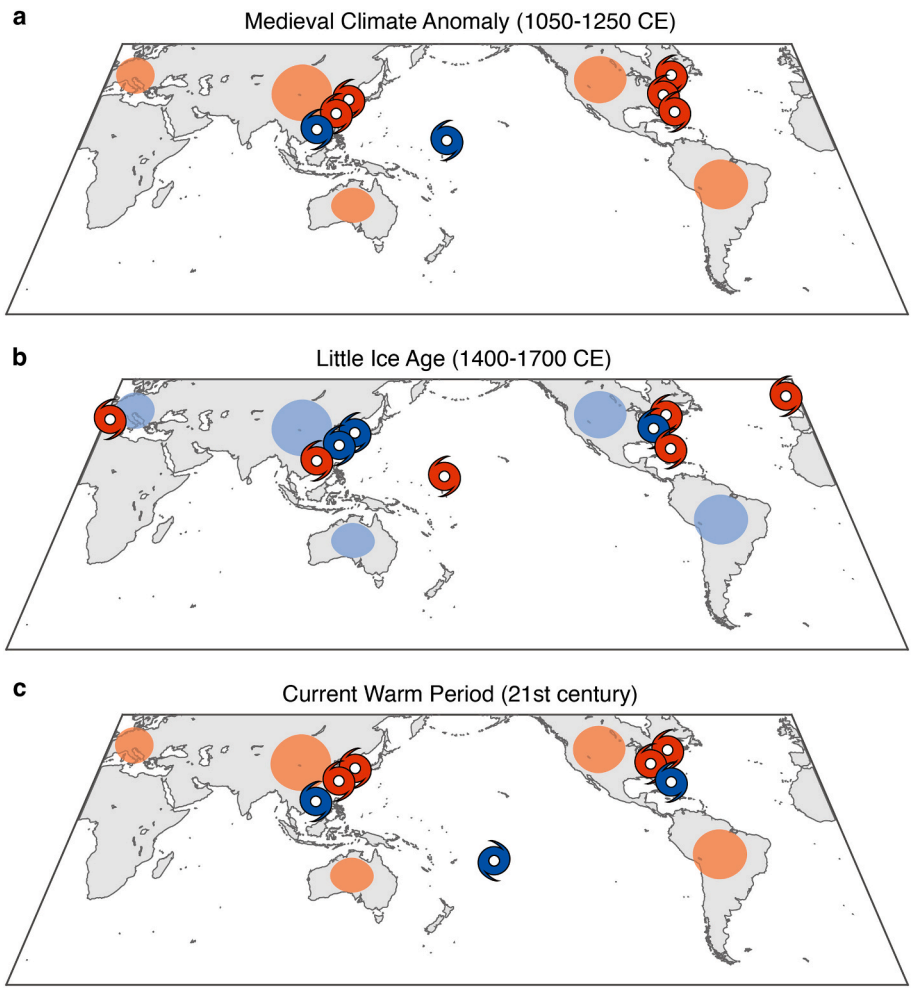

Fig. 9. Hypothetical diagram of variation of storm activity in the last millennium. (a) Storm activity during the Medieval Climate Anomaly in 1050–1250 CE, (b) the Little Ice Age in 1400–1700 CE, and (c) the Current Warm Period in 2000–2022 CE. Red and Blue storm icons show high and low storm activity compared to the mean condition in the last millennium, respectively. Red and blue shades show relatively warm and cool condition compared to the condition in last millennium, respectively. Temperature variation is based on PAGES2k Consortium (2017, 2013). (For interpretation of the references to colour in this figure legend, the reader is referred to the web version of this article.)

basins. Denniston et al. (2015) reported that stalagmite records from northern Australia showed isotopic peaks corresponding to extreme precipitation events in 50–400 CE, 850–1450 CE, and 20th century, and decreasing in 500–850 CE and 1460–1650 CE. They posited that the variability of these extreme precipitation events is driven by ENSO variability (Denniston et al., 2015).

Flood deposit records associated with heavy precipitation in North Island, New Zealand show periods of sustained high storm frequency with 10 events per century at 4900–4600 years BP and 2100–1800 years BP. Fitzsimons and Howarth (2022) reported that from a 10 k-year lakebed flood sediment record from South Island, New Zealand, the frequency of precipitation events was low between 10,000–8000 years BP, moderate between 8000 and 5500 years BP, and high between 5500 and 4000 years BP. In the late Holocene, event frequency was low between 4000 and 700 years BP, but has been increasing from 700 years BP to the present (Fitzsimons and Howarth, 2022).

Terry and Lau (2018) conducted surveys of boulders launched during recent TC and previous events at Taveuni Island, Fiji. In 2016, Category 5 cyclone Winston made landfall on Fiji, breaking the reef edge and launching a carbonate boulder onto the reef flat (Terry and Lau, 2018). U—Th dating and hydrodynamic calculations indicate that past wave events in the last 400 years also provided boulders with wave forces comparable to that of Winston (Terry and Etienne, 2014; Terry and Lau, 2018). Thus, Winston was the largest storm on observation record to land on Fiji following an unusual track, but possibly not unprecedented on the centennial-scale.

The central South Pacific, including French Polynesia, is less frequently affected by TCs than the islands of the western South Pacific, although evidences of past storm events have been reported. Lau et al. (2016) described the distribution of 286 boulders in French Polynesia and performed U—Th dating of corals in boulders. The concentration of ages coincides with the period around 1300 CE and the period when the SST was high on the Great Barrier Reef, but it does not coincide with the period of about 280 years 1436–1718 CE, which overlaps with the LIA (Lau et al., 2016). Two large boulders (77 t and 68 t) may have been transported to the reef flat by a powerful cyclone in 1867, based on the dating results with historical records (Lau et al., 2016). There are no boulders dated after 1900 CE, suggesting that no wave events of similar magnitude have been experienced in the past 100 years (Lau et al., 2016).

Toomey et al. (2013) provided a record of storms over the last 5000 years from coarse-grained event deposits within the back-reef lagoon deposits surrounding Taha'a, French Polynesia. The Taha'a record indicated the presence of a higher coarse-grained overwash flux at 2900–500 years BP and an earlier active period at 5000–3800 years BP compared to the present (Toomey et al., 2013). The authors found that there is a pattern of inter-basin storm activity that is in phase with the high storm activity in Bahamas and anti-phase with low storm activity in

southwestern Japan during 2900–500 years BP (Toomey et al., 2013).

In summary, in the western South Pacific, although individual paleotempestological records show variability on centennial to millennial scales, there is no consistent trend across the entire basin. Factors that make detection difficult are that the absolute number of storm records is small, that proxies related to precipitation and floods can in principle detect precipitation events other than storms, and that storms are less frequently than other basins. Although inconclusive, there is some evidence to suggest that storms have been inactive in the central South Pacific over the past century or more. Therefore, it is possible that the region may experience increased storm activity by natural centennial-scale variability in the future.

4.5. Summary

Paleotempestological studies have revealed variations in the variability of past TC activity in the western North Atlantic, Europe, western North Pacific, and western South Pacific. In the western North Atlantic, while variations were observed in the northern (New England), central (Florida), and southern (Bahamas) regions, La Niña-like climate patterns and the relatively warmer conditions are thought to be the factors that stimulated TC activity. In Europe, there is evidence of widely synchronized and active storm activity, with a period of 1500 years associated with the Bond events. In the western North Pacific, the temperature variability in the basin and the global and the shift of associated atmospheric circulation are the dominant drivers of TC activity although the ENSO plays a subdominant role on the change in TC track. No consistent trend has been identified in the western South Pacific yet. These inter-basin differences are attributed to variations in the primary factors controlling fluctuation in storm activity in each basin (Table 3). Bond events have a significant impact on the climate of the North Atlantic Ocean by influencing thermohaline circulation and Arctic climate, but they are relatively less pronounced in distant regions such as East Asia and the Southern Hemisphere due to teleconnection relationships. This suggests that the climate patterns with direct relationships are stronger than those with teleconnection relationships. Nonetheless, the importance of the ENSO in many basins underscores the considerable impact of it on global climate and TC activity, which is consistent with observational records and modeling results.

It is still unclear that whether globally consistent variations in storm activity exist. Limitations in detection are due to the lack of absolute number, spatial heterogeneity, and proxy type bias of paleotempestological records. Considering the chaotic behavior of TCs, the absolute number of paleotempestological records is still insufficient to capture their variability. In order to detect robust regional, global trends, and inter-basin differences, it is essential to densify paleotempestological records in all regions, analyze trends in subregions within the basin, and correlate findings with time-series records of paleoclimate proxies. Especially, more investigation is necessary in the Indian Ocean, Central Pacific, East to Southeast Asia, and eastern North Pacific, where there are still few records. Finally, storm activity is characterized by many factors such as intensity, size, path, and speed. Different paleotempestological records can capture different characteristics of their activity. Therefore, diversifying the type of paleotempestological records is useful for understanding the multifaceted characteristics of storms.

Table 3
Possible dominant drivers of paleostorm activity.

Region	Dominant climatic factor
Western North Atlantic	ENSO, SST
Europe	Bond events, NAO, WEPA
Western North Pacific	SST, ENSO, ITCZ
Eastern North Pacific	Unknown
Western South Pacific	Unknown
Indian Ocean	Unknown

It is hypothesized that the variation pattern of storm activity may vary by region due to differences in the impact and timing of climate events. For instance, the effects of the LIA are remarkable in the northern hemisphere at high latitudes and in the North Atlantic Ocean, but not in the southern hemisphere. Also, the coldest period of the LIA may have occurred in the 15th century in the central-eastern Pacific and in the 17th century in northwestern Europe and southeastern North America (Neukom et al., 2019). Differences in the impact and timing of climate events are thought to produce differences in the variability of storm activities.

5. Paleoclimate modeling for tropical cyclone activity

Over the past decade, modeling has been conducted to understand TC activity under the paleoclimate condition. Many of them are contributed by the effort of the Paleoclimate Modeling Intercomparison Project (PMIP), whose goals are to identify common responses of atmospheric general circulation models to imposed paleoclimate conditions, to compare model results with paleoclimate data, and to provide results for the analysis and interpretation of paleoclimate data. PMIP pays particular attention to paleoclimate condition and associated impacts (e.g., changes in TC activity) during the Last Glacial Maximum (~21 ka) and Mid-Holocene (~6 ka). In this chapter, we focus on the results of the Holocene, when there are many paleotempestological records, and summarize previous studies in paleoclimate simulation (Table 4).

Climate indices have been proposed to better describe favorable conditions for TC genesis and development, helping us to understand the distribution of TC activity in representative climate conditions. Potential Intensity (PI) is the theoretical maximum intensity of TC that can be thermodynamically developed in a certain environmental field (Emanuel, 1986, 1988). Genesis Potential Index (GPI) is an index of the susceptibility of TC generation in a certain environmental field, which consists of vorticity in the lower layer, vertical wind shear (Camargo et al., 2007). Positive GPI has a positive effect on the generation of TC. Korty et al. (2012) experimented changes in thermodynamic factors important to TC generation over the middle Holocene and pre-industrial millennia, using the PMIP Phase 2 climate model. Their results showed that the thermodynamic factors are stable in both periods, but the orbital variability and volcanic activity have detectable effects. Korty et al. (2012) found that changes in mid-Holocene solar radiation altered the seasonal cycle of potential intensity in the northern hemisphere, leaving the southern hemisphere, where solar radiation was weaker than today, slightly more favorable for TC development than pre-industrial conditions.

Table 4
Publication of paleoclimate modeling.

Paper	Period	Study area	Method	Ensemble
Korty et al. (2012)	850–1850 CE Mid-Holocene (6 ka)	Global	Climatic index	Yes
Koh and Brierley (2015)	Pre-Industrial Mid-Holocene	Global	Climatic index	Yes
Yan et al. (2015)	Last 2 k years	Global	Climatic index	No
Yan et al. (2017a)	Last 1 k years	Western North Pacific	Climatic index	Yes
Kozar et al. (2013)	850–1999 CE	North Atlantic	Downscaling	No
Pausata et al. (2017)	Pre-Industrial Mid-Holocene	Global	Downscaling Climatic index	No
Dandoy et al. (2021)	Pre-Industrial Mid-Holocene	North Atlantic	Downscaling Climatic index	No

Koh and Brierley (2015) used the five climate models of PMIP Phase 3 to calculate the factors involved in TC generation. They found that changes in GPI during the middle Holocene were asymmetric with respect to the equator, i.e., decreasing in the northern hemisphere and increasing in the southern hemisphere (Koh and Brierley, 2015). This is due to the effects of seasonal variations in solar radiation. On the other hand, enhanced seasonality in the middle Holocene could drive localized changes in TC genesis potential by influencing the strength of monsoon and the displacement of the ITCZ. (Koh and Brierley, 2015).

Yan et al. (2015) investigated the response of many factors (PI, SST,

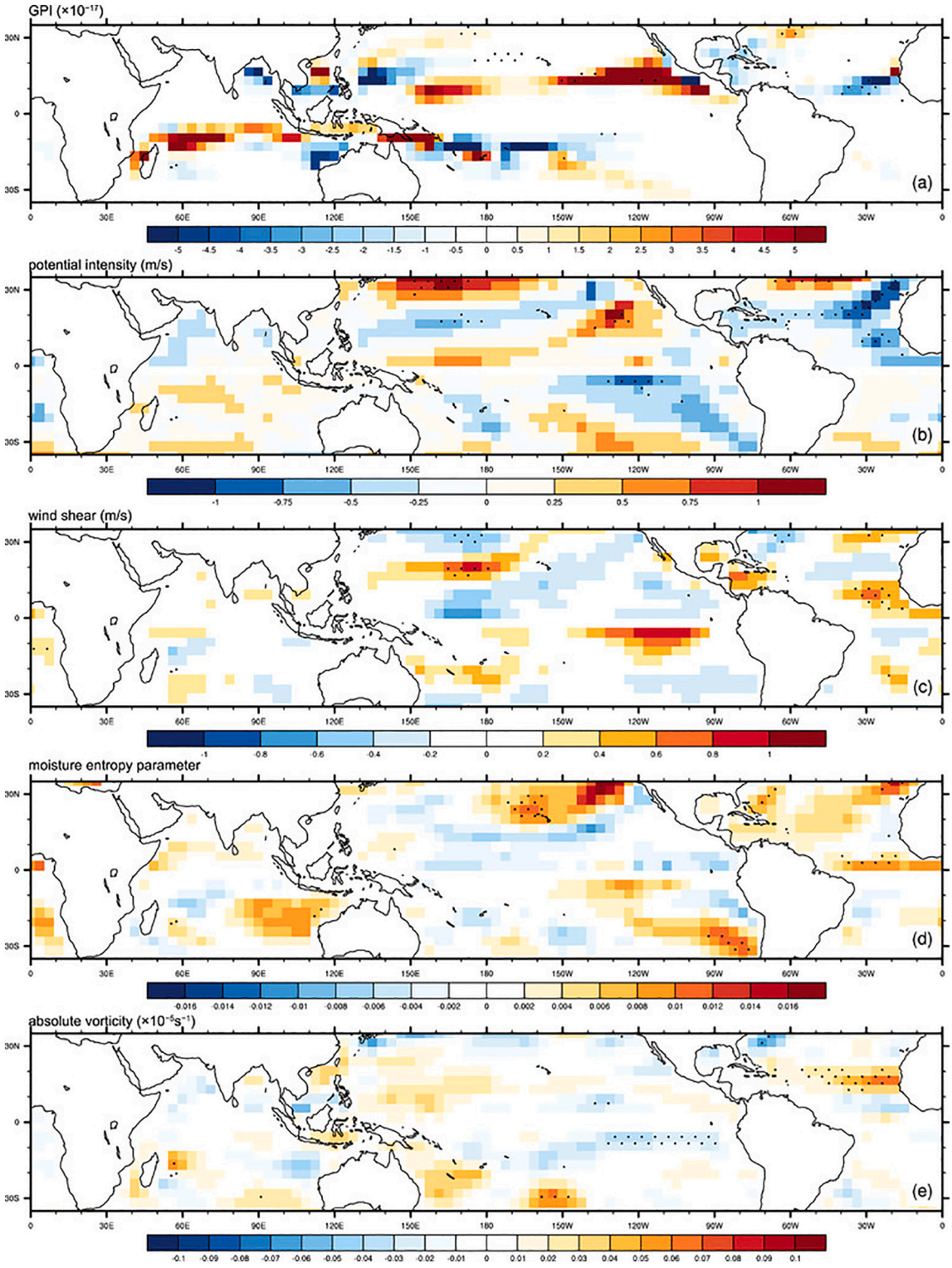

Fig. 10. Differences in the large-scale climatic environments between the Medieval Climate Anomaly and the Little Ice Age, simulated by a global climate model (Yan et al., 2015). Panels show (a) Genesis Potential Index, (b) potential intensity, (c) wind shear, (d) moisture entropy parameter, and (e) absolute vorticity. Dotted areas are significant at 95% confidence level from a two-tailed Student's *t*-test. This figure is from Yan et al. (2015). © American Meteorological Society. Used with permission.

vertical wind shear, mid-level relative humidity, vorticity, and GPI) to external forcing over a relatively long period of the past 2000 years (Fig. 10). These factors generally showed no long-term trends over the past 2000 years (Yan et al., 2015). Basin-specific GPIs have changed relatively recently: favorable conditions for TC genesis in the western North Pacific from 1600 CE to the present, decreases in the western South Pacific from the late 1800s to the present, increases in the North Indian Ocean after 1900 CE, and in the South Indian Ocean after 1800 CE (Yan et al., 2015). In the North Atlantic, the GPI gradually increased over the past 2000 years, with favorable conditions for TC activity during 1250–1350 CE and 1850–2000 CE (Yan et al., 2015). These results suggest that the environment affecting TC activity has changed markedly in the last few hundred years compared to the past 2000 years.

With particular attention to the past 1000 years, Yan et al. (2017a) investigated the consensus among 11 models by comparing results of indices related to TC generation in the western North Pacific. Multimodel ensemble averages showed that many indices (potential intensity, relative humidity in the middle layer) increased during the MCA and decreased during the LIA (Yan et al., 2017a). Consequently, GPI was favorably (adversely) conditioned at MCA (LIA), especially in the northern part of the western North Pacific (Yan et al., 2017a).

Statistical and mechanical downscale models allow analysis of track data to calculate developmental and migration processes. Kozar et al. (2013) simulated the generation, development and migration of TCs in the North Atlantic over the past 1000 years for the first time, using statistical and dynamical downscaling techniques developed by Emanuel et al. (2006). As a result, it was found that the number of TC occurrences in the whole basin on a multidecadal scale correlates well with the number of landfalling hurricanes. This supports the ability to assess long-term changes in TC-climatology using paleotempestological records.

Pausata et al. (2017) computed global TC activity in the Mid-Holocene (~6 ka) using the high-resolution Earth System model and dynamical downscaling techniques. They found that, under the middle Holocene condition, TC numbers were predicted to remain almost unchanged or slightly decrease in the entire Northern Hemisphere, and to increase in the Southern Hemisphere due to the changes in the orbital forcing, which is similar to previous studies using the index (Koh and Brierley, 2015; Korty et al., 2012). On a regional scale, they projected an increase in TC in South Asia and a widespread decrease in TC in the western Pacific Ocean, an increase in the Caribbean and coastal waters, and a decrease in the tropical North Atlantic Ocean relative to the pre-industrial condition (Pausata et al., 2017). Additionally, Pausata et al. (2017) found that vegetation developing in the Sahara and reduced dust emissions during the middle Holocene, enhanced the changes in TC activity seen by orbital forcing alone. In particular, the strengthening of the West African monsoon associated with greening of the Sahara affected the entire tropics and possibly caused an increase in TC activity in both hemispheres during the middle Holocene (Pausata et al., 2017).

With regards to atmospheric dynamics such as the African Easterly Waves, Dandoy et al. (2021) have conducted dynamical downscale modeling to reveal TC behavior in the North Atlantic during the middle Holocene. Their results showed that the main development region of TCs shifted northward, the TC turning point shifted eastward north of 20°N, and the TC landfalls decreased in the north of Florida during the middle Holocene, compared to the pre-industrial climate (Dandoy et al., 2021). Sahara greening and reduction of dust would have likely strengthened these patterns (Dandoy et al., 2021). Overall, Dandoy et al. (2021) predicted an increased proportion of more intense hurricanes and longer life spans in the mid-Holocene compared to pre-industrial times.

Early research that investigated changes in the indices related to TC activity did not simulate storms directly due to lack of access to the outputs required for downscaling (Koh and Brierley, 2015; Korty et al., 2012). These studies are based on the assumption that the GPI, which captures the effects of factors on TC generation in modern climates, also works in various climatic conditions. The agreement between the GPI distribution and the track density distribution based on the downscale model confirms this assumption and supports the validity of the GPI even in the paleoclimate.

In summary, paleoclimate modeling over the past decade has revealed the following:

- There was little change in total absolute numbers of global TCs throughout the Holocene. Especially in the middle Holocene, when the climate was extreme, the simulation based on the PMIP protocol shows a maximum change of ~10%.
- Under the middle Holocene climatic conditions, both climate index (e.g., GPI and PI) and downscale models predicted little change in the number of TC occurrences in the Northern Hemisphere and an increase in the Southern Hemisphere.
- In the Middle Holocene, there were locally predicted increase in TC in South Asia and widespread decrease in the open western Pacific Ocean, increase in the Caribbean coasts, and decrease in the open tropical North Atlantic Ocean.
- Over the past 2000 years, the annual variability of simulated potential intensity of TCs in each basin is small, generally 3–10 m/s.
- Compared to LIA, MCA had higher GPI in the Northeast Pacific, South Indian Ocean, and northern Northwest Pacific, while both GPI and potential intensity were relatively lower in the North Atlantic.
- Changes between hemispheres and basins are relatively consistent between models.

6. Synthesis of paleostorm studies and future goals

Comparison between paleoclimate modeling results and paleotempestological studies is useful not only for the evaluation of models by the paleotempestological evidences but also the interpretation of paleostorm variability. Paleotempestological evidence and modeling results in the western North Pacific show interesting agreement. Modeling for the last millennium indicate that the favorable index TC generation in the western North Pacific increased during the MCA and decreased during the LIA (Yan et al., 2017; Fig. 10). This result is consistent with the overwash record in the southwest Japan (Woodruff et al., 2009) and the historical record in the Philippines (García-Herrera et al., 2007). Marine sediment records off the east coast of China also suggest that TC activity was higher in the MCA than in the LIA (Yang et al., 2022; Zhou et al., 2019). Therefore, the modeling result supports the hypothesis that the warm period such as the MCA caused more favorable conditions for TC generation and development in the western North Pacific compared to the cold period such as the LIA (Fig. 9).

Interestingly, when Kozar et al. (2013) compared landfall frequencies of hurricanes inferred from sediment records at eight sites in North America with landfall frequencies at the same eight sites based on a downscale modeling, both time-series changes were did not match. The simulation result of the GPI is also inconsistent with the variations seen on the paleotempestological records in the North Atlantic (Yan et al., 2015; Fig. 10). This discrepancy is due to both the limited number of paleotempestological records and climate model flaws as mentioned in the previous chapters. The former effect is relatively small due to the relatively high density of records collected along the North Atlantic coast (Oliva et al., 2017). On the other hand, the model has a limitation that they do not take into account internal climate variability such as ENSO, which is known to have a large impact on TC activity in the North Atlantic.

Paleotempestological records indicate periods of high and quiet periods of storm activity on a centennial time scale, suggesting a relationship between storm activity and climate variability such as ENSO and NAO (Chapter 4). Numerous paleoclimate records have confirmed that the positions and intensities of paleoclimate modes (e.g., ENSO and NAO) and internal factors (e.g., AMOC and ITCZ) fluctuated on various

time scales (Chapter 3; Figs. 4, 5).

The impact of single-phase dominance of long-term climate modes on TC activity is complex. This is because longer (centennial) periods dominated by a single phase of climate mode (e.g., El Niño event in ENSO) may change the thermodynamic environment in a different way than high-frequency (seasonal to decadal) transients (Korty et al., 2012). For example, the El Niño event is partly responsible for suppressing Atlantic TC activity due to the rapid warming of the atmosphere and lagging surface temperature there (Tang and Neelin, 2004), but as the Atlantic SST equilibrates with warmer atmospheric conditions, permanent El Niño conditions can have the opposite effect (Korty et al., 2012). To verify whether and how TC activity is driven by internal climate variability, as suggested by paleotempestological records, model experiments considering patterns of internal climate change should be conducted.

Despite the importance of climate modeling, the environmental conditions used in experiments are limited. Previous studies have mainly focused on the LGM and the middle Holocene (~6 ka). Orbital factors, aerosols, and vegetation differ between the MCA, which is a relatively recent warming period, and the Holocene Thermal Maximum, which is older but comparable to the present warming. Therefore, by conducting experiments targeting various periods, it is possible to evaluate the sensitivity of forcing to changes in TC activity. Model experiments during past cold events (e.g., Bond events) will also be useful in interpreting weakening effects of thermohaline circulation due to global warming, as predicted by many simulations.

Declaration of competing interest

The authors declare that they have no known competing financial interests or personal relationships that could have appeared to influence the work reported in this paper.

Data availability

The data that has been used is confidential.

Acknowledgement

This research was supported by research funding from JSPS KAKENHI (grant numbers JP21J22319 and JP21H04508). The authors thank the two anonymous reviewers and the handling editor, Dr. Jingping Xu, for valuable comments which helped to improve the manuscript.

References

Aharon, P., Lambert, W.J., 2009. Radiocarbon deficiencies of US Gulf Coast lakes compromise paleo-hurricane records. Quat. Res. 71, 266–270. https://doi.org/10.1016/j.yqres.2009.01.004.

Alley, R.B., Ágústsdóttir, A.M., 2005. The 8k event: Cause and consequences of a major Holocene abrupt climate change. Quat. Sci. Rev. 24, 1123–1149. https://doi.org/10.1016/j.quascirev.2004.12.004.

Autret, R., Dodet, G., Fichaut, B., Suanez, S., David, L., Leckler, F., Ardhuin, F., Ammann, J., Grandjean, P., Allemand, P., Filipot, J.F., 2016. A comprehensive hydro-geomorphic study of cliff-top storm deposits on Banneg Island during winter 2013–2014. Mar. Geol. 382, 37–55. https://doi.org/10.1016/j.margeo.2016.09.014.

Autret, R., Dodet, G., Suanez, S., Roudaut, G., Fichaut, B., 2018. Long–term variability of supratidal coastal boulder activation in Brittany (France). Geomorphology 304, 184–200. https://doi.org/10.1016/j.geomorph.2017.12.028.

Ayache, M., Swingedouw, D., Mary, Y., Eynaud, F., Colin, C., 2018. Multi-centennial variability of the AMOC over the Holocene: a new reconstruction based on multiple proxy-derived SST records. Glob. Planet. Chang. 170, 172–189. https://doi.org/10.1016/j.gloplacha.2018.08.016.

Bagnold, R.A., 1954. Experiments on a gravity-free dispersion of large solid spheres in a Newtonian fluid under shear. Proc. R. Soc. London. Ser. A. Math. Phys. Sci. 225, 49–63. https://doi.org/10.1098/rspa.1954.0186.

Baker, A.J., Hodges, K.I., Schiemann, R.K.H., Vidale, P.L., 2021. Historical variability and lifecycles of North Atlantic midlatitude cyclones originating in the tropics. J. Geophys. Res. Atmos. 126, 1–18. https://doi.org/10.1029/2020JD033924.

Baldini, L.M., McDermott, F., Baldini, J.U.L., Arias, P., Cueto, M., Fairchild, I.J., Hoffmann, D.L., Mattey, D.P., Müller, W., Nita, D.C., Ontañón, R., Garciá-Moncó, C., Richards, D.A., 2015. Regional temperature, atmospheric circulation, and sea-ice variability within the Younger Dryas Event constrained using a speleothem from northern Iberia. Earth Planet. Sci. Lett. 419, 101–110. https://doi.org/10.1016/j.epsl.2015.03.015.

Baldini, L.M., Baldini, J.U.L., McElwaine, J.N., Frappier, A.B., Asmerom, Y., Liu, K., Prufer, K.M., Ridley, H.E., Polyak, V., Kennett, D.J., Macpherson, C.G., Aquino, V.V., Awe, J., Breitenbach, S.F.M., 2016. Persistent northward North Atlantic tropical cyclone track migration over the past five centuries. Sci. Rep. 6, 37522. https://doi.org/10.1038/srep37522.

Banerjee, C., Bevere, L., Corti, D.T., Finucane, J., Lechner, R., 2023. Natural catastrophes and inflation in 2022 : a perfect storm 34.

Basher, R.E., Zheng, X., 1995. Tropical Cyclones in the Southwest Pacific: spatial patterns and Relationships to Southern Oscillation and Sea Surface Temperature. J. Clim. 8, 1249–1260. https://doi.org/10.1175/1520-0442(1995)008<1249:TCITSP>2.0.CO;2.

Bendixen, M., Clemmensen, L.B., Kroon, A., 2013. Sandy berm and beach-ridge formation in relation to extreme sea-levels: a Danish example in a micro-tidal environment. Mar. Geol. 344, 53–64. https://doi.org/10.1016/j.margeo.2013.07.006.

Bentley, A.M., Bosart, L.F., Keyser, D., 2019. A climatology of extratropical cyclones leading to extreme weather events over central and eastern North America. Mon. Weather Rev. 147, 1471–1490. https://doi.org/10.1175/MWR-D-18-0453.1.

Bereiter, B., Eggleston, S., Schmitt, J., Nehrbass-Ahles, C., Stocker, T.F., Fischer, H., Kipfstuhl, S., Chappellaz, J., 2015. Revision of the EPICA Dome C CO2 record from 800 to 600-kyr before present. Geophys. Res. Lett. 42, 542–549. https://doi.org/10.1002/2014GL061957.

Bereiter, B., Shackleton, S., Baggenstos, D., Kawamura, K., Severinghaus, J., 2018. Mean global ocean temperatures during the last glacial transition. Nature 553, 39–44. https://doi.org/10.1038/nature25152.

Berkelhammer, M., Sinha, A., Stott, L., Cheng, H., Pausata, F.S.R., Yoshimura, K., 2013. An abrupt shift in the Indian Monsoon 4000 years ago. In: Climates, Landscapes, and Civilizations., pp. 75–88. https://doi.org/10.1029/2012GM001207.

Bhardwaj, P., Pattanaik, D.R., Singh, O., 2019. Tropical cyclone activity over Bay of Bengal in relation to El Niño-Southern Oscillation. Int. J. Climatol. 39, 5452–5469. https://doi.org/10.1002/joc.6165.

Bianchette, T.A., Liu, K., McCloskey, T.A., 2022. A 4000-year paleoenvironmental reconstruction and extreme event record from Laguna Nuxco, Guerrero, Mexico. Palaeogeogr. Palaeoclimatol. Palaeoecol. 594, 110933 https://doi.org/10.1016/j.palaeo.2022.110933.

Black, B.A., Andersson, C., Butler, P.G., Carroll, M.L., DeLong, K.L., Reynolds, D.J., Schöne, B.R., Scourse, J., Van Der Sleen, P., Wanamaker, A.D., Witbaard, R., 2019. The revolution of crossdating in marine palaeoecology and palaeoclimatology. Biol. Lett. 15 https://doi.org/10.1098/rsbl.2018.0665.

Boldt, K.V., Lane, P., Woodruff, J.D., Donnelly, J.P., 2010. Calibrating a sedimentary record of overwash from Southeastern New England using modeled historic hurricane surges. Mar. Geol. 275, 127–139. https://doi.org/10.1016/j.margeo.2010.05.002.

Bond, G., Kromer, B., Beer, J., Muscheler, R., Evans, M.N., Showers, W., Hoffmann, S., Lotti-Bond, R., Hajdas, I., Bonani, G., 2001. Persistent solar influence on North Atlantic climate during the Holocene. Science 80-.). 294, 2130–2136. https://doi.org/10.1126/science.1065680.

Boudreault, M., Caron, L.P., Camargo, S.J., 2017. Reanalysis of climate influences on Atlantic tropical cyclone activity using cluster analysis. J. Geophys. Res. 122, 4258–4280. https://doi.org/10.1002/2016JD026103.

Bova, S., Rosenthal, Y., Liu, Z., Godad, S.P., Yan, M., 2021. Seasonal origin of the thermal maxima at the Holocene and the last interglacial. Nature 589, 548–553. https://doi.org/10.1038/s41586-020-03155-x.

Bradley, R.S., 2014. Paleoclimatology: Reconstructing Climates of the Quaternary: Third Edition. In: Paleoclimatology: Reconstructing Climates of the Quaternary: Third Edition. https://doi.org/10.1016/C2009-0-18310-1.

Bramante, J.F., Ford, M.R., Kench, P.S., Ashton, A.D., Toomey, M.R., Sullivan, R.M., Karnauskas, K.B., Ummenhofer, C.C., Donnelly, J.P., 2020. Increased typhoon activity in the Pacific deep tropics driven by Little Ice Age circulation changes. Nat. Geosci. 13, 806–811. https://doi.org/10.1038/s41561-020-00656-2.

Brandon, C.M., Woodruff, J.D., Lane, D.P., Donnelly, J.P., 2013. Tropical cyclone wind speed constraints from resultant storm surge deposition: a 2500 year reconstruction of hurricane activity from St. Marks, FL. Geochem. Geophys. Geosyst. 14, 2993–3008. https://doi.org/10.1002/ggge.20217.

Brandon, C.M., Woodruff, J.D., Donnelly, J.P., Sullivan, R.M., 2014. How unique was Hurricane Sandy? Sedimentary reconstructions of extreme flooding from New York harbor. Sci. Rep. 4, 7366. https://doi.org/10.1038/srep07366.

Bregy, J.C., Wallace, D.J., Minzoni, R.T., Cruz, V.J., 2018. 2500-year paleotempestological record of intense storms for the northern Gulf of Mexico, United States. Mar. Geol. 396, 26–42. https://doi.org/10.1016/j.margeo.2017.09.009.

Bregy, J.C., Maxwell, J.T., Robeson, S.M., Harley, G.L., Elliott, E.A., Heeter, K.J., 2022. US Gulf Coast tropical cyclone precipitation influenced by volcanism and the North Atlantic subtropical high. Commun. Earth Environ. 3, 164. https://doi.org/10.1038/s43247-022-00494-7.

Brill, D., May, S.M., Engel, M., Reyes, M., Pint, A., Opitz, S., Dierick, M., Gonzalo, L.A., Esser, S., Brückner, H., 2016. Typhoon Haiyan's sedimentary record in coastal environments of the Philippines and its palaeotempestological implications. Nat. Hazards Earth Syst. Sci. 16, 2799–2822. https://doi.org/10.5194/nhess-16-2799-2016.

Bristow, C.S., Pucillo, K., 2006. Quantifying rates of coastal progradation from sediment volume using GPR and OSL: the Holocene fill of Guichen Bay, south-east South

Australia. Sedimentology 53, 769–788. https://doi.org/10.1111/j.1365-3091.2006.00792.x.
Brooke, B.P., Huang, Z., Nicholas, W.A., Oliver, T.S.N., Tamura, T., Woodroffe, C.D., Nichol, S.L., 2019. Relative sea-level records preserved in Holocene beach-ridge strandplains – An example from tropical northeastern Australia. Mar. Geol. 411, 107–118. https://doi.org/10.1016/j.margeo.2019.02.005.
Brown, A.L., Reinhardt, E.G., van Hengstum, P.J., Pilarczyk, J.E., 2014. A coastal Yucatan sinkhole records intense hurricane events. J. Coast. Res. 30, 418–428. https://doi.org/10.2112/JCOASTRES-D-13-00069.1.
Burnett, A.C., Sheshadri, A., Silvers, L.G., Robinson, T., 2021. Tropical cyclone frequency under varying SSTs in Aquaplanet Simulations. Geophys. Res. Lett. 48, 1–9. https://doi.org/10.1029/2020GL091980.
Burpee, R.W., 1972. The origin and structure of Easterly Waves in the Lower Troposphere of North Africa. J. Atmos. Sci. 29, 77–90. https://doi.org/10.1175/1520-0469(1972)029<0077:TOASOE>2.0.CO;2.
Caesar, L., McCarthy, G.D., Thornalley, D.J.R., Cahill, N., Rahmstorf, S., 2021. Current Atlantic Meridional Overturning Circulation weakest in last millennium. Nat. Geosci. 14, 118–120. https://doi.org/10.1038/s41561-021-00699-z.
Camargo, S.J., Sobel, A.H., 2005. Western North Pacific tropical cyclone intensity and ENSO. J. Clim. 18, 2996–3006. https://doi.org/10.1175/JCLI3457.1.
Camargo, S.J., Emanuel, K.A., Sobel, A.H., 2007. Use of a genesis potential index to diagnose ENSO effects on tropical cyclone genesis. J. Clim. 20, 4819–4834. https://doi.org/10.1175/JCLI4282.1.
Carré, M., Sachs, J.P., Purca, S., Schauer, A.J., Braconnot, P., Falcón, R.A., Julien, M., Lavallée, D., 2014. Holocene history of ENSO variance and asymmetry in the eastern tropical Pacific. Science (80-.) 345, 1045–1048. https://doi.org/10.1126/science.1252220.
Castagno, K.A., Donnelly, J.P., Woodruff, J.D., 2021. Grain-size analysis of hurricane-induced event beds in a New England Salt Marsh, Massachusetts, USA. J. Coast. Res. 37, 326–335. https://doi.org/10.2112/JCOASTRES-D-19-00159.1.
Castelle, B., Dodet, G., Masselink, G., Scott, T., 2017. A new climate index controlling winter wave activity along the Atlantic coast of Europe: the West Europe Pressure Anomaly. Geophys. Res. Lett. 44, 1384–1392. https://doi.org/10.1002/2016GL072379.
Castelle, B., Dodet, G., Masselink, G., Scott, T., 2018. Increased winter-mean wave height, variability, and periodicity in the Northeast Atlantic over 1949–2017. Geophys. Res. Lett. 45, 3586–3596. https://doi.org/10.1002/2017GL076884.
Causon Deguara, J., Gauci, R., 2017. Evidence of extreme wave events from boulder deposits on the south-east coast of Malta (Central Mediterranean). Nat. Hazards 86, 543–568. https://doi.org/10.1007/s11069-016-2525-4.
Chaumillon, E., Bertin, X., Fortunato, A.B., Bajo, M., Schneider, J.L., Dezileau, L., Walsh, J.P., Michelot, A., Chauveau, E., Créach, A., Hénaff, A., Sauzeau, T., Waeles, B., Gervais, B., Jan, G., Baumann, J., Breilh, J.F., Pedreros, R., 2017. Storm-induced marine flooding: lessons from a multidisciplinary approach. Earth-Sci. Rev. 165, 151–184. https://doi.org/10.1016/j.earscirev.2016.12.005.
Chen, T., Cobb, K.M., Roff, G., Zhao, J., Yang, H., Hu, M., Zhao, K., 2018. Coral-derived western Pacific tropical sea surface temperatures during the last millennium. Geophys. Res. Lett. 45, 3542–3549. https://doi.org/10.1002/2018GL077619.
Clemmensen, L.B., Murray, A., Heinemeier, J., de Jong, R., 2009. The evolution of Holocene coastal dunefields, Jutland, Denmark: a record of climate change over the past 5000 years. Geomorphology 105, 303–313. https://doi.org/10.1016/j.geomorph.2008.10.003.
Clemmensen, L.B., Nielsen, L., Bendixen, M., Murray, A., 2012. Morphology and sedimentary architecture of a beach-ridge system (Anholt, the Kattegat sea): a record of punctuated coastal progradation and sea-level change over the past ~1000 years. Boreas 41, 422–434. https://doi.org/10.1111/j.1502-3885.2012.00250.x.
Clemmensen, L.B., Glad, A.C., Kroon, A., 2016. Storm flood impacts along the shores of micro-tidal inland seas: a morphological and sedimentological study of the Vesterlyng beach, the Belt Sea, Denmark. Geomorphology 253, 251–261. https://doi.org/10.1016/j.geomorph.2015.10.020.
Cobb, K.M., Charles, C.D., Cheng, H., Edwards, R.L., 2003. El Niño/Southern Oscillation and tropical Pacific climate during the last millennium. Nature 424, 271–276. https://doi.org/10.1038/nature01779.
Collins, E.S., Scott, D.B., Gayes, P.T., 1999. Hurricane records on the South Carolina coast: can they be detected in the sediment record? Quat. Int. 56, 15–26. https://doi.org/10.1016/S1040-6182(98)00013-5.
Collins-Key, S.A., Altman, J., 2021. Detecting tropical cyclones from climate- and oscillation-free tree-ring width chronology of longleaf pine in south-central Georgia. Glob. Planet. Chang. 201, 103490 https://doi.org/10.1016/j.gloplacha.2021.103490.
Conroy, J.L., Overpeck, J.T., Cole, J.E., Shanahan, T.M., Steinitz-Kannan, M., 2008. Holocene changes in eastern tropical Pacific climate inferred from a Galápagos lake sediment record. Quat. Sci. Rev. 27, 1166–1180. https://doi.org/10.1016/j.quascirev.2008.02.015.
Cook, E.R., Krusic, P.J., Anchukaitis, K.J., Buckley, B.M., Nakatsuka, T., Sano, M., 2013. Tree-ring reconstructed summer temperature anomalies for temperate East Asia since 800 C.E. Clim. Dyn. 41, 2957–2972. https://doi.org/10.1007/s00382-012-1611-x.
Cook, B.I., Smerdon, J.E., Seager, R., Cook, E.R., 2014. Pan-Continental Droughts in North America over the Last Millennium. J. Clim. 27, 383–397. https://doi.org/10.1175/JCLI-D-13-00100.1.
Cox, R., Zentner, D.B., Kirchner, B.J., Cook, M.S., 2012. Boulder ridges on the Aran Islands (Ireland): recent movements caused by storm waves, not tsunamis. J. Geol. 120, 249–272. https://doi.org/10.1086/664787.
Cox, R., Jahn, K.L., Watkins, O.G., Cox, P., 2018. Extraordinary boulder transport by storm waves (west of Ireland, winter 2013–2014), and criteria for analysing coastal boulder deposits. Earth-Sci. Rev. 177, 623–636. https://doi.org/10.1016/j.earscirev.2017.12.014.
Cox, R., O'boyle, L., Cytrynbaum, J., 2019. Imbricated coastal boulder deposits are formed by storm waves, and can preserve a long-term storminess record. Sci. Rep. 9, 1–12. https://doi.org/10.1038/s41598-019-47254-w.
Cox, R., Ardhuin, F., Dias, F., Autret, R., Beisiegel, N., Earlie, C.S., Herterich, J.G., Kennedy, A., Paris, R., Raby, A., Schmitt, P., Weiss, R., 2020. Systematic review shows that work done by storm waves can be misinterpreted as tsunami-related because commonly used hydrodynamic equations are flawed. Front. Mar. Sci. 7, 4. https://doi.org/10.3389/fmars.2020.00004.
D'Agostino, R., Lionello, P., 2017. Evidence of global warming impact on the evolution of the Hadley Circulation in ECMWF centennial reanalyses. Clim. Dyn. 48, 3047–3060. https://doi.org/10.1007/s00382-016-3250-0.
Daloz, A.S., Camargo, S.J., 2018. Is the poleward migration of tropical cyclone maximum intensity associated with a poleward migration of tropical cyclone genesis? Clim. Dyn. 50, 705–715. https://doi.org/10.1007/s00382-017-3636-7.
Dandoy, S., Pausata, F.S.R., Camargo, S.J., Laprise, R., Winger, K., Emanuel, K., 2021. Atlantic hurricane response to Saharan greening and reduced dust emissions during the mid-Holocene. Clim. Past 17, 675–701. https://doi.org/10.5194/cp-17-675-2021.
Das, O., Wang, Y., Donoghue, J., Xu, X., Coor, J., Elsner, J., Xu, Y., 2013. Reconstruction of paleostorms and paleoenvironment using geochemical proxies archived in the sediments of two coastal lakes in northwest Florida. Quat. Sci. Rev. 68, 142–153. https://doi.org/10.1016/j.quascirev.2013.02.014.
Degeai, J.P., Devillers, B., Dezileau, L., Oueslati, H., Bony, G., 2015. Major storm periods and climate forcing in the Western Mediterranean during the Late Holocene. Quat. Sci. Rev. 129, 37–56. https://doi.org/10.1016/j.quascirev.2015.10.009.
Delworth, T.L., Mann, M.E., 2000. Observed and simulated multidecadal variability in the Northern Hemisphere. Clim. Dyn. 16, 661–676. https://doi.org/10.1007/s003820000075.
Denniston, R.F., Villarini, G., Gonzales, A.N., Wyrwoll, K.H., Polyak, V.J., Ummenhofer, C.C., Lachniet, M.S., Wanamaker, A.D., Humphreys, W.F., Woods, D., Cugley, J., 2015. Extreme rainfall activity in the Australian tropics reflects changes in the El Niño/Southern Oscillation over the last two millennia. Proc. Natl. Acad. Sci. USA 112, 4576–4581. https://doi.org/10.1073/pnas.1422270112.
Denommee, K.C., Bentley, S.J., Droxler, A.W., 2015. Climatic controls on hurricane patterns: a 1200-y near-annual record from Lighthouse Reef. Belize. Sci. Rep. 4, 3876. https://doi.org/10.1038/srep03876.
Dezileau, L., Sabatier, P., Blanchemanche, P., Joly, B., Swingedouw, D., Cassou, C., Castaings, J., Martinez, P., Von Grafenstein, U., 2011. Intense storm activity during the Little Ice Age on the French Mediterranean coast. Palaeogeogr. Palaeoclimatol. Palaeoecol. 299, 289–297. https://doi.org/10.1016/j.palaeo.2010.11.009.
Dezileau, L., Pérez-Ruzafa, A., Blanchemanche, P., Degeai, J.-P., Raji, O., Martinez, P., Marcos, C., Von Grafenstein, U., 2016. Extreme storms during the last 6500 years from lagoonal sedimentary archives in the Mar Menor (SE Spain). Clim. Past 12, 1389–1400. https://doi.org/10.5194/cp-12-1389-2016.
Dixit, Y., Hodell, D.A., Petrie, C.A., 2014. Abrupt weakening of the summer monsoon in Northwest India ~4100 yr ago. Geology 42, 339–342. https://doi.org/10.1130/G35236.1.
Donnelly, J.P., Woodruff, J.D., 2007. Intense hurricane activity over the past 5,000 years controlled by El Niño and the West African monsoon. Nature 447, 465–468. https://doi.org/10.1038/nature05834.
Donnelly, C., Kraus, N., Larson, M., 2006. State of Knowledge on Measurement and Modeling of Coastal Overwash. J. Coast. Res. 224, 965–991. https://doi.org/10.2112/04-0431.1.
Donnelly, J.P., Hawkes, A.D., Lane, P., MacDonald, D., Shuman, B.N., Toomey, M.R., van Hengstum, P.J., Woodruff, J.D., 2015. Climate forcing of unprecedented intense-hurricane activity in the last 2000 years. Earth's Futur. 3, 49–65. https://doi.org/10.1002/2014EF000274.
Dullaart, J.C.M., Muis, S., Bloemendaal, N., Chertova, M.V., Couasnon, A., Aerts, J.C.J.H., 2021. Accounting for tropical cyclones more than doubles the global population exposed to low-probability coastal flooding. Commun. Earth Environ. 2, 1–11. https://doi.org/10.1038/s43247-021-00204-9.
Eisenstein, L., Schulz, B., Qadir, G.A., Pinto, J.G., Knippertz, P., 2022. Identification of high-wind features within extratropical cyclones using a probabilistic random forest-Part 1: Method and case studies. Weather Clim. Dyn. 3, 1157–1182. https://doi.org/10.5194/wcd-3-1157-2022.
Elsner, J.B., 2003. Tracking hurricanes. Bull. Am. Meteorol. Soc. 84, 353–356. https://doi.org/10.1175/BAMS-84-3-353.
Emanuel, K.A., 1986. An Air-Sea Interaction Theory for Tropical Cyclones. Part I: Steady-State Maintenance.
Emanuel, K.A., 1988. The maximum intensity of hurricanes. J. Atmos. Sci. 45, 1143–1155. https://doi.org/10.1175/1520-0469(1988)045<1143:TMIOH>2.0.CO;2.
Emanuel, K., 2021. Atlantic tropical cyclones downscaled from climate reanalyses show increasing activity over past 150 years. Nat. Commun. 12, 7027. https://doi.org/10.1038/s41467-021-27364-8.
Emanuel, K., Ravela, S., Vivant, E., Risi, C., 2006. A statistical deterministic approach to hurricane risk assessment. Bull. Am. Meteorol. Soc. 87, 299–314. https://doi.org/10.1175/BAMS-87-3-299.
Erb, M.P., McKay, N.P., Steiger, N., Dee, S., Hancock, C., Ivanovic, R.F., Gregoire, L.J., Valdes, P., 2022. Reconstructing Holocene temperatures in time and space using paleoclimate data assimilation. Clim. Past 18, 2599–2629. https://doi.org/10.5194/cp-18-2599-2022.

Ercolani, C., Muller, J., Collins, J., Savarese, M., Squiccimara, L., 2015. Intense Southwest Florida hurricane landfalls over the past 1000 years. Quat. Sci. Rev. 126, 17–25. https://doi.org/10.1016/j.quascirev.2015.08.008.
Erdmann, W., Kelletat, D., Scheffers, A., 2018. Boulder transport by storms – Extreme-waves in the coastal zone of the Irish west coast. Mar. Geol. 399, 1–13. https://doi.org/10.1016/j.margeo.2018.02.003.
Etienne, S., Paris, R., 2010. Boulder accumulations related to storms on the south coast of the Reykjanes Peninsula (Iceland). Geomorphology 114, 55–70. https://doi.org/10.1016/j.geomorph.2009.02.008.
Fairbridge, R.W., Hillaire-Marcel, C., 1977. An 8,000-yr palaeoclimatic record of the "Double-Hale" 45-yr solar cycle. Nature 268, 413–416. https://doi.org/10.1038/268413a0.
Fairchild, I.J., Baker, A., 2012. Speleothem Science, Speleothem Science: From Process to Past Environments. Wiley. https://doi.org/10.1002/9781444361094.
Fairchild, I.J., Smith, C.L., Baker, A., Fuller, L., Spötl, C., Mattey, D., McDermott, F., 2006. Modification and preservation of environmental signals in speleothems. Earth-Sci. Rev. 75, 105–153. https://doi.org/10.1016/j.earscirev.2005.08.003.
Felton, C.S., Subrahmanyam, B., Murty, V.S.N., 2013. ENSO-modulated cyclogenesis over the Bay of Bengal. J. Clim. 26, 9806–9818. https://doi.org/10.1175/JCLI-D-13-00134.1.
Fichaut, B., Suanez, S., 2011. Quarrying, transport and deposition of cliff-top storm deposits during extreme events: Banneg Island. Brittany. Mar. Geol. 283, 36–55. https://doi.org/10.1016/j.margeo.2010.11.003.
Fitzsimons, S., Howarth, J., 2022. Developing lacustrine sedimentary records of storminess in southwestern New Zealand. Quat. Sci. Rev. 277, 107355 https://doi.org/10.1016/j.quascirev.2021.107355.
Fleitmann, D., Burns, S.J., Mangini, A., Mudelsee, M., Kramers, J., Villa, I., Neff, U., Al-Subbary, A.A., Buettner, A., Hippler, D., Matter, A., 2007. Holocene ITCZ and Indian monsoon dynamics recorded in stalagmites from Oman and Yemen (Socotra). Quat. Sci. Rev. 26, 170–188. https://doi.org/10.1016/j.quascirev.2006.04.012.
Forsyth, A.J., Nott, J., Bateman, M.D., 2010. Beach ridge plain evidence of a variable late-Holocene tropical cyclone climate, North Queensland, Australia. Palaeogeogr. Palaeoclimatol. Palaeoecol. 297, 707–716. https://doi.org/10.1016/j.palaeo.2010.09.024.
Forsyth, A.J., Nott, J., Bateman, M.D., Beaman, R.J., 2012. Juxtaposed beach ridges and foredunes within a ridge plain - Wonga Beach, northeast Australia. Mar. Geol. 307–310, 111–116. https://doi.org/10.1016/j.margeo.2012.02.012.
Frank, W.M., Young, G.S., 2007. The interannual variability of tropical cyclones. Mon. Weather Rev. 135, 3587–3598. https://doi.org/10.1175/MWR3435.1.
Frappier, A.B., 2008. A stepwise screening system to select storm-sensitive stalagmites: taking a targeted approach to speleothem sampling methodology. Quat. Int. 187, 25–39. https://doi.org/10.1016/j.quaint.2007.09.042.
Frappier, A.B., Sahagian, D., Carpenter, S.J., González, L.A., Frappier, B.R., 2007. Stalagmite stable isotope record of recent tropic cyclone events. Geology 35, 111–114. https://doi.org/10.1130/G23145A.1.
Gagan, M.K., Ayliffe, L.K., Beck, J.W., Cole, J.E., Druffel, E.R.M., Dunbar, R.B., Schrag, D. P., 2000. New views of tropical paleoclimates from corals. Quat. Sci. Rev. 19, 45–64. https://doi.org/10.1016/S0277-3791(99)00054-2.
García-Herrera, R., Ribera, P., Hernández, E., Gimero, L., 2007. Northwest Pacific typhoons documented by the Philippine Jesuits, 1566-1900. J. Geophys. Res. Atmos. 112, 1–12. https://doi.org/10.1029/2006JD007370.
Gischler, E., Shinn, E.A., Oschmann, W., Fiebig, J., Buster, N.A., 2008. A 1500-year holocene caribbean climate archive from the Blue Hole, lighthouse reef, belize. J. Coast. Res. 24, 1495–1505. https://doi.org/10.2112/07-0891.1.
Goff, J., Chagué-Goff, C., Nichol, S., Jaffe, B., Dominey-Howes, D., 2012. Progress in palaeotsunami research. Sediment. Geol. 243–244, 70–88. https://doi.org/10.1016/j.sedgeo.2011.11.002.
Goldenberg, S.B., Landsea, C.W., Mestas-Nuñez, A.M., Gray, W.M., 2001. The recent increase in Atlantic hurricane activity: causes and implications. Science (80-.) 293, 474–479. https://doi.org/10.1126/science.1060040.
Goslin, J., Clemmensen, L.B., 2017. Proxy records of Holocene storm events in coastal barrier systems: Storm-wave induced markers. Quat. Sci. Rev. 174, 80–119. https://doi.org/10.1016/j.quascirev.2017.08.026.
Goto, K., Chavanich, S.A., Imamura, F., Kunthasap, P., Matsui, T., Minoura, K., Sugawara, D., Yanagisawa, H., 2007. Distribution, origin and transport process of boulders deposited by the 2004 Indian Ocean tsunami at Pakarang Cape, Thailand. Sediment. Geol. 202, 821–837. https://doi.org/10.1016/j.sedgeo.2007.09.004.
Goto, K., Okada, K., Imamura, F., 2009. Characteristics and hydrodynamics of boulders transported by storm waves at Kudaka Island, Japan. Mar. Geol. 262, 14–24. https://doi.org/10.1016/j.margeo.2009.03.001.
Goto, K., Kawana, T., Imamura, F., 2010a. Historical and geological evidence of boulders deposited by tsunamis, southern Ryukyu Islands, Japan. Earth-Sci. Rev. 102, 77–99. https://doi.org/10.1016/j.earscirev.2010.06.005.
Goto, K., Miyagi, K., Kawamata, H., Imamura, F., 2010b. Discrimination of boulders deposited by tsunamis and storm waves at Ishigaki Island, Japan. Mar. Geol. 269, 34–45. https://doi.org/10.1016/j.margeo.2009.12.004.
Goto, K., Miyagi, K., Kawana, T., Takahashi, J., Imamura, F., 2011. Emplacement and movement of boulders by known storm waves - Field evidence from the Okinawa Islands, Japan. Mar. Geol. 283, 66–78. https://doi.org/10.1016/j.margeo.2010.09.007.
Gray, W.M., 1968. Global view of the oriigin of tropical disturbances and storms. Mon. Weather Rev. 96, 669–700. https://doi.org/10.1175/1520-0493(1968)096<0669:GVOTOO>2.0.CO;2.
Greer, L., Swart, P.K., 2006. Decadal cyclicity of regional mid-Holocene precipitation: evidence from Dominican coral proxies. Paleoceanography 21, 1–17. https://doi.org/10.1029/2005PA001166.
Grise, K.M., Davis, S.M., 2020. Hadley cell expansion in CMIP6 models. Atmos. Chem. Phys. 20, 5249–5268. https://doi.org/10.5194/acp-20-5249-2020.
Grottoli, A.G., Eakin, C.M., 2007. A review of modern coral δ18O and Δ14C proxy records. Earth-Sci. Rev. 81, 67–91. https://doi.org/10.1016/j.earscirev.2006.10.001.
Grove, C.A., Nagtegaal, R., Zinke, J., Scheufen, T., Koster, B., Kasper, S., McCulloch, M. T., van den Bergh, G., Brummer, G.J.A., 2010. River runoff reconstructions from novel spectral luminescence scanning of massive coral skeletons. Coral Reefs 29, 579–591. https://doi.org/10.1007/s00338-010-0629-y.
Haig, J., Nott, J., Reichart, G.J., 2014. Australian tropical cyclone activity lower than at any time over the past 550-1,500 years. Nature 505, 667–670. https://doi.org/10.1038/nature12882.
Han, Y., Jiang, W., Jiang, L., Yong, Y., Yue, Y., Li, Y., Yu, K., 2023. Influences of climate change on tropical cyclones: an insight into the Western North Pacific over the past two millennia. Glob. Planet. Chang. 231, 104319 https://doi.org/10.1016/j.gloplacha.2023.104319.
Hanna, E., Cappelen, J., Allan, R., Jónsson, T., Le Blanco, F., Lillington, T., Hickey, K., 2008. New insights into north European and North Atlantic surface pressure variability, storminess, and related climatic change since 1830. J. Clim. 21, 6739–6766. https://doi.org/10.1175/2008JCLI2296.1.
Hansom, J.D., Hall, A.M., 2009. Magnitude and frequency of extra-tropical North Atlantic cyclones: a chronology from cliff-top storm deposits. Quat. Int. 195, 42–52. https://doi.org/10.1016/j.quaint.2007.11.010.
Harley, G.L., Grissino-Mayer, H.D., Horn, S.P., 2011. The dendrochronology of Pinus elliottii in the lower Florida Keys: chronology development and climate response. Tree-Ring Res. 67, 39–50. https://doi.org/10.3959/2010-3.1.
Haug, G.H., Hughen, K.A., Sigman, D.M., Peterson, L.C., Röhl, U., 2001. Southward migration of the intertropical convergence zone through the holocene. Science (80-.) 293, 1304–1308. https://doi.org/10.1126/science.1059725.
Hawkes, A.D., Horton, B.P., 2012. Sedimentary record of storm deposits from Hurricane Ike, Galveston and San Luis Islands, Texas. Geomorphology 171–172, 180–189. https://doi.org/10.1016/j.geomorph.2012.05.017.
Hein, C.J., Fitzgerald, D.M., De Souza, L.H.P., Georgiou, I.Y., Buynevich, I.V., Klein, A.H. D.F., De Menezes, J.T., Cleary, W.J., Scolaro, T.L., 2016. Complex coastal change in response to autogenic basin infilling: an example from a sub-tropical Holocene strandplain. Sedimentology 63, 1362–1395. https://doi.org/10.1111/sed.12265.
Hemphill-Haley, E., Kelsey, H.M., Graehl, N.A., Casso, M., Caldwell, D., Loofbourrow, C., Robinson, M., Vermeer, J., Southwick, E., 2019. Recent sandy deposits at five northern California coastal wetlands—Stratigraphy, diatoms, and implications for storm and tsunami hazards. Sci. Investig. Rep. 187 https://doi.org/10.3133/sir20185111.
Hetzinger, S., Pfeiffer, M., Dullo, W.-C., Keenlyside, N., Latif, M., Zinke, J., 2008. Caribbean coral tracks Atlantic Multidecadal Oscillation and past hurricane activity. Geology 36, 11. https://doi.org/10.1130/G24321A.1.
Hippensteel, S.P., 2011. Spatio-lateral continuity of hurricane deposits in back-barrier marshes. Geol. Soc. Am. Bull. 123, 2277–2294. https://doi.org/10.1130/B30261.1.
Hippensteel, S.P., Garcia, W.J., 2014. Micropaleontological evidence of prehistoric hurricane strikes from southeastern North Carolina. J. Coast. Res. 298, 1157–1172. https://doi.org/10.2112/jcoastres-d-12-00180.1.
Hippensteel, S.P., Martin, R.E., 1999. Foraminifera as an indicator of overwash deposits, Barrier Island sediment supply, and Barrier Island evolution: Folly Island, South Carolina. Palaeogeogr. Palaeoclimatol. Palaeoecol. 149, 115–125. https://doi.org/10.1016/S0031-0182(98)00196-5.
Hobgood, J., 2005. Tropical cyclones. In: Oliver, J.E. (Ed.), Encyclopedia of World Climatology. Springer, Netherlands, pp. 750–755. https://doi.org/10.1007/1-4020-3266-8_213.
Hurrell, J.W., Kushnir, Y., Visbeck, M., 2001. The North Atlantic Oscillation. Science 80-.). 291, 603–605. https://doi.org/10.1126/science.1058761.
Imamura, F., Goto, K., Ohkubo, S., 2008. A numerical model for the transport of a boulder by tsunami. J. Geophys. Res. Ocean. 113, 1–12. https://doi.org/10.1029/2007JC004170.
Intergovernmental Panel on Climate Change (IPCC), 2021. Climate Change 2021 – The Physical Science Basis, Cambridge University Press, Cambridge, United Kingdom and New York, NY, USA. https://doi.org/10.1017/9781009157896.
Isdale, P.J., Stewart, B.J., Tickle, K.S., Lough, J.M., 1998. Palaeohydrological variation in a tropical river catchment: a reconstruction using fluorescent bands in corals of the Great Barrier Reef, Australia. Holocene 8, 1–8. https://doi.org/10.1191/095968398670905088.
Kaufman, D.S., Broadman, E., 2023. Revisiting the Holocene global temperature conundrum. Nature 614, 425–435. https://doi.org/10.1038/s41586-022-05536-w.
Kaufman, D.S., Ager, T.A., Anderson, N.J., Anderson, P.M., Andrews, J.T., Bartlein, P.J., Brubaker, L.B., Coats, L.L., Cwynar, L.C., Duvall, M.L., Dyke, A.S., Edwards, M.E., Eisner, W.R., Gajewski, K., Geirsdóttir, A., Hu, F.S., Jennings, A.E., Kaplan, M.R., Kerwin, M.W., Lozhkin, A.V., MacDonald, G.M., Miller, G.H., Mock, C.J., Oswald, W. W., Otto-Bliesner, B.L., Porinchu, D.F., Rühland, K., Smol, J.P., Steig, E.J., Wolfe, B. B., 2004. Holocene thermal maximum in the western Arctic (0-180°W). Quat. Sci. Rev. 23, 529–560. https://doi.org/10.1016/j.quascirev.2003.09.007.
Kaufman, D., McKay, N., Routson, C., Erb, M., Dätwyler, C., Sommer, P.S., Heiri, O., Davis, B., 2020a. Holocene global mean surface temperature, a multi-method reconstruction approach. Sci. Data 7, 1–13. https://doi.org/10.1038/s41597-020-0530-7.
Kaufman, D., McKay, N., Routson, C., Erb, M., Davis, B., Heiri, O., Jaccard, S., Tierney, J., Dätwyler, C., Axford, Y., Brussel, T., Cartapanis, O., Chase, B., Dawson, A., de Vernal, A., Engels, S., Jonkers, L., Marsicek, J., Moffa-Sánchez, P., Morrill, C., Orsi, A., Rehfeld, K., Saunders, K., Sommer, P.S., Thomas, E., Tonello, M., Tóth, M., Vachula, R., Andreev, A., Bertrand, S., Biskaborn, B., Bringué, M., Brooks, S.,

Caniupán, M., Chevalier, M., Cwynar, L., Emile-Geay, J., Fegyveresi, J., Feurdean, A., Finsinger, W., Fortin, M.-C., Foster, L., Fox, M., Gajewski, K., Grosjean, M., Hausmann, S., Heinrichs, M., Holmes, N., Ilyashuk, B., Ilyashuk, E., Juggins, S., Khider, D., Koinig, K., Langdon, P., Larocque-Tobler, I., Li, J., Lotter, A., Luoto, T., Mackay, A., Magyari, E., Malevich, S., Mark, B., Massaferro, J., Montade, V., Nazarova, L., Novenko, E., Pařil, P., Pearson, E., Peros, M., Pienitz, R., Płóciennik, M., Porinchu, D., Potito, A., Rees, A., Reinemann, S., Roberts, S., Rolland, N., Salonen, S., Self, A., Seppä, H., Shala, S., St-Jacques, J.-M., Stenni, B., Syrykh, L., Tarrats, P., Taylor, K., van den Bos, V., Velle, G., Wahl, E., Walker, I., Wilmshurst, J., Zhang, E., Zhilich, S., 2020b. A global database of Holocene paleotemperature records. Sci. Data 7, 115. https://doi.org/10.1038/s41597-020-0445-3.

Kench, P.S., McLean, R.F., Owen, S.D., Tuck, M., Ford, M.R., 2018. Storm-deposited coral blocks: a mechanism of island genesis, Tutaga island, Funafuti atoll, Tuvalu. Geology 46, 915–918. https://doi.org/10.1130/G45045.1.

Kiage, L.M., Deocampo, D., Mccloskey, T.A., Bianchette, T.A., Hursey, M., 2011. A 1900-year paleohurricane record from Wassaw Island, Georgia, USA. J. Quat. Sci. 26, 714–722. https://doi.org/10.1002/jqs.1494.

Kilbourne, K.H., Moyer, R.P., Quinn, T.M., Grottoli, A.G., 2011. Testing coral-based tropical cyclone reconstructions: an example from Puerto Rico. Palaeogeogr. Palaeoclimatol. Palaeoecol. 307, 90–97. https://doi.org/10.1016/j.palaeo.2011.04.027.

Klotzbach, P.J., Gray, W.M., 2008. Multidecadal variability in North Atlantic tropical cyclone activity. J. Clim. 21, 3929–3935. https://doi.org/10.1175/2008JCLI2162.1.

Klotzbach, P.J., Wood, K.M., Schreck, C.J., Bowen, S.G., Patricola, C.M., Bell, M.M., 2022. Trends in global tropical cyclone activity: 1990–2021. Geophys. Res. Lett. 49, 1–11. https://doi.org/10.1029/2021GL095774.

Knapp, P.A., Hadley, K.S., 2012. A 300-year history of Pacific Northwest windstorms inferred from tree rings. Glob. Planet. Chang. 92–93, 257–266. https://doi.org/10.1016/j.gloplacha.2012.06.002.

Knapp, P.A., Soulé, P.T., Maxwell, J.T., Ortegren, J.T., Mitchell, T.J., 2021. Tropical cyclone precipitation regimes since 1750 and the Great Suppression of 1843–1876 along coastal North Carolina, USA. Int. J. Climatol. 41, 200–210. https://doi.org/10.1002/joc.6615.

Knight, J.B., Jaeger, H.M., Nagel, S.R., 1993. Vibration-induced size separation in granular media: the convection connection. Phys. Rev. Lett. 70, 3728–3731. https://doi.org/10.1103/PhysRevLett.70.3728.

Knutson, T., Camargo, S.J., Chan, J.C.L., Emanuel, K., Ho, C.H., Kossin, J., Mohapatra, M., Satoh, M., Sugi, M., Walsh, K., Wu, L., 2019. Tropical cyclones and climate change assessment: Part I: Detection and Attribution. Bull. Am. Meteorol. Soc. 100, 1987–2007. https://doi.org/10.1175/BAMS-D-18-0189.1.

Kobashi, T., Menviel, L., Jeltsch-Thömmes, A., Vinther, B.M., Box, J.E., Muscheler, R., Nakaegawa, T., Pfister, P.L., Döring, M., Leuenberger, M., Wanner, H., Ohmura, A., 2017. Volcanic influence on centennial to millennial Holocene Greenland temperature change. Sci. Rep. 7, 1441. https://doi.org/10.1038/s41598-017-01451-7.

Koh, J.H., Brierley, C.M., 2015. Tropical cyclone genesis potential across palaeoclimates. Clim. Past 11, 1433–1451. https://doi.org/10.5194/cp-11-1433-2015.

Kohila, B.S., Dezileau, L., Boussetta, S., Melki, T., Kallel, N., 2021. Review article: Extreme marine events revealed by lagoonal sedimentary records in Ghar El Melh during the last 2500 years in the northeast of Tunisia. Nat. Hazards Earth Syst. Sci. 21, 3645–3661. https://doi.org/10.5194/nhess-21-3645-2021.

Kongsen, S., Phantuwongraj, S., Choowong, M., 2021a. Distinguishing late Holocene storm deposit from shore-normal beach sediments from the Gulf of Thailand. Front. Earth Sci. 9, 1–18. https://doi.org/10.3389/feart.2021.625926.

Kongsen, S., Phantuwongraj, S., Choowong, M., Chawchai, S., Chaiwongsaen, N., Fuengfu, S., Vu, D.T.A., Tuan, D.Q., Preusser, F., 2021b. Barrier island sediments reveal storm surge and fluvial flood events in the past centuries at Thua Thien Hue, central Vietnam. Front. Ecol. Evol. 9, 1–22. https://doi.org/10.3389/fevo.2021.746143.

Kortekaas, S., Dawson, A.G., 2007. Distinguishing tsunami and storm deposits: an example from Martinhal, SW Portugal. Sediment. Geol. 200, 208–221. https://doi.org/10.1016/j.sedgeo.2007.01.004.

Korty, R.L., Camargo, S.J., Galewsky, J., 2012. Variations in tropical cyclone genesis factors in simulations of the Holocene epoch. J. Clim. 25, 8196–8211. https://doi.org/10.1175/JCLI-D-12-00033.1.

Kossin, J.P., Emanuel, K.A., Vecchi, G.A., 2014. The poleward migration of the location of tropical cyclone maximum intensity. Nature 509, 349–352. https://doi.org/10.1038/nature13278.

Kossin, J.P., Emanuel, K.A., Camargo, S.J., 2016. Past and projected changes in western North Pacific tropical cyclone exposure. J. Clim. 29, 5725–5739. https://doi.org/10.1175/JCLI-D-16-0076.1.

Kossin, J.P., Knapp, K.R., Olander, T.L., Velden, C.S., 2020. Global increase in major tropical cyclone exceedance probability over the past four decades. Proc. Natl. Acad. Sci. 117, 11975–11980. https://doi.org/10.1073/pnas.1920849117.

Kozar, M.E., Mann, M.E., Emanuel, K.A., Evans, J.L., 2013. Long-term variations of North Atlantic tropical cyclone activity downscaled from a coupled model simulation of the last millennium. J. Geophys. Res. Atmos. 118 https://doi.org/10.1002/2013JD020380, 13,383-13,392.

Kuleshov, Y., Qi, L., Fawcett, R., Jones, D., 2008. On tropical cyclone activity in the Southern Hemisphere: trends and the ENSO connection. Geophys. Res. Lett. 35, 1–5. https://doi.org/10.1029/2007GL032983.

Lambert, W.J., Aharon, P., Rodriguez, A.B., 2008. Catastrophic hurricane history revealed by organic geochemical proxies in coastal lake sediments: a case study of Lake Shelby, Alabama (USA). J. Paleolimnol. 39, 117–131. https://doi.org/10.1007/s10933-007-9101-6.

Lane, P., Donnelly, J.P., Woodruff, J.D., Hawkes, A.D., 2011. A decadally-resolved paleohurricane record archived in the late Holocene sediments of a Florida sinkhole. Mar. Geol. 287, 14–30. https://doi.org/10.1016/j.margeo.2011.07.001.

Larson, J., Zhou, Y., Higgins, R.W., 2005. Characteristics of landfalling tropical cyclones in the United States and Mexico: climatology and interannual variability. J. Clim. 18, 1247–1262. https://doi.org/10.1175/JCLI3317.1.

Lases-Hernández, F., Medina-Elizalde, M., Benoit Frappier, A., 2020. Drip water δ18O variability in the northeastern Yucatán Peninsula, Mexico: Implications for tropical cyclone detection and rainfall reconstruction from speleothems. Geochim. Cosmochim. Acta 285, 237–256. https://doi.org/10.1016/j.gca.2020.07.008.

Lau, A.Y.A., Autret, R., 2020. Spatial patterns of subaerial coarse clasts. In: Geological Records of Tsunamis and Other Extreme Waves. Elsevier, pp. 513–546. https://doi.org/10.1016/B978-0-12-815686-5.00024-9.

Lau, A.Y.A., Terry, J.P., Ziegler, A.D., Switzer, A.D., Lee, Y., Etienne, S., 2016. Understanding the history of extreme wave events in the Tuamotu Archipelago of French Polynesia from large carbonate boulders on Makemo Atoll, with implications for future threats in the central South Pacific. Mar. Geol. 380, 174–190. https://doi.org/10.1016/j.margeo.2016.04.018.

Lawrence, R.J., Gedzelman, D.S., 1996. Low stable isotope ratios of tropical cyclone rains. Geophys. Res. Lett. 23, 527–530. https://doi.org/10.1029/96GL00425.

Leatherman, S.P., Williams, A.T., 1983. Vertical sedimentation units in a barrier island washover fan. Earth Surf. Process. Landf. 8, 141–150. https://doi.org/10.1002/esp.3290080205.

Lee, T.-C., Knutson, R.T., Kamahori, H., Ying, M., 2012. Impacts of climate change on tropical cyclones in the Western North Pacific Basin. Part II: Late twenty-first century projections. Trop. Cyclone Res. Rev 1, e241. https://doi.org/10.6057/2012TCRR02.08.

Lee, T.-C., Knutson, T.R., Nakaegawa, T., Ying, M., Cha, E.J., 2020. Third assessment on impacts of climate change on tropical cyclones in the Typhoon Committee Region – Part I: Observed changes, detection and attribution. Trop. Cyclone Res. Rev. 9, 1–22. https://doi.org/10.1016/j.tcrr.2020.03.001.

Lewis, D.B., Finkelstein, D.B., Grissino-Mayer, H.D., Mora, C.I., Perfect, E., 2011. A multitree perspective of the tree ring tropical cyclone record from longleaf pine (Pinus palustris Mill.), Big Thicket National Preserve, Texas, United States. J. Geophys. Res. 116, 1–7. https://doi.org/10.1029/2009jg001194.

Liao, X., Holloway, C.E., Feng, X., Liu, C., Lyu, X., Xue, Y., Bao, R., Li, J., Qiao, F., 2023. Observed Interannual Relationship between ITCZ Position and Tropical Cyclone Frequency. J. Clim. 36, 5587–5603. https://doi.org/10.1175/JCLI-D-22-0865.1.

Lin, N., Emanuel, K.A., Smith, J.A., Vanmarcke, E., 2010. Risk assessment of hurricane storm surge for New York City. J. Geophys. Res. Atmos. 115, 1–11. https://doi.org/10.1029/2009JD013630.

Lindhorst, S., Schutter, I., 2014. Polar gravel beach-ridge systems: Sedimentary architecture, genesis, and implications for climate reconstructions (South Shetland Islands/Western Antarctic Peninsula). Geomorphology 221, 187–203. https://doi.org/10.1016/j.geomorph.2014.06.013.

Liu, K.-B., 2004. Paleotempestology: Principels, methods, and examples from gluf coast lake sediments. In: Hurricanes and Typhoons: Past, Present, and Future., pp. 13–57.

Liu, K., Fearn, M.L., 1993. Lake-sediment record of late Holocene hurricane activities from coastal Alabama. Geology 21, 793. https://doi.org/10.1130/0091-7613(1993)021<0793:LSROLH>2.3.CO;2.

Liu, K., Fearn, M.L., 2000. Reconstruction of prehistoric landfall frequencies of catastrophic hurricanes in northwestern Florida from lake sediment records. Quat. Res. 54, 238–245. https://doi.org/10.1006/qres.2000.2166.

Liu, K., Shen, C., Louie, K. Sheun, 2001. A 1,000-year history of typhoon landfalls in Guangdong, Southern China, reconstructed from Chinese historical documentary records. Ann. Assoc. Am. Geogr. 91, 453–464. https://doi.org/10.1111/0004-5608.00253.

Lough, J.M., 2007. Tropical river flow and rainfall reconstructions from coral luminescence: Great Barrier Reef, Australia. Paleoceanography 22, 1–16. https://doi.org/10.1029/2006PA001377.

Lough, J.M., 2010. Climate records from corals. Wiley Interdiscip. Rev. Clim. Chang. 1, 318–331. https://doi.org/10.1002/wcc.39.

Lough, J.M., 2011. Great Barrier Reef coral luminescence reveals rainfall variability over northeastern Australia since the 17th century. Paleoceanography 26, n/a-n/a. https://doi.org/10.1029/2010PA002050.

Mann, M.E., 2021. Beyond the hockey stick: climate lessons from the Common Era. Proc. Natl. Acad. Sci. 118, 1–9. https://doi.org/10.1073/pnas.2112797118.

Mann, M.E., Woodruff, J.D., Donnelly, J.P., Zhang, Z., 2009a. Atlantic hurricanes and climate over the past 1,500 years. Nature 460, 880–883. https://doi.org/10.1038/nature08219.

Mann, M.E., Zhang, Z., Rutherford, S., Bradley, R.S., Hughes, M.K., Shindell, D., Ammann, C., Faluvegi, G., Ni, F., 2009b. Global signatures and dynamical origins of the Little Ice Age and Medieval Climate Anomaly. Science (80-.) 326, 1256–1260. https://doi.org/10.1126/science.1177303.

Marcott, S.A., Shakun, J.D., Clark, P.U., Mix, A.C., 2013. A Reconstruction of Regional and Global Temperature for the past 11,300 years. Science (80-.) 339, 1198–1201. https://doi.org/10.1126/science.1228026.

Masselink, G., van Heteren, S., 2014. Response of wave-dominated and mixed-energy barriers to storms. Mar. Geol. 352, 321–347. https://doi.org/10.1016/j.margeo.2013.11.004.

Masselink, G., Castelle, B., Scott, T., Dodet, G., Suanez, S., Jackson, D., Floc'h, F., 2016. Extreme wave activity during 2013/2014 winter and morphological impacts along the Atlantic coast of Europe. Geophys. Res. Lett. 43, 2135–2143. https://doi.org/10.1002/2015GL067492.

Matero, I.S.O., Gregoire, L.J., Ivanovic, R.F., Tindall, J.C., Haywood, A.M., 2017. The 8.2 ka cooling event caused by Laurentide ice saddle collapse. Earth Planet. Sci. Lett. 473, 205–214. https://doi.org/10.1016/j.epsl.2017.06.011.
Matthews, T., Murphy, C., Wilby, R.L., Harrigan, S., 2014. Stormiest winter on record for Ireland and UK. Nat. Clim. Chang. 4, 738–740. https://doi.org/10.1038/nclimate2336.
May, S.M., Brill, D., Engel, M., Scheffers, A., Pint, A., Opitz, S., Wennrich, V., Squire, P., Kelletat, D., Uckner, H.B., 2015a. Traces of historical tropical cyclones and tsunamis in the Ashburton Delta (North-west Australia). Sedimentology 62, 1546–1572. https://doi.org/10.1111/sed.12192.
May, S.M., Engel, M., Brill, D., Cuadra, C., Lagmay, A.M.F., Santiago, J., Suarez, J.K., Reyes, M., Brückner, H., 2015b. Block and boulder transport in Eastern Samar (Philippines) during Supertyphoon Haiyan. Earth Surf. Dyn. 3, 543–558. https://doi.org/10.5194/esurf-3-543-2015.
May, S.M., Brill, D., Leopold, M., Callow, J.N., Engel, M., Scheffers, A., Opitz, S., Norpoth, M., Brückner, H., 2017. Chronostratigraphy and geomorphology of washover fans in the Exmouth Gulf (NW Australia) – a record of tropical cyclone activity during the late Holocene. Quat. Sci. Rev. 169, 65–84. https://doi.org/10.1016/j.quascirev.2017.05.023.
Mayewski, P.A., Rohling, E.E., Stager, J.C., Karlén, W., Maasch, K.A., Meeker, L.D., Meyerson, E.A., Gasse, F., van Kreveld, S., Holmgren, K., Lee-Thorp, J., Rosqvist, G., Rack, F., Staubwasser, M., Schneider, R.R., Steig, E.J., 2004. Holocene climate variability. Quat. Res. 62, 243–255. https://doi.org/10.1016/j.yqres.2004.07.001.
McCloskey, T.A., Keller, G., 2009. 5000 year sedimentary record of hurricane strikes on the central coast of Belize. Quat. Int. 195, 53–68. https://doi.org/10.1016/j.quaint.2008.03.003.
McCloskey, T.A., Liu, K., 2012. A sedimentary-based history of hurricane strikes on the southern Caribbean coast of Nicaragua. Quat. Res. (United States) 78, 454–464. https://doi.org/10.1016/j.yqres.2012.07.003.
McCloskey, T.A., Liu, K., 2013. A 7000 year record of paleohurricane activity from a coastal wetland in Belize. Holocene 23, 278–291. https://doi.org/10.1177/0959683612460782.
McGregor, H.V., Evans, M.N., Goosse, H., Leduc, G., Martrat, B., Addison, J.A., Mortyn, P.G., Oppo, D.W., Seidenkrantz, M.S., Sicre, M.A., Phipps, S.J., Selvaraj, K., Thirumalai, K., Filipsson, H.L., Ersek, V., 2015. Robust global ocean cooling trend for the pre-industrial Common Era. Nat. Geosci. 8, 671–677. https://doi.org/10.1038/ngeo2510.
Medina-Elizalde, M., Burns, S.J., Polanco-Martínez, J.M., Beach, T., Lases-Hernández, F., Shen, C.C., Wang, H.C., 2016a. High-resolution speleothem record of precipitation from the Yucatan Peninsula spanning the Maya Preclassic Period. Glob. Planet. Chang. 138, 93–102. https://doi.org/10.1016/j.gloplacha.2015.10.003.
Medina-Elizalde, M., Polanco-Martínez, J.M., Lases-Hernández, F., Bradley, R., Burns, S., 2016b. Testing the "tropical storm" hypothesis of Yucatan Peninsula climate variability during the Maya Terminal Classic Period. Quat. Res. (United States) 86, 111–119. https://doi.org/10.1016/j.yqres.2016.05.006.
Merlis, T.M., Held, I.M., 2019. Aquaplanet Simulations of Tropical Cyclones. Curr. Clim. Chang. Rep. 5, 185–195. https://doi.org/10.1007/s40641-019-00133-y.
Miller, D.L., Mora, C.I., Grissino-Mayer, H.D., Mock, C.J., Uhle, M.E., Sharp, Z., 2006. Tree-ring isotope records of tropical cyclone activity. Proc. Natl. Acad. Sci. USA 103, 14294–14297. https://doi.org/10.1073/pnas.0606549103.
Minamidate, K., Goto, K., Watanabe, M., Roeber, V., Toguchi, K., Sannoh, M., Nakashima, Y., Kan, H., 2020. Millennial scale maximum intensities of typhoon and storm wave in the northwestern Pacific Ocean inferred from storm deposited reef boulders. Sci. Rep. 10, 7218. https://doi.org/10.1038/s41598-020-64100-6.
Minamidate, K., Goto, K., Kan, H., 2022. Numerical estimation of maximum possible sizes of paleo-earthquakes and tsunamis from storm-derived boulders. Earth Planet. Sci. Lett. 579, 117354 https://doi.org/10.1016/j.epsl.2021.117354.
Monecke, K., Templeton, C.K., Finger, W., Houston, B., Luthi, S., McAdoo, B.G., Meilianda, E., Storms, J.E.A., Walstra, D.J., Amna, R., Hood, N., Karmanocky, F.J., Nurjanah, Rusydy, I., Sudrajat, S.U., 2015. Beach ridge patterns in West Aceh, Indonesia, and their response to large earthquakes along the northern Sunda trench. Quat. Sci. Rev. 113, 159–170. https://doi.org/10.1016/j.quascirev.2014.10.014.
Moon, I.J., Kim, S.H., Chan, J.C.L., 2019. Climate change and tropical cyclone trend. Nature. https://doi.org/10.1038/s41586-019-1222-3.
Moore, L.J., Durán Vinent, O., Ruggiero, P., 2016. Vegetation control allows autocyclic formation of multiple dunes on prograding coasts. Geology 44, 559–562. https://doi.org/10.1130/G37778.1.
Morton, R.A., Richmond, B.M., Jaffe, B.E., Gelfenbaum, G., 2006. Reconnaissance Investigation of Caribbean Extreme Wave Deposits – Preliminary Observations, Interpretations, and Research Directions, USGS, Open-File Report, 41 p. https://doi.org/10.3133/ofr20061293.
Morton, R.A., Gelfenbaum, G., Jaffe, B.E., 2007. Physical criteria for distinguishing sandy tsunami and storm deposits using modern examples. Sediment. Geol. 200, 184–207. https://doi.org/10.1016/j.sedgeo.2007.01.003.
Moy, C.M., Seltzer, G.O., Rodbell, D.T., Anderson, D.M., 2002. Variability of El Niño/Southern Oscillation activity at millennial timescales during the Holocene epoch. Nature 420, 162–165. https://doi.org/10.1038/nature01194.
Munksgaard, N.C., Zwart, C., Kurita, N., Bass, A., Nott, J., Bird, M.I., 2015. Stable isotope anatomy of tropical cyclone ita, North-Eastern Australia, April 2014. PLoS One 10, 1–15. https://doi.org/10.1371/journal.pone.0119728.
Mylroie, J.E., Carew, J.L., Moore, A.I., 1995. Blue holes: Definition and genesis. Carbonates Evaporites 10, 225–233. https://doi.org/10.1007/BF03175407.
Nakamura, A., Yokoyama, Y., Maemoku, H., Yagi, H., Okamura, M., Matsuoka, H., Miyake, N., Osada, T., Adhikari, D.P., Dangol, V., Ikehara, M., Miyairi, Y., Matsuzaki, H., 2016. Weak monsoon event at 4.2 ka recorded in sediment from Lake Rara, Himalayas. Quat. Int. 397, 349–359. https://doi.org/10.1016/j.quaint.2015.05.053.
Nanayama, F., Shigeno, K., Satake, K., Shimokawa, K., Koitabashi, S., Miyasaka, S., Ishii, M., 2000. Sedimentary differences between the 1993 Hokkaido-nansei-oki tsunami and the 1959 Miyakojima typhoon at Taisei, southwestern Hokkaido, northern Japan. Sediment. Geol. 135, 255–264. https://doi.org/10.1016/S0037-0738(00)00076-2.
Nandasena, N.A.K., Tanaka, N., 2013. Boulder transport by high energy: Numerical model-fitting experimental observations. Ocean Eng. 57, 163–179. https://doi.org/10.1016/j.oceaneng.2012.09.012.
Nandasena, N.A.K., Paris, R., Tanaka, N., 2011. Reassessment of hydrodynamic equations: minimum flow velocity to initiate boulder transport by high energy events (storms, tsunamis). Mar. Geol. 281, 70–84. https://doi.org/10.1016/j.margeo.2011.02.005.
Nandasena, N.A.K., Tanaka, N., Sasaki, Y., Osada, M., 2013. Boulder transport by the 2011 Great East Japan tsunami: Comprehensive field observations and whither model predictions? Mar. Geol. 346, 292–309. https://doi.org/10.1016/j.margeo.2013.09.015.
Neukom, R., Steiger, N., Gómez-Navarro, J.J., Wang, J., Werner, J.P., 2019. No evidence for globally coherent warm and cold periods over the preindustrial Common Era. Nature 571, 550–554. https://doi.org/10.1038/s41586-019-1401-2.
Nguetsop, V.F., Servant-Vildary, S., Servant, M., 2004. Late Holocene climatic changes in West Africa, a high resolution diatom record from equatorial Cameroon. Quat. Sci. Rev. 23, 591–609. https://doi.org/10.1016/j.quascirev.2003.10.007.
Noji, M., Imamura, F., Syuto, N., 1993. Developing the method of tsunami boulder transport calculation. Coast. Eng. Japan Soc. Civ. Eng. 40, 176–180.
Nott, J., 1997. Extremely high-energy wave deposits inside the Great Barrier Reef, Australia: determining the cause-tsunami or tropical cyclone. Mar. Geol. 141, 193–207. https://doi.org/10.1016/S0025-3227(97)00063-7.
Nott, J., 2003. Waves, coastal boulder deposits and the importance of the pre-transport setting. Earth Planet. Sci. Lett. 210, 269–276. https://doi.org/10.1016/S0012-821X(03)00104-3.
Nott, J., 2011. A 6000 year tropical cyclone record from Western Australia. Quat. Sci. Rev. 30, 713–722. https://doi.org/10.1016/j.quascirev.2010.12.004.
Nott, J., Forsyth, A., 2012. Punctuated global tropical cyclone activity over the past 5,000 years. Geophys. Res. Lett. 39, 1–5. https://doi.org/10.1029/2012GL052236.
Nott, J., Hayne, M., 2001. High frequency of 'super-cyclones' along the Great Barrier Reef over the past 5,000 years. Nature 413, 508–512. https://doi.org/10.1038/35097055.
Nott, J., Smithers, S., Walsh, K., Rhodes, E., 2009. Sand beach ridges record 6000 year history of extreme tropical cyclone activity in northeastern Australia. Quat. Sci. Rev. 28, 1511–1520. https://doi.org/10.1016/j.quascirev.2009.02.014.
Nott, J., Chague-Goff, C., Goff, J., Sloss, C., Riggs, N., 2013. Anatomy of sand beach ridges: evidence from severe Tropical Cyclone Yasi and its predecessors, northeast Queensland, Australia. J. Geophys. Res. Earth Surf. 118, 1710–1719. https://doi.org/10.1002/jgrf.20122.
Nyberg, J., Malmgren, B.A., Winter, A., Jury, M.R., Kilbourne, K.H., Quinn, T.M., 2007. Low Atlantic hurricane activity in the 1970s and 1980s compared to the past 270 years. Nature 447, 698–701. https://doi.org/10.1038/nature05895.
O'Brien, M.P., Morison, J.R., 1952. The forces exerted by waves on objects. Trans. Am. Geophys. Union 33, 32–38. https://doi.org/10.1017/CBO9781107415324.004.
Oliva, F., Peros, M., Viau, A., 2017. A review of the spatial distribution of and analytical techniques used in paleotempestological studies in the western North Atlantic Basin. Prog. Phys. Geogr. Earth Environ. 41, 171–190. https://doi.org/10.1177/0309133316683899.
Olsen, J., Anderson, N.J., Knudsen, M.F., 2012. Variability of the North Atlantic Oscillation over the past 5,200 years. Nat. Geosci. 5, 808–812. https://doi.org/10.1038/ngeo1589.
Orme, L.C., Davies, S.J., Duller, G.A.T., 2015. Reconstructed centennial variability of late Holocene storminess from Cors Fochno, Wales, UK. J. Quat. Sci. 30, 478–488. https://doi.org/10.1002/jqs.2792.
Ortega, P., Lehner, F., Swingedouw, D., Masson-Delmotte, V., Raible, C.C., Casado, M., Yiou, P., 2015. A model-tested North Atlantic Oscillation reconstruction for the past millennium. Nature 523, 71–74. https://doi.org/10.1038/nature14518.
Osman, M.B., Tierney, J.E., Zhu, J., Tardif, R., Hakim, G.J., King, J., Poulsen, C.J., 2021. Globally resolved surface temperatures since the last Glacial Maximum. Nature 599, 239–244. https://doi.org/10.1038/s41586-021-03984-4.
PAGES2k Consortium, 2013. Continental-scale temperature variability during the past two millennia. Nat. Geosci. 6, 339–346. https://doi.org/10.1038/ngeo1797.
PAGES2k Consortium, 2017. A global multiproxy database for temperature reconstructions of the Common Era. Sci. Data 4, 170088. https://doi.org/10.1038/sdata.2017.88.
Paris, R., Wassmer, P., Sartohadi, J., Lavigne, F., Barthomeuf, B., Desgages, E., Grancher, D., Baumert, P., Vautier, F., Brunstein, D., Gomez, C., 2009. Tsunamis as geomorphic crises: lessons from the December 26, 2004 tsunami in Lhok Nga, West Banda Aceh (Sumatra, Indonesia). Geomorphology 104, 59–72. https://doi.org/10.1016/j.geomorph.2008.05.040.
Paris, R., Naylor, L.A., Stephenson, W.J., 2011. Boulders as a signature of storms on rock coasts. Mar. Geol. 283, 1–11. https://doi.org/10.1016/j.margeo.2011.03.016.
Pausata, F.S.R., Emanuel, K.A., Chiacchio, M., Diro, G.T., Zhang, Q., Sushama, L., Stager, J.C., Donnelly, J.P., 2017. Tropical cyclone activity enhanced by Sahara greening and reduced dust emissions during the African Humid Period. Proc. Natl. Acad. Sci. USA 114, 6221–6226. https://doi.org/10.1073/pnas.1619111114.
Peros, M., Gregory, B., Matos, F., Reinhardt, E., Desloges, J., 2015. Late-Holocene record of lagoon evolution, climate change, and hurricane activity from southeastern Cuba. Holocene 25, 1483–1497. https://doi.org/10.1177/0959683615585844.

Phantuwongraj, S., Choowong, M., Nanayama, F., Hisada, K.I., Charusiri, P., Chutakositkanon, V., Pailoplee, S., Chabangbon, A., 2013. Coastal geomorphic conditions and styles of storm surge washover deposits from Southern Thailand. Geomorphology 192, 43–58. https://doi.org/10.1016/j.geomorph.2013.03.016.
Pinto, J.G., Zacharias, S., Fink, A.H., Leckebusch, G.C., Ulbrich, U., 2009. Factors contributing to the development of extreme North Atlantic cyclones and their relationship with the NAO. Clim. Dyn. 32, 711–737. https://doi.org/10.1007/s00382-008-0396-4.
Poussait, P.M., Myneni, S.C.B., Lanzirotti, A., 2006. Tropical dendrochemistry: a novel approach to estimate age and growth from ringless trees. Geophys. Res. Lett. 33, 1–5. https://doi.org/10.1029/2006GL026929.
Rahmstorf, S., Box, J.E., Feulner, G., Mann, M.E., Robinson, A., Rutherford, S., Schaffernicht, E.J., 2015. Exceptional twentieth-century slowdown in Atlantic Ocean overturning circulation. Nat. Clim. Chang. 5, 475–480. https://doi.org/10.1038/nclimate2554.
Raji, O., Dezileau, L., Von Grafenstein, U., Niazi, S., Snoussi, M., Martinez, P., 2015. Extreme sea events during the last millennium in the northeast of Morocco. Nat. Hazards Earth Syst. Sci. 15, 203–211. https://doi.org/10.5194/nhess-15-203-2015.
Renssen, H., Seppä, H., Crosta, X., Goosse, H., Roche, D.M., 2012. Global characterization of the Holocene thermal Maximum. Quat. Sci. Rev. 48, 7–19. https://doi.org/10.1016/j.quascirev.2012.05.022.
Rimbu, N., Lohmann, G., Kim, J.-H., Arz, H.W., Schneider, R., 2003. Arctic/North Atlantic Oscillation signature in Holocene sea surface temperature trends as obtained from alkenone data. Geophys. Res. Lett. 30, 2000–2003. https://doi.org/10.1029/2002GL016570.
Rodysill, J.R., Donnelly, J.P., Sullivan, R., Lane, P.D., Toomey, M., Woodruff, J.D., Hawkes, A.D., MacDonald, D., d'Entremont, N., McKeon, K., Wallace, E., van Hengstum, P.J., 2020. Historically unprecedented Northern Gulf of Mexico hurricane activity from 650 to 1250 CE. Sci. Rep. 10, 1–17. https://doi.org/10.1038/s41598-020-75874-0.
Rovere, A., Casella, E., Harris, D.L., Lorscheid, T., Nandasena, N.A.K., Dyer, B., Sandstrom, M.R., Stocchi, P., D'Andrea, W.J., Raymo, M.E., 2017. Giant boulders and Last interglacial storm intensity in the North Atlantic. Proc. Natl. Acad. Sci. 114, 12144–12149. https://doi.org/10.1073/pnas.1712433114.
Russell, J.O., Aiyyer, A., White, J.D., Hannah, W., 2017. Revisiting the connection between African Easterly Waves and Atlantic tropical cyclogenesis. Geophys. Res. Lett. 44, 587–595. https://doi.org/10.1002/2016GL071236.
Sabatier, P., Dezileau, L., Colin, C., Briqueu, L., Bouchette, F., Martinez, P., Siani, G., Raynal, O., Von Grafenstein, U., 2012. 7000 years of paleostorm activity in the NW Mediterranean Sea in response to Holocene climate events. Quat. Res. 77, 1–11. https://doi.org/10.1016/j.yqres.2011.09.002.
Sallenger, J., 2000. Storm impact scale for barrier islands. J. Coast. Res. 16, 890–895.
Sánchez-Murillo, R., Durán-Quesada, A.M., Esquivel-Hernández, G., Rojas-Cantillano, D., Birkel, C., Welsh, K., Sánchez-Llull, M., Alonso-Hernández, C.M., Tetzlaff, D., Soulsby, C., Boll, J., Kurita, N., Cobb, K.M., 2019. Deciphering key processes controlling rainfall isotopic variability during extreme tropical cyclones. Nat. Commun. 10, 1–10. https://doi.org/10.1038/s41467-019-12062-3.
Scheffers, A.M., Scheffers, S.R., Kelletat, D.H., Squire, P., Collins, L., Feng, Y., Zhao, J., Joannes-Boyau, R., May, S.M., Schellmann, G., Freeman, H., 2012. Coarse clast ridge sequences as suitable archives for past storm events? Case study on the Houtman Abrolhos, Western Australia. J. Quat. Sci. 27, 713–724. https://doi.org/10.1002/jqs.2558.
Schmitt, D., Gischler, E., Anselmetti, F.S., Vogel, H., 2020. Caribbean cyclone activity: an annually-resolved Common Era record. Sci. Rep. 10, 1–17. https://doi.org/10.1038/s41598-020-68633-8.
Schreck, C.J., Knapp, K.R., Kossin, J.P., 2014. The impact of best track discrepancies on global tropical cyclone climatologies using IBTrACS. Mon. Weather Rev. 142, 3881–3899. https://doi.org/10.1175/MWR-D-14-00021.1.
Scileppi, E., Donnelly, J.P., 2007. Sedimentary evidence of hurricane strikes in western long Island, New York. Geochem. Geophys. Geosyst. 8, 1–25. https://doi.org/10.1029/2006GC001463.
Scott, D.B., Collins, E.S., Gayes, P.T., Wright, E., 2003. Records of prehistoric hurricanes on the South Carolina coast based on micropaleontological and sedimentological evidence, with comparison to other Atlantic Coast records. Geol. Soc. Am. Bull. 115, 1027–1039. doi.org/10.1130/B25011.1.
Sedgwick, P.E., Davis, R.A., 2003. Stratigraphy of washover deposits in Florida: Implications for recognition in the stratigraphic record. Mar. Geol. 200, 31–48. https://doi.org/10.1016/S0025-3227(03)00163-4.
Sharmila, S., Walsh, K.J.E., 2018. Recent poleward shift of tropical cyclone formation linked to Hadley cell expansion. Nat. Clim. Chang. 8, 730–736. https://doi.org/10.1038/s41558-018-0227-5.
Short, A.D., 2006. Australian beach systems - nature and distribution. J. Coast. Res. 22, 11–27. https://doi.org/10.2112/05A-0002.1.
Soria, J.L.A., Switzer, A.D., Pilarczyk, J.E., Siringan, F.P., Khan, N.S., Fritz, H.M., 2017. Typhoon Haiyan overwash sediments from Leyte Gulf coastlines show local spatial variations with hybrid storm and tsunami signatures. Sediment. Geol. 358, 121–138. https://doi.org/10.1016/j.sedgeo.2017.06.006.
Sorrel, P., Tessier, B., Demory, F., Delsinne, N., Mouazé, D., 2009. Evidence for millennial-scale climatic events in the sedimentary infilling of a macrotidal estuarine system, the Seine estuary (NW France). Quat. Sci. Rev. 28, 499–516. https://doi.org/10.1016/j.quascirev.2008.11.009.
Sorrel, P., Debret, M., Billeaud, I., Jaccard, S.L., McManus, J.F., Tessier, B., 2012. Persistent non-solar forcing of Holocene storm dynamics in coastal sedimentary archives. Nat. Geosci. 5, 892–896. https://doi.org/10.1038/ngeo1619.
Spahni, R., Chappellaz, J., Stocker, T.F., Loulergue, L., Hausammann, G., Kawamura, K., Flückiger, J., Schwander, J., Raynaud, D., Masson-Delmotte, V., Jouzel, J., 2005. Atmospheric methane and nitrous oxide of the Late Pleistocene from Antarctic Ice Cores. Science (80-.) 310, 1317–1321. https://doi.org/10.1126/science.1120132.
Spiske, M., Jaffe, B.E., 2009. Sedimentology and hydrodynamic implications of a coarse-grained hurricane sequence in a carbonate reef setting. Geology 37, 839–842. https://doi.org/10.1130/G30173A.1.
Steinhilber, F., Beer, J., Fröhlich, C., 2009. Total solar irradiance during the Holocene. Geophys. Res. Lett. 36, 1–5. https://doi.org/10.1029/2009GL040142.
Steinman, B.A., Abbott, M.B., Mann, M.E., Ortiz, J.D., Feng, S., Pompeani, D.P., Stansell, N.D., Anderson, L., Finney, B.P., Bird, B.W., 2014. Ocean-atmosphere forcing of centennial hydroclimate variability in the Pacific Northwest. Geophys. Res. Lett. 41, 2553–2560. https://doi.org/10.1002/2014GL059499.
Stockdon, H.F., Holman, R.A., Howd, P.A., Sallenger, A.H., 2006. Empirical parameterization of setup, swash, and runup. Coast. Eng. 53, 573–588. https://doi.org/10.1016/j.coastaleng.2005.12.005.
Stott, L., Cannariato, K., Thunell, R., Haug, G.H., Koutavas, A., Lund, S., 2004. Decline of surface temperature and salinity in the western tropical pacific ocean in the holocene epoch. Nature 431, 56–59. https://doi.org/10.1038/nature02903.
Studholme, J., Gulev, S., 2018. Concurrent changes to hadley circulation and the meridional distribution of tropical cyclones. J. Clim. 31, 4367–4389. https://doi.org/10.1175/JCLI-D-17-0852.1.
Studholme, J., Fedorov, A.V., Gulev, S.K., Emanuel, K., Hodges, K., 2022. Poleward expansion of tropical cyclone latitudes in warming climates. Nat. Geosci. 15, 14–28. https://doi.org/10.1038/s41561-021-00859-1.
Sugawara, D., 2021. Numerical modeling of tsunami: advances and future challenges after the 2011 Tohoku earthquake and tsunami. Earth-Sci. Rev. 214, 103498 https://doi.org/10.1016/j.earscirev.2020.103498.
Sullivan, R.M., van Hengstum, P.J., Coats, S.J., Donnelly, J.P., Tamalavage, A.E., Winkler, T.S., Albury, N.A., 2021. Hydroclimate dipole drives multi-centennial variability in the Western Tropical North Atlantic Margin during the Middle and Late Holocene. Paleoceanogr. Paleoclimatol. 36, 1–16. https://doi.org/10.1029/2020PA004184.
Switzer, A.D., Jones, B.G., 2008. Setup, deposition, and sedimentary characteristics of two storm overwash deposits, Abrahams Bosom Beach, southeastern Australia. J. Coast. Res. 24, 189–200. https://doi.org/10.2112/05-0487.1.
Tamura, T., 2012. Beach ridges and prograded beach deposits as palaeoenvironment records. Earth-Sci. Rev. 114, 279–297. https://doi.org/10.1016/j.earscirev.2012.06.004.
Tamura, T., Nicholas, W.A., Oliver, T.S.N., Brooke, B.P., 2018. Coarse-sand beach ridges at Cowley Beach, north-eastern Australia: their formative processes and potential as records of tropical cyclone history. Sedimentology 65, 721–744. https://doi.org/10.1111/sed.12402.
Tamura, T., Oliver, T.S.N., Cunningham, A.C., Woodroffe, C.D., 2019. Recurrence of extreme coastal erosion in SE Australia beyond historical timescales inferred from beach ridge morphostratigraphy. Geophys. Res. Lett. 46, 4705–4714. https://doi.org/10.1029/2019GL083061.
Tan, M., Liu, T., Hou, J., Qin, X., Zhang, H., Li, T., 2003. Cyclic rapid warming on centennial-scale revealed by a 2650-year stalagmite record of warm season temperature. Geophys. Res. Lett. 30 https://doi.org/10.1029/2003GL017352.
Tan, L., Shen, C.C., Löwemark, L., Chawchai, S., Lawrence Edwards, R., Cai, Y., Breitenbach, S.F.M., Cheng, H., Chou, Y.C., Duerrast, H., Partin, J.W., Cai, W., Chabangborn, A., Gao, Y., Kwiecien, O., Wu, C.C., Shi, Z., Hsu, H.H., Wohlfarth, B., 2019. Rainfall variations in central Indo-Pacific over the past 2,700 y. Proc. Natl. Acad. Sci. USA 116, 17201–17206. https://doi.org/10.1073/pnas.1903167116.
Tang, B.H., Neelin, J.D., 2004. ENSO Influence on Atlantic hurricanes via tropospheric warming. Geophys. Res. Lett. 31, 1–4. https://doi.org/10.1029/2004GL021072.
Tao, S., Liu, K., Yu, K., Shi, Q., Yan, H., Zhang, H., Wang, L., Huang, Z., Chen, T., 2021. Poleward shift in tropical cyclone tracks in the Northwest Pacific during warm periods: past and future. Paleoceanogr. Paleoclimatol. 36, 1–20. https://doi.org/10.1029/2021PA004367.
Terry, J.P., Etienne, S., 2014. Potential for timing high-energy marine inundation events in the recent geological past through age-dating of reef boulders in Fiji. Geosci. Lett. 1, 14. https://doi.org/10.1186/s40562-014-0014-8.
Terry, J.P., Lau, A.Y.A., 2018. Magnitudes of nearshore waves generated by tropical cyclone Winston, the strongest landfalling cyclone in South Pacific records. Unprecedented or unremarkable? Sediment. Geol. 364, 276–285. https://doi.org/10.1016/j.sedgeo.2017.10.009.
Terry, J.P., Dunne, K., Jankaew, K., 2016a. Prehistorical frequency of high-energy marine inundation events driven by typhoons in the Bay of Bangkok (Thailand), interpreted from coastal carbonate boulders. Earth Surf. Process. Landf. 41, 553–562. https://doi.org/10.1002/esp.3873.
Terry, J.P., Oliver, G.J.H., Friess, D.A., 2016b. Ancient high-energy storm boulder deposits on Ko Samui, Thailand, and their significance for identifying coastal hazard risk. Palaeogeogr. Palaeoclimatol. Palaeoecol. 454, 282–293. https://doi.org/10.1016/j.palaeo.2016.04.046.
Terry, J.P., Goff, J., Jankaew, K., 2018. Major typhoon phases in the upper Gulf of Thailand over the last 1.5 millennia, determined from coastal deposits on rock islands. Quat. Int. 487, 87–98. https://doi.org/10.1016/j.quaint.2018.04.022.
Thomas, E.R., Wolff, E.W., Mulvaney, R., Steffensen, J.P., Johnsen, S.J., Arrowsmith, C., White, J.W.C., Vaughn, B., Popp, T., 2007. The 8.2 ka event from Greenland ice cores. Quat. Sci. Rev. 26, 70–81. https://doi.org/10.1016/j.quascirev.2006.07.017.
Thompson, D.W.J., Wallace, J.M., 1998. The Arctic oscillation signature in the wintertime geopotential height and temperature fields. Geophys. Res. Lett. 25, 1297–1300. https://doi.org/10.1029/98GL00950.
Toomey, M.R., Donnelly, J.P., Woodruff, J.D., 2013. Reconstructing mid-late Holocene cyclone variability in the Central Pacific using sedimentary records from Tahaa,

French Polynesia. Quat. Sci. Rev. 77, 181–189. https://doi.org/10.1016/j.quascirev.2013.07.019.
Trouet, V., Esper, J., Graham, N.E., Baker, A., Scourse, J.D., Frank, D.C., 2009. Persistent positive north atlantic oscillation mode dominated the medieval climate anomaly. Science (80-.) 324, 78–80. https://doi.org/10.1126/science.1166349.
Trouet, V., Scourse, J.D., Raible, C.C., 2012. North Atlantic storminess and Atlantic Meridional Overturning Circulation during the last Millennium: Reconciling contradictory proxy records of NAO variability. Glob. Planet. Chang. 84–85, 48–55. https://doi.org/10.1016/j.gloplacha.2011.10.003.
Trouet, V., Harley, G.L., Domínguez-Delmás, M., 2016. Shipwreck rates reveal Caribbean tropical cyclone response to past radiative forcing. Proc. Natl. Acad. Sci. USA 113, 3169–3174. https://doi.org/10.1073/pnas.1519566113.
Uda, T., 2003. Typhoon and the battle of Bun-ei and Koan. J. Japan Sea Rim Stud. 9, 51–59.
Vaganov, E.A., Anchukaitis, K.J., Evans, M.N., 2011. How well understood are the processes that create dendroclimatic records? A mechanistic model of the climatic control on conifer tree-ring growth dynamics. In: Dendroclimatology. Developments in Paleoenvironmental Research. Springer, Dordrecht, pp. 37–75. https://doi.org/10.1007/978-1-4020-5725-0_3.
van Hengstum, P.J., Donnelly, J.P., Toomey, M.R., Albury, N.A., Lane, P., Kakuk, B., 2014. Heightened hurricane activity on the Little Bahama Bank from 1350 to 1650 AD. Cont. Shelf Res. 86, 103–115. https://doi.org/10.1016/j.csr.2013.04.032.
van Hengstum, P.J., Donnelly, J.P., Fall, P.L., Toomey, M.R., Albury, N.A., Kakuk, B., 2016. The intertropical convergence zone modulates intense hurricane strikes on the western North Atlantic margin. Sci. Rep. 6, 21728. https://doi.org/10.1038/srep21728.
van Hengstum, P.J., Winkler, T.S., Tamalavage, A.E., Sullivan, R.M., Little, S.N., MacDonald, D., Donnelly, J.P., Albury, N.A., 2020. Holocene sedimentation in a blue hole surrounded by carbonate tidal flats in the Bahamas: Autogenic versus allogenic processes. Mar. Geol. 419 https://doi.org/10.1016/j.margeo.2019.106051.
Vecchi, G.A., Landsea, C., Zhang, W., Villarini, G., Knutson, T., 2021. Changes in Atlantic major hurricane frequency since the late-19th century. Nat. Commun. 12, 1–9. https://doi.org/10.1038/s41467-021-24268-5.
Walker, M.J.C., Berkelhammer, M., Björck, S., Cwynar, L.C., Fisher, D.A., Long, A.J., Lowe, J.J., Newnham, R.M., Rasmussen, S.O., Weiss, H., 2012. Formal subdivision of the Holocene Series/Epoch: a Discussion Paper by a Working Group of INTIMATE (Integration of ice-core, marine and terrestrial records) and the Subcommission on Quaternary Stratigraphy (International Commission on Stratigraphy). J. Quat. Sci. 27, 649–659. https://doi.org/10.1002/jqs.2565.
Wallace, E.J., Donnelly, J.P., Hengstum, P.J., Wiman, C., Sullivan, R.M., Winkler, T.S., D'Entremont, N.E., Toomey, M., Albury, N., 2019. Intense hurricane activity over the past 1500 years at South Andros Island, The Bahamas. Paleoceanogr. Paleoclimatol. 34, 1761–1783. https://doi.org/10.1029/2019PA003665.
Wallace, E., Donnelly, J., van Hengstum, P., Winkler, T., Dizon, C., LaBella, A., Lopez, I., D'Entremont, N., Sullivan, R., Woodruff, J., Hawkes, A., Maio, C., 2021a. Regional shifts in paleohurricane activity over the last 1500 years derived from blue hole sediments offshore of Middle Caicos Island. Quat. Sci. Rev. 268, 107126 https://doi.org/10.1016/j.quascirev.2021.107126.
Wallace, E.J., Coats, S., Emanuel, K., Donnelly, J.P., 2021b. Centennial-scale shifts in storm frequency captured in paleohurricane records from the Bahamas arise predominantly from random variability. Geophys. Res. Lett. 48 https://doi.org/10.1029/2020GL091145.
Wallace, E.J., Donnelly, J.P., van Hengstum, P.J., Winkler, T.S., McKeon, K., MacDonald, D., D'Entremont, N.E., Sullivan, R.M., Woodruff, J.D., Hawkes, A.D., Maio, C., 2021c. 1,050 years of hurricane strikes on Long Island in the Bahamas. Paleoceanogr. Paleoclimatol. 36, 1–22. https://doi.org/10.1029/2020PA004156.
Walsh, K.J.E., McBride, J.L., Klotzbach, P.J., Balachandran, S., Camargo, S.J., Holland, G., Knutson, T.R., Kossin, J.P., Lee, T., Sobel, A., Sugi, M., 2016. Tropical cyclones and climate change. WIREs Clim. Chang. 7, 65–89. https://doi.org/10.1002/wcc.371.
Wang, B., Chan, J.C.L., 2002. How strong ENSO events affect tropical storm activity over the western North Pacific. J. Clim. 15, 1643–1658. https://doi.org/10.1175/1520-0442(2002)015<1643:HSEEAT>2.0.CO;2.
Wang, Y., Cheng, H., Edwards, R.L., He, Y., Kong, X., An, Z., Wu, J., Kelly, M.J., Dykoski, C.A., Li, X., 2005. The holocene Asian monsoon: links to solar changes and North Atlantic climate. Science 80-.). 308, 854–857. https://doi.org/10.1126/science.1106296.
Wanner, H., Butikofer, J., 2008. Holocene bond cycles: real or imaginary? Geografie 113, 338–350. https://doi.org/10.37040/geografie2008113040338.
Wanner, H., Brönnimann, S., Casty, C., Gyalistras, D., Luterbacher, J., Schmutz, C., Stephenson, D.B., Xoplaki, E., 2001. North Atlantic Oscillation – concepts and studies. Surv. Geophys. 22, 321–382. https://doi.org/10.1023/A:1014217317898.
Wanner, H., Beer, J., Bütikofer, J., Crowley, T.J., Cubasch, U., Flückiger, J., Goosse, H., Grosjean, M., Joos, F., Kaplan, J.O., Küttel, M., Müller, S.A., Prentice, I.C., Solomina, O., Stocker, T.F., Tarasov, P., Wagner, M., Widmann, M., 2008. Mid- to Late Holocene climate change: an overview. Quat. Sci. Rev. 27, 1791–1828. https://doi.org/10.1016/j.quascirev.2008.06.013.
Wanner, H., Wanner, H., Mercolli, L., Mercolli, L., Grosjean, M., Grosjean, M., Ritz, S.P., 2015. Holocene climate variability and change; a data-based review. J. Geol. Soc. Lond. 172, 254–263. https://doi.org/10.1144/jgs2013-101.
Watanabe, M., Goto, K., Bricker, J.D., Imamura, F., 2018. Are inundation limit and maximum extent of sand useful for differentiating tsunamis and storms? An example from sediment transport simulations on the Sendai Plain, Japan. Sediment. Geol. 364, 204–216. https://doi.org/10.1016/j.sedgeo.2017.12.026.
Watanabe, M., Goto, K., Imamura, F., Kennedy, A., Sugawara, D., Nakamura, N., Tonosaki, T., 2019. Modeling boulder transport by coastal waves on cliff topography: Case study at Hachijo Island, Japan. Earth Surf. Process. Landf. 2956, 2939–2956. https://doi.org/10.1002/esp.4684.
Watanabe, M., Goto, K., Imamura, F., 2020. Reconstruction of transport modes and flow parameters from coastal boulders. In: Geological Records of Tsunamis and Other Extreme Waves. Elsevier, pp. 617–639. https://doi.org/10.1016/B978-0-12-815686-5.00028-6.
White, W.B., 2007. Paleoclimate records from speleothems in limestone caves. In: Studies of Cave Sediments: Physical and Chemical Records of Paleoclimate. https://doi.org/10.1007/978-1-4020-5766-3_9.
Williams, H.F.L., 2012. Magnitude of Hurricane Ike storm surge sedimentation: implications for coastal marsh aggradation. Earth Surf. Process. Landf. 37, 901–906. https://doi.org/10.1002/esp.3252.
Williams, H.F.L., 2015. Contrasting styles of Hurricane Irene washover sedimentation on three east coast barrier islands: Cape Lookout, North Carolina; Assateague Island, Virginia; and Fire Island, New York. Geomorphology 231, 182–192. https://doi.org/10.1016/j.geomorph.2014.11.027.
Williams, H.F.L., Choowong, M., Phantuwongraj, S., Surakietchai, P., Thongkhao, T., Kongsen, S., Simon, E., 2016. Geologic records of Holocene typhoon strikes on the Gulf of Thailand coast. Mar. Geol. 372, 66–78. https://doi.org/10.1016/j.margeo.2015.12.014.
Winkler, T.S., van Hengstum, P.J., Donnelly, J.P., Wallace, E.J., Sullivan, R.M., MacDonald, D., Albury, N.A., 2020. Revising evidence of hurricane strikes on Abaco Island (the Bahamas) over the last 700 years. Sci. Rep. 10, 1–17. https://doi.org/10.1038/s41598-020-73132-x.
Winkler, T.S., van Hengstum, P.J., Donnelly, J.P., Wallace, E.J., Albury, N.A., D'Entremont, N., Hawkes, A.D., Maio, C.V., Roberts, J., Sullivan, R.M., Woodruff, J. D., 2023. More Frequent Hurricane Passage Across the Bahamian Archipelago During the Little Ice Age. Paleoceanogr. Paleoclimatology 38. https://doi.org/10.1029/2023PA004623.
Winkler, T.S., van Hengstum, P.J., Donnelly, J.P., Wallace, E.J., D'Entremont, N., Hawkes, A.D., Maio, C.V., Sullivan, R.M., Woodruff, J.D., 2022. Oceanic passage of hurricanes across Cay Sal Bank in the Bahamas over the last 530 years. Mar. Geol. 443, 106653 https://doi.org/10.1016/j.margeo.2021.106653.
WMO, 2021. WMO Atlas of Mortality and Economic Losses from Weather, Climate and Water Extremes.
WMO, 2021a. Review for the Forty Years of the Wmo Tropical Cyclone.
Woodruff, J.D., Donnelly, J.P., Emanuel, K., Lane, P., 2008a. Assessing sedimentary records of paleohurricane activity using modeled hurricane climatology. Geochem. Geophys. Geosyst. 9 https://doi.org/10.1029/2008GC002043.
Woodruff, J.D., Donnelly, J.P., Mohrig, D., Geyer, W.R., 2008b. Reconstructing relative flooding intensities responsible for hurricane-induced deposits from Laguna Playa Grande, Vieques, Puerto Rico. Geology 36, 391–394. https://doi.org/10.1130/G24731A.1.
Woodruff, J.D., Donnelly, J.P., Okusu, A., 2009. Exploring typhoon variability over the mid-to-late Holocene: evidence of extreme coastal flooding from Kamikoshiki, Japan. Quat. Sci. Rev. 28, 1774–1785. https://doi.org/10.1016/j.quascirev.2009.02.005.
Woodruff, J.D., Kanamaru, K., Kundu, S., Cook, T.L., 2015. Depositional evidence for the Kamikaze typhoons and links to changes in typhoon climatology. Geology 43, 91–94. https://doi.org/10.1130/G36209.1.
Yan, Q., Korty, R., Zhang, Z., 2015. Tropical cyclone genesis factors in a simulation of the last two millennia: results from the Community Earth System Model. J. Clim. 28, 7182–7202. https://doi.org/10.1175/JCLI-D-15-0054.1.
Yan, Q., Wei, T., Zhang, Z., 2017a. Variations in large-scale tropical cyclone genesis factors over the western North Pacific in the PMIP3 last millennium simulations. Clim. Dyn. 48, 957–970. https://doi.org/10.1007/s00382-016-3120-9.
Yan, X., Zhang, R., Knutson, T.R., 2017b. The role of Atlantic overturning circulation in the recent decline of Atlantic major hurricane frequency. Nat. Commun. 8, 1695. https://doi.org/10.1038/s41467-017-01377-8.
Yang, Y., Xu, T., Zhang, X., Ma, L., Lone, M.A., Jiang, X., 2021. Typhoon rainfall impact on drip water δ^{18}O in Xianyun cave, Southeast China. Hydrol. Process. 35, 1–13. https://doi.org/10.1002/hyp.14062.
Yang, Y., Piper, D.J.W., Xu, M., Gao, J., Jia, J., Normandeau, A., Chu, D., Zhou, L., Wang, Y.P., Gao, S., 2022. Northwestern Pacific tropical cyclone activity enhanced by increased Asian dust emissions during the Little Ice Age. Nat. Commun. 13, 1712. https://doi.org/10.1038/s41467-022-29386-2.
Yap, W., Switzer, A.D., Gouramanis, C., Marzinelli, E., Wijaya, W., Yan, Y.T., Dominey-Howes, D., Labbate, M., Srinivasalu, S., Jankaew, K., Lauro, F.M., 2021. Environmental DNA signatures distinguish between tsunami and storm deposition in overwash sand. Commun. Earth Environ. 2, 1–15. https://doi.org/10.1038/s43247-021-00199-3.
Yu, K.F., Zhao, J.X., Collerson, K.D., Shi, Q., Chen, T.G., Wang, P.X., Liu, T.S., 2004. Storm cycles in the last millennium recorded in Yongshu Reef, southern South China Sea. Palaeogeogr. Palaeoclimatol. Palaeoecol. 210, 89–100. https://doi.org/10.1016/j.palaeo.2004.04.002.
Yu, K.-F., Zhao, J.-X., Shi, Q., Meng, Q.-S., 2009. Reconstruction of storm/tsunami records over the last 4000 years using transported coral blocks and lagoon sediments in the southern South China Sea. Quat. Int. 195, 128–137. https://doi.org/10.1016/j.quaint.2008.05.004.
Zhang, P., Cheng, H., Edwards, R.L., Chen, F., Wang, Y., Yang, X., Liu, Jian, Tan, M., Wang, X., Liu, Jinghua, An, C., Dai, Z., Zhou, J., Zhang, D., Jia, J., Jin, L., Johnson, K. R., 2008. A test of climate, sun, and culture relationships from an 1810-year Chinese cave record. Science (80-.) 322, 940–942. https://doi.org/10.1126/science.1163965.
Zhang, R., Sutton, R., Danabasoglu, G., Kwon, Y.O., Marsh, R., Yeager, S.G., Amrhein, D. E., Little, C.M., 2019. A review of the role of the Atlantic meridional overturning

circulation in atlantic multidecadal variability and associated climate impacts. Rev. Geophys. 57, 316–375. https://doi.org/10.1029/2019RG000644.
Zhao, J. Xin, Neil, D.T., Feng, Y. Xing, Yu, K. Fu, Pandolfi, J.M., 2009. High-precision U-series dating of very young cyclone-transported coral reef blocks from Heron and Wistari reefs, southern Great Barrier Reef, Australia. Quat. Int. 195, 122–127. https://doi.org/10.1016/j.quaint.2008.06.004.
Zhou, X., Liu, Z., Yan, Q., Zhang, X., Yi, L., Yang, W., Xiang, R., He, Y., Hu, B., Liu, Y., Shen, Y., 2019. Enhanced tropical cyclone intensity in the western North Pacific during warm periods over the last two millennia. Geophys. Res. Lett. 46, 9145–9153. https://doi.org/10.1029/2019GL083504.
Zhou, L., Gao, S., Jia, J., Yang, Y., Tong, C., Wang, A., 2021. Paleo-typhoon events as indicated by coral reef boulder deposits on the southern coast of Hainan Island, China. Front. Mar. Sci. 8, 1–13. https://doi.org/10.3389/fmars.2021.746773.